arXiv:2504.02547v1 [stat.ME] 3 Apr 2025

A smooth multi-group Gaussian Mixture Model for cellwise robust covariance estimation

Patricia Puchhammer
patricia.puchhammer@tuwien.ac.at

Ines Wilms
i.wilms@maastrichtuniversity.nl

Peter Filzmoser
peter.filzmoser@tuwien.ac.at

April 4, 2025

Abstract

Are data groups which are pre-defined by expert opinions or medical diagnoses corresponding to groups based on statistical modeling? For which reason might observations be inconsistent? This contribution intends to answer both questions by proposing a novel multi-group Gaussian mixture model that accounts for the given group context while allowing high flexibility. This is achieved by assuming that the observations of a particular group originate not from a single distribution but from a Gaussian mixture of all group distributions. Moreover, the model provides robustness against cellwise outliers, thus against atypical data cells of the observations. The objective function can be formulated as a likelihood problem and optimized efficiently. We also derive the theoretical breakdown point of the estimators, an innovative result in this context to quantify the degree of robustness to cellwise outliers. Simulations demonstrate the excellent performance and the advantages to alternative models and estimators. Applications from different areas illustrate the strength of the method, particularly in investigating observations which are on the overlap of different groups.

1 Introduction

The continuous increase in data volumes confronts statisticians with increasingly complex data structures. External information in addition to the measured features is often available and can be leveraged in the analysis. An example of external information are data with a partitioning of the observations into groups. This can be either a partition such as healthy persons and patients, but it could also be related to an expert grouping or to groups based on some hypothesis.

However, in contrast to traditional classification tasks, the group information is considered uncertain to some extent, and thus the intended groups need more flexible modeling. Examples common in the medical context are progressive diseases, where patients are in transition from a healthy status towards more and more sever stages of a disease. Overall, groups cannot be dissociated from each other leading to a multi-group setting for the analysis.

Analyzing the groups separately might offer some insight, but overall trends or connections between groups would be lost or at least difficult to extract. On the other extreme, removing the grouping structure also poses analytical obstacles. Methodologies that assume identically distributed observations might fail because of the lack of coherency between the groups. Other approaches based on multiple distributions, such as mixture models or clustering methods, can deliver groups of data, however, they are not necessarily connected to the provided grouping and thus model something we might not be interested in. Therefore, more flexible models that can account for an underlying, possibly smooth connection among data groups defined by external information on a prior partition are needed to draw proper insights from data sets often present in real life.

There are many practical problem settings of this kind: When analyzing spatial data, as in the geosciences, underlying structures such as terrain type or country borders can dictate the grouping structure. Although the underlying basis are (continuous) spatial coordinates, the focus for the analysis still lies on the specifics of provided groups, but also on their common characteristics. The same applies to time-series data structured by some fixed time interval, such as months or years, or by specific events. An important area where separation based on smooth external variables is common is medicine, where many diagnoses are based on continuous measurements with specific thresholds. An example is diabetes, where the diagnosis is based on measured blood sugar. Moreover, even if the diagnosis is not based on continuous external variables, most diseases are progressive, so measured features vary in a smooth way between people with different health conditions. Thus, taking the diagnosis classification as granted will not only lead to mistakes, but also misses information of persons being at a transition, as well as the reasons for this transition. The idea extends to many other fields, such as groups based on socio-economic status, or failure of components due to abrasion in industrial technology.

When it comes to real-life data, outliers are often present. Their effect on data analysis should be minimized to obtain robust and reliable results. Especially in settings with complex data structures, they can be masked more easily and can have a greater effect on the results if not detected. With multivariate data, outlying observations can be entirely different from the data majority, or they can just differ in single variables. The latter are called cellwise outliers, and methods were developed for their identification in one coherent data set, such as the *detecting deviating data cells* algorithm (DDC, Rousseeuw and Bossche, 2018), or the *cellMCD* estimator (Raymaekers and Rousseeuw, 2023) for cellwise robust covariance estimation. A cellwise robust version of a Gaussian mixture model was recently proposed by Zaccaria et al. (2024, cellGMM)

– however, the method is limited to delivering the best clusters independent of prior information from the grouping structure.

We extend the setting of Gaussian mixture models (GMMs) to multi-group data sets to address the additional focus given by the pre-defined groups. Assuming that a smooth process underlies the partition into groups, we model each group having a main distribution and being mixed with distributions of other groups. This allows us to match the resulting distributions to the pre-defined groups and to put unusual observations into a bigger context. An observation can either be unusual in the original group and might fit better to another group, indicating a possible mismatch, or an observation is generally unusual because of possibly outlying cells. For a mismatch, it is worth checking the group assignment for errors. In case of outlying cells, these may refer to unreliable or extreme measurements that should either be corrected or removed for further analysis. By specifying the probabilities of group membership for each observation, we can also shed light on the transition mechanisms of observations moving from their predefined group to another one, and thus identify potentially influential variables during this transition.

The remainder of the paper is structured as follows. Section 2 provides more detailed information on the relevant literature, as well as an introduction to the model setup and the objective function. Section 3 details the algorithm and hyperparameter settings. Theoretical results on robustness properties are reported in Section 4, and experimental simulation results on robustness are described in Section 5. Three real-life data examples from meteorology, medicine and oenology, the science of wine and wine making, are illustrated in Section 6, and Section 7 concludes.

2 Methodology

We introduce the multi-group Gaussian mixture model in Section 2.1. The objective function based on the log-likelihood is proposed in Section 2.2, and finally connections and differences to related methods are discussed in Section 2.3.

2.1 Model and notation

Let $\boldsymbol{X}_1, \boldsymbol{X}_2, \ldots, \boldsymbol{X}_N$ be data sets from N groups consisting of independent observations $\boldsymbol{X}_g = ((\boldsymbol{x}_{g,1})', \ldots, (\boldsymbol{x}_{g,n_g})')' \in \mathbb{R}^{n_g \times p}$ per group $g = 1, \ldots, N$ of the same p variables. Let $n = \sum_{g=1}^{N} n_g$, and assume that observations $\boldsymbol{x}_{g,i}$ from group g, $i = 1, \ldots, n_g$, originate from a Gaussian mixture

$$\boldsymbol{x}_{g,i} \sim \mathcal{N}(\boldsymbol{\mu}_k, \boldsymbol{\Sigma}_k) \text{ with probability } \pi_{g,k} \geq 0 \tag{1}$$

for $k = 1, \ldots, N$. Note that observations of a particular group can originate not only from a single distribution but from a Gaussian mixture of all group distributions. In the multi-group setting we assume that a pre-specified group

is more coherent than the combined data, and thus it consists of a main distribution assigned to it. Therefore, we enforce $\pi_{g,g} \geq \alpha \geq 0.5$, where the constant α specifies how coherent each group should be.

Based on Equation (1) it follows that the expected value and the covariance of any $\boldsymbol{x}_g$ from group g are

$$\begin{aligned}\mathbb{E}[\boldsymbol{x}_g] &= \sum_{k=1}^{N} \pi_{g,k}\boldsymbol{\mu}_k, \\ \mathrm{Cov}[\boldsymbol{x}_g] &= \sum_{k=1}^{N} \pi_{g,k}\boldsymbol{\Sigma}_k + \sum_{k=1}^{N} \pi_{g,k}(\boldsymbol{\mu}_k - \mathbb{E}[\boldsymbol{x}_g])(\boldsymbol{\mu}_k - \mathbb{E}[\boldsymbol{x}_g])', \end{aligned} \tag{2}$$

see Appendix A for the derivation. The covariance corresponding to group g is then a smoothed covariance consisting of the covariance from the major distribution, $\boldsymbol{\Sigma}_g$, with a minimum weight of α, and of the other covariance matrices $\boldsymbol{\Sigma}_k$, with weights $\pi_{g,k}$ specifying the amount of overlap to other distributions as well as the variability of the means around the expected value.

In the following we define our notation used throughout the paper. The multivariate normal density with mean $\boldsymbol{\mu}_k$ and covariance $\boldsymbol{\Sigma}_k$ of an observation $\boldsymbol{x}_{g,i}$ is denoted by

$$\varphi(\boldsymbol{x}_{g,i}; \boldsymbol{\mu}_k, \boldsymbol{\Sigma}_k) = \frac{\exp\left(-\frac{1}{2}(\boldsymbol{x}_{g,i} - \boldsymbol{\mu}_k)'\boldsymbol{\Sigma}_k^{-1}(\boldsymbol{x}_{g,i} - \boldsymbol{\mu}_k)\right)}{\sqrt{(2\pi)^p \det \boldsymbol{\Sigma}_k}}.$$

Since outlying cells will be considered missing in the likelihood, observed and missing cells of $\boldsymbol{x}_{g,i}$ are denoted by a binary vector $\boldsymbol{w}_{g,i} = (w_{g,i1}, \ldots, w_{g,ip})$, where a value of 1 indicates observed variables, and 0 indicates missing or outlying values. We will put $(\boldsymbol{w}_{g,i})$ as superscript, as in $\boldsymbol{x}_{g,i}^{(\boldsymbol{w}_{g,i})}$, $\boldsymbol{\mu}_k^{(\boldsymbol{w}_{g,i})}$ and $\boldsymbol{\Sigma}_k^{(\boldsymbol{w}_{g,i})}$, if we only consider the subset of variables that are observed, i.e. $\{j : w_{g,ij} = 1, j = 1, \ldots, p\}$. Moreover, for any binary vectors $\boldsymbol{w}$ and $\tilde{\boldsymbol{w}}$, the notation $\boldsymbol{\Sigma}_k^{(\boldsymbol{w}|\tilde{\boldsymbol{w}})}$ denotes the submatrix of $\boldsymbol{\Sigma}_k$ that includes rows and columns indicated by $\boldsymbol{w}$ and $\tilde{\boldsymbol{w}}$, respectively. Also, $(1 - \boldsymbol{w})$ indicates missing cells instead of observed ones, $\{j : w_{g,ij} = 0, j = 1, \ldots, p\}$.

When considering the multivariate normal density $\varphi(\boldsymbol{x}_{g,i}^{(\boldsymbol{w}_{g,i})}; \boldsymbol{\mu}_k^{(\boldsymbol{w}_{g,i})}, \boldsymbol{\Sigma}_k^{(\boldsymbol{w}_{g,i})})$ of a partially observed observation, conventions regarding fully non-observed observations ($\boldsymbol{w}_{g,i} = \boldsymbol{0}$) are as follows. The density $\varphi(\boldsymbol{x}_{g,i}^{(\boldsymbol{w}_{g,i})}; \boldsymbol{\mu}_k^{(\boldsymbol{w}_{g,i})}, \boldsymbol{\Sigma}_k^{(\boldsymbol{w}_{g,i})})$ and the covariance determinant $\det(\boldsymbol{\Sigma}_k^{(\boldsymbol{w}_{g,i})})$ are equal to 1, the squared Mahalanobis distance $(\boldsymbol{x}_{g,i}^{(\boldsymbol{w}_{g,i})} - \boldsymbol{\mu}_k^{(\boldsymbol{w}_{g,i})})'(\boldsymbol{\Sigma}_k^{(\boldsymbol{w}_{g,i})})^{-1}(\boldsymbol{x}_{g,i}^{(\boldsymbol{w}_{g,i})} - \boldsymbol{\mu}_k^{(\boldsymbol{w}_{g,i})})$ is equal to zero.

2.2 Objective function

For our cellwise robust estimation of the statistical model described above we denote the model parameters that need to be estimated as $\boldsymbol{\pi} = (\pi_{g,k})_{g,k=1}^N$, $\boldsymbol{\mu} = (\boldsymbol{\mu}_k)_{k=1}^N$ and $\boldsymbol{\Sigma} = (\boldsymbol{\Sigma}_k)_{k=1}^N$, and their estimates as $\hat{\boldsymbol{\pi}} = (\hat{\pi}_{g,k})_{g,k=1}^N$, $\hat{\boldsymbol{\mu}} = (\hat{\boldsymbol{\mu}}_k)_{k=1}^N$ and $\hat{\boldsymbol{\Sigma}} = (\hat{\boldsymbol{\Sigma}}_k)_{k=1}^N$.

Based on the proposed model in Equation (1) we use a likelihood approach to estimate the parameters. Robustness against cellwise outliers is achieved by considering outlying cells to be missing values indicated by a set of matrices $\boldsymbol{W} = (\boldsymbol{W}_g)_{g=1}^N$ consisting of binary vectors $\boldsymbol{w}_{g,i}, i = 1, \ldots, n_g$, which also need to be estimated, $\hat{\boldsymbol{W}} = (\hat{\boldsymbol{W}}_g)_{g=1}^N$. These missing values are removed from the likelihood estimation by using the observed likelihood.

For defining the objective function, the approach of the cellMCD (Raymaekers and Rousseeuw, 2023) is extended. We combine the observed log-likelihood for the model described in Equation (1) with a penalty term for the number of missing cells. The estimators are then the minimizers of the *observed penalized log-likelihood* $\mathrm{Obj}(\boldsymbol{\pi}, \boldsymbol{\mu}, \boldsymbol{\Sigma}, \boldsymbol{W})$, defined as

$$\sum_{g=1}^{N}\sum_{i=1}^{n_g}\left[-2\ln\left(\sum_{k=1}^{N}\pi_{g,k}\varphi\left(\boldsymbol{x}_{g,i}^{(\boldsymbol{w}_{g,i})};\boldsymbol{\mu}_k^{(\boldsymbol{w}_{g,i})},\boldsymbol{\Sigma}_{reg,k}^{(\boldsymbol{w}_{g,i})}\right)\right)+\sum_{j=1}^{p}q_{g,ij}(1-w_{g,ij})\right] \tag{3}$$

subject to the constraints

$$\boldsymbol{\Sigma}_{reg,k} = (1-\rho_k)\boldsymbol{\Sigma}_k + \rho_k \boldsymbol{T}_k \tag{4}$$

$$\sum_{i=1}^{n_g} w_{g,ij} \geq h_g \qquad \forall j = 1, \ldots, p, \forall g = 1, \ldots, N \tag{5}$$

$$\sum_{k=1}^{N} \pi_{g,k} = 1 \qquad \forall g = 1, \ldots, N \tag{6}$$

$$\pi_{g,g} \geq \alpha \geq 0.5. \tag{7}$$

The first part of Equation (3) is the observed likelihood of each observation $\boldsymbol{x}_{g,i}$ given a missingness pattern $\boldsymbol{w}_{g,i}$. The second part introduces the penalty term to reduce the number of flagged cells and increases accuracy as also shown in Raymaekers and Rousseeuw (2023). Flagging a cell of an observation $x_{g,ij}$ costs a value of $q_{g,ij}$ in the objective function. The penalty constant $q_{g,ij}$ is derived by the notion of a standardized residual. If the (absolute) residual is atypically large (measured by a χ^2-quantile), the minimizing effects on the likelihood exceed the additional cost flagging the cell. If the residual is too small, it will not be flagged and included in the estimation. In that way, only clearly outlying cells are flagged and overflagging is reduced. For more details on choosing $q_{g,ij}$, we refer to Section 3.4.

Regarding the constraints, Equation (4) provides regularization of the covariance matrices by a convex combination with a regular diagonal matrix $\boldsymbol{T}_k$ of univariate robust scale for group k, and a regularization factor $\rho_k > 0$, similar to the MRCD (Boudt et al., 2020). Regularity provides stability for grouped data settings, where groups can also consist of just a few observations, as well as for high-dimensional settings. The proposed values for ρ_k and $\boldsymbol{T}_k$ are described in more detail in Section 3.4.

The number of cells flagged per group and variable is constrained by Equation (5), where at least half of the cells per group need to be included in the parameter estimation of the mixture model, $h_g \geq \lceil 0.5 n_g \rceil$. However, due to the possible instability of the covariance estimation between two variables, we set the default value to $h_g = \lceil 0.75 n_g \rceil$ and thus allow for a maximum of 25% of flagged cells per variable and group.

Lastly, the two constraints in Equations (6) and (7) originate from the proposed multi-group GMM. The parameter α specifies how strict the model is regarding the pre-defined groups. A value of $\alpha = 1$ allows no group change of observations from their given groups. When α decreases, more and more flexibility among the groups is allowed. Therefore, a gradual increase in flexibility can illuminate observations located in the transition between groups.

2.3 Connections to related work

Our method combines elements of clustering via mixture models, robustness, missing data, and multi-group data analysis.

Regarding robustness, many methods exist for the rowwise setting, where an entire observation is considered an outlier (Maronna et al., 2019). A recent rise in methodologies is visible for the cellwise paradigm, introduced by Alqallaf et al. (2009), where single cells of an observation are considered outlying. Standard rowwise robust estimators of covariance and location are the Minimum Covariance Determinant (MCD; Rousseeuw, 1984, 1985) estimator, typically proposed for $n \geq 5p$ (with n the number of observations and p the number of variables), and its regularized version, the Minimum Regularized Covariance Determinant (MRCD; Boudt et al., 2020) estimator. Both search for a subset of observations that minimize the resulting sample covariance.

In the cellwise paradigm, the cellwise robust MCD (cellMCD; Raymaekers and Rousseeuw, 2023) is a recent proposal to extend the likelihood formulation of the MCD to the cellwise outlier setting, leveraging the idea that outlying cells can be considered to be missing values in the estimation procedure. The objective function of the cellMCD consists of the observed likelihood (Little and Rubin, 2019), where outlying cells are declared as missing, plus a penalty term reducing the number of flagged cells and thus increasing estimation accuracy. The objective function is then optimized in an iterative manner, switching between covariance and location estimation via an Expected Maximization (EM) algorithm and updating flagged outlying cells. Again, $n \geq 5p$ is suggested. An alternative in high-dimensional settings is the covariance estimator of Öllerer and Croux (2015) based on pairwise correlations.

Regarding finite mixture models, rowwise robust proposals for standard GMMs (Neykov et al., 2007) were recently extended to cellwise robustness (cellGMM, Zaccaria et al., 2024). Similar to the cellMCD, the objective function consists of an observed likelihood incorporating the mixture model and a penalty term. However, due to the model structure, the penalty weights need to be estimated for each observation separately in the first step before the outliers can be flagged more accurately in the second step. While cellGMM is cellwise robust

and allows for multiple distributions, it does not account for the pre-defined grouping structure and estimated clusters are not directly matched to the given groups.

One rowwise robust method that is applicable in the scenario described above is the spatially smoothed MRCD (ssMRCD) estimation proposed by Puchhammer and Filzmoser (2024). Originally developed for spatial data, it relies on predefined groups that are connected by a bigger picture, and in contrast to a standard GMM also provides a match between pre-defined groups and covariance and location estimates. However, the ssMRCD is not formulated as a mixture model, as it yields a covariance estimate for a group by incorporating overall and group-wise information, where the group contributions are prespecified by weights. For achieving robustness, the ssMRCD estimator targets the determinant of specific covariance matrices, similar to MCD and MRCD.

Compared to the ssMRCD, there are certain advantages of the proposed probabilistic model-based approach when it comes to selecting hyperparameters. While the amount of smoothing and the smoothing weights need to be prespecified for the ssMRCD estimator, which correspond to the mixture weights in the specified mixture model, here these parameters can be estimated within the probabilistic model. Also the amount of flexibility (referred to as smoothing for the ssMRCD) is not a fixed parameter given to the model, but it can vary between groups and is only restricted by the hyperparameter α.

3 Algorithm

The algorithm for the multi-group GMM consists of two steps, iteratively minimizing the objective function over two sets of parameters, similar to Raymaekers and Rousseeuw (2023). The W-step minimizes over $\boldsymbol{W}$ and the Expectation Minimization (Maximization) (EM, Dempster et al., 1977; McLachlan and Krishnan, 2008) step minimizes over $(\boldsymbol{\pi}, \boldsymbol{\mu}, \boldsymbol{\Sigma})$. Especially the EM-step is adapted to the multi-group setting by accounting for constraint (7) and by regularizing the covariance, see Equation (4). Given initial starting values for the parameters described in Appendix C.1,we iteratively repeat the W-step and the EM-step until the estimated covariance matrices have converged. A pseudo code of the main algorithmic structure is given in Algorithm 1.

3.1 W-Step

The calculation of the $(\tau+1)$-th step is based on the estimated parameters in the τ-th step, $\hat{\boldsymbol{\pi}}^\tau = (\hat{\pi}^\tau_{g,k})^N_{g,k=1}$, $\hat{\boldsymbol{\mu}}^\tau = (\hat{\boldsymbol{\mu}}^\tau_k)^N_{k=1}, \hat{\boldsymbol{\Sigma}}^\tau = (\hat{\boldsymbol{\Sigma}}^\tau_k)^N_{k=1}$, $\hat{\boldsymbol{W}}^\tau = (\hat{\boldsymbol{W}}^\tau_g)^N_{g=1}$. Here, we minimize the objective function Equation (3) corresponding to the parameter $\boldsymbol{W}$. For an estimate $\hat{\boldsymbol{W}}^\tau$, a copy $\tilde{\boldsymbol{W}}$ is defined and modified for each variable step by step to reduce the objective function value, starting with $j = 1$. Although the exact results depend on the order of the variables, Raymaekers and Rousseeuw (2023) have shown by simulations that this effect is small or even negligible.

Based on the fixed variable j, for each group g and observation i we calculate the difference in the objective function for including the cell in the estimation, $\tilde{w}_{g,ij} = 1$ $({}_1\tilde{\boldsymbol{w}}_{g,i})$ and flagging the cell, $\tilde{w}_{g,ij} = 0$ $({}_0\tilde{\boldsymbol{w}}_{g,i})$ while all other entries stay unmodified. Note that the results are order independent regarding groups or observations. Thus, the difference $\Delta_{g,ij}$ is

$$\begin{aligned}\Delta_{g,ij} = &-2\ln\left(\sum_{k=1}^{N}\hat{\pi}_{g,k}^{\tau}\varphi\left(\boldsymbol{x}_{g,i}^{({}_1\tilde{\boldsymbol{w}}_{g,i})};\hat{\boldsymbol{\mu}}_k^{\tau({}_1\tilde{\boldsymbol{w}}_{g,i})},\hat{\boldsymbol{\Sigma}}_{reg,k}^{\tau\ ({}_1\tilde{\boldsymbol{w}}_{g,i})}\right)\right)\\ &+2\ln\left(\sum_{k=1}^{N}\hat{\pi}_{g,k}^{\tau}\varphi\left(\boldsymbol{x}_{g,i}^{({}_0\tilde{\boldsymbol{w}}_{g,i})};\hat{\boldsymbol{\mu}}_k^{\tau({}_0\tilde{\boldsymbol{w}}_{g,i})},\hat{\boldsymbol{\Sigma}}_{reg,k}^{\tau\ ({}_0\tilde{\boldsymbol{w}}_{g,i})}\right)\right) - q_{g,ij}.\end{aligned}$$

For all observations with $\Delta_{g,ij} < 0$, we set $\tilde{w}_{g,ij}$ equal to 1 for further calculations. If there are less than h_g observations per group g with $\Delta_{g,ij} < 0$, we set those $\tilde{w}_{g,ij}$ equal to 1 for which $\Delta_{g,ij}$ is among the lowest h_g values of $\{\Delta_{g,ij} : i = 1, \ldots, n_g\}$. Then, the same procedure is applied to the next variable with the updated $\tilde{\boldsymbol{W}}$, until the flagging is updated for all variables. Overall, the updated $\tilde{\boldsymbol{W}}$ after all variables is the next estimate $\hat{\boldsymbol{W}}^{\tau+1}$. We always modify $\tilde{\boldsymbol{W}}$ such that the objective function is at least not increasing given the constraints, and thus the whole W-step does not increase the objective function value.

3.2 EM-Step

Given $\hat{\boldsymbol{W}}^{\tau+1}$, the parameters of the mixture model can be estimated to minimize the unpenalized observed likelihood of the GMM with missing values thus minimizing the overall objective function. Eirola et al. (2014) provide an EM-based algorithm for GMMs with missing data that will be adapted to the multi-group setting incorporating the additional constraints given by Equations (4) and (7). More details and derivations are provided in Appendix C.2.

The expected probability that observation $\boldsymbol{x}_{g,i}$ is from distribution k conditional on the observed values indicated by $\hat{\boldsymbol{w}}_{g,i}^{\tau+1}$ and on the previous estimates $\hat{\boldsymbol{\pi}}^{\tau} = (\hat{\pi}_{g,k}^{\tau})_{g,k=1}^{N}$, $\hat{\boldsymbol{\mu}}^{\tau} = (\hat{\boldsymbol{\mu}}_k^{\tau})_{k=1}^{N}$, $\hat{\boldsymbol{\Sigma}}^{\tau} = (\hat{\boldsymbol{\Sigma}}_k^{\tau})_{k=1}^{N}$, is

$$\hat{t}_{g,i,k}^{\tau+1} = \frac{\hat{\pi}_{g,k}^{\tau}\varphi\left(\boldsymbol{x}_{g,i}^{(\hat{\boldsymbol{w}}_{g,i}^{\tau+1})};\hat{\boldsymbol{\mu}}_k^{\tau(\hat{\boldsymbol{w}}_{g,i}^{\tau+1})},\hat{\boldsymbol{\Sigma}}_{reg,k}^{\tau\ (\hat{\boldsymbol{w}}_{g,i}^{\tau+1})}\right)}{\sum_{l=1}^{N}\hat{\pi}_{g,l}^{\tau}\varphi\left(\boldsymbol{x}_{g,i}^{(\hat{\boldsymbol{w}}_{g,i}^{\tau+1})};\hat{\boldsymbol{\mu}}_l^{\tau(\hat{\boldsymbol{w}}_{g,i}^{\tau+1})},\hat{\boldsymbol{\Sigma}}_{reg,l}^{\tau\ (\hat{\boldsymbol{w}}_{g,i}^{\tau+1})}\right)}. \tag{8}$$

Due the constraints in Equation (7) and (6), the mixture probability updates are adapted according to

$$\hat{\pi}_{g,g}^{\tau+1} = \max\left\{\alpha, \frac{1}{n_g}\sum_{i=1}^{n_g}\hat{t}_{g,i,g}^{\tau+1}\right\}, \quad \hat{\pi}_{g,k}^{\tau+1} = (1-\hat{\pi}_{g,g}^{\tau+1})\frac{\frac{1}{n_g}\sum_{i=1}^{n_g}\hat{t}_{g,i,k}^{\tau+1}}{1-\frac{1}{n_g}\sum_{i=1}^{n_g}\hat{t}_{g,i,g}^{\tau+1}}.$$

Further, for an observation $\boldsymbol{x}_{g,i}$ with current missingness pattern $\hat{\boldsymbol{w}}_{g,i}^{\tau+1}$, the conditional expectation $\hat{\boldsymbol{x}}_{g,i}^{\tau+1}$ assuming that $\boldsymbol{x}_{g,i}$ comes from distribution k is

calculated by

$$\hat{\boldsymbol{x}}_{g,i}^{\tau+1(1-\hat{\boldsymbol{w}}_{g,i}^{\tau+1})} = \hat{\boldsymbol{\mu}}_k^{\tau(1-\hat{\boldsymbol{w}}_{g,i}^{\tau+1})} + \hat{\boldsymbol{\Sigma}}_{reg,k}^{\tau\ (1-\hat{\boldsymbol{w}}_{g,i}^{\tau+1}|\hat{\boldsymbol{w}}_{g,i}^{\tau+1})} \times \left(\hat{\boldsymbol{\Sigma}}_{reg,k}^{\tau\ (\hat{\boldsymbol{w}}_{g,i}^{\tau+1}|\hat{\boldsymbol{w}}_{g,i}^{\tau+1})}\right)^{-1} \left(\boldsymbol{x}_{g,i}^{(\hat{\boldsymbol{w}}_{g,i}^{\tau+1})} - \hat{\boldsymbol{\mu}}_k^{\tau(\hat{\boldsymbol{w}}_{g,i}^{\tau+1})}\right) \tag{9}$$

$$\hat{\boldsymbol{x}}_{g,i}^{\tau+1(\hat{\boldsymbol{w}}_{g,i}^{\tau+1})} = \boldsymbol{x}_{g,i}^{(\hat{\boldsymbol{w}}_{g,i}^{\tau+1})}. \tag{10}$$

The new estimate for $\hat{\boldsymbol{\mu}}_k^{\tau+1}$ is then

$$\hat{\boldsymbol{\mu}}_k^{\tau+1} = \frac{1}{\bar{t}_k} \sum_{g=1}^{N} \sum_{i=1}^{n_g} \hat{t}_{g,i,k}^{\tau+1} \hat{\boldsymbol{x}}_{g,i}^{\tau+1}$$

with $\bar{t}_k = \sum_{g=1}^{N} \sum_{i=1}^{n_g} \hat{t}_{g,i,k}^{\tau+1}$.

For estimating the covariance based on $\hat{\boldsymbol{x}}_{g,i}^{\tau+1}$, an additional term needs to be added. Assuming that observation $\boldsymbol{x}_{g,i}$ originates from distribution k, the correction term is calculated according to

$$\tilde{\boldsymbol{\Sigma}}_{reg,k}^{\tau\ (1-\hat{\boldsymbol{w}}_{g,i}^{\tau+1}|1-\hat{\boldsymbol{w}}_{g,i}^{\tau+1})} = \hat{\boldsymbol{\Sigma}}_{reg,k}^{\tau\ (1-\hat{\boldsymbol{w}}_{g,i}^{\tau+1}|1-\hat{\boldsymbol{w}}_{g,i}^{\tau+1})} - \hat{\boldsymbol{\Sigma}}_{reg,k}^{\tau\ (1-\hat{\boldsymbol{w}}_{g,i}^{\tau+1}|\hat{\boldsymbol{w}}_{g,i}^{\tau+1})} \times \left(\hat{\boldsymbol{\Sigma}}_{reg,k}^{\tau\ (\hat{\boldsymbol{w}}_{g,i}^{\tau+1}|\hat{\boldsymbol{w}}_{g,i}^{\tau+1})}\right)^{-1} \hat{\boldsymbol{\Sigma}}_{reg,k}^{\tau\ (\hat{\boldsymbol{w}}_{g,i}^{\tau+1}|1-\hat{\boldsymbol{w}}_{g,i}^{\tau+1})}$$

for unobserved variables, $\hat{\boldsymbol{w}}_{g,i}^{\tau+1}$ equal to 0, and 1 otherwise. The new estimate $\hat{\boldsymbol{\Sigma}}_{reg,k}^{\tau+1}$ is then calculated as

$$\hat{\boldsymbol{\Sigma}}_{reg,k}^{\tau+1} = \rho_k \boldsymbol{T}_k + (1-\rho_k) \frac{1}{\bar{t}_k} \sum_{g=1}^{N} \sum_{i=1}^{n_g} \hat{t}_{g,i,k}^{\tau+1} \left[(\hat{\boldsymbol{x}}_{g,i}^{\tau+1} - \hat{\boldsymbol{\mu}}_k^{\tau+1})(\hat{\boldsymbol{x}}_{g,i}^{\tau+1} - \hat{\boldsymbol{\mu}}_k^{\tau+1})' + \tilde{\boldsymbol{\Sigma}}_{reg,k}^{\tau} \right].$$

3.3 Convergence of the algorithm

The algorithm iterates between the W-step and the EM-step until the maximal absolute change in any entry of all covariance matrices, $\max_{k,j,j'} |\hat{\Sigma}_{reg,k,jj'}^{\tau} - \hat{\Sigma}_{reg,k,jj'}^{\tau+1}|$, is smaller than $\epsilon_{conv} = 10^{-4}$.

Since the regularization of the covariance matrices acts on the maximization step of the EM-algorithm, the same argumentation as in Proposition 6 from Raymaekers and Rousseeuw (2023) can be applied to show that each W-step and EM-step reduce the objective function or leaves it unchanged while all constraints are fulfilled. Thus, the algorithm converges to a local minimum.

3.4 Choice of hyperparameters

In the objective function (3), the parameters ρ_k, $\boldsymbol{T}_k$ and $q_{g,ij}$ are used but not yet specified.

First, regarding the regularization, we choose a diagonal matrix $\boldsymbol{T}_k$ consisting of robust univariate scale estimates for observations from group k, $\boldsymbol{T}_k = \text{diag}(\hat{\sigma}_{k,1}, \ldots, \hat{\sigma}_{k,p})$. Here, we choose the univariate MCD estimator applied to each variable separately. For the amount of regularization we opt for a condition number of 100 for each covariance. However, due to multiple groups, this is not always possible since $\boldsymbol{T}_k$ could vary heavily and possibly already have a higher condition number for one specific k. Thus, the condition number to achieve for distribution k is $\kappa_k = \max(1.1 \operatorname{cond} \boldsymbol{T}_k, 100)$, where the factor 1.1 allows for multivariate data input if the condition number of $\boldsymbol{T}_k$ is high. Given the initial estimates $\hat{\boldsymbol{\Sigma}}_k^0$, the regularization factor ρ_k is chosen as small as possible and such that the condition number fulfills $\rho_k \boldsymbol{T}_k + (1-\rho_k)\hat{\boldsymbol{\Sigma}}_k^0 \leq \kappa_k$.

Second, the penalty weights $q_{g,ij}$ are chosen per observation and variable. In the cellMCD algorithm (Raymaekers and Rousseeuw, 2023), the weights only depend on the initial estimate of the conditional variance per variable j, and a cell is flagged if

$$\ln(C_{ij}) + \ln(2\pi) + (x_{ij} - \hat{x}_{ij})^2 / C_{ij} > q_j,$$

where $\hat{x}_{ij}$ and C_{ij} are conditional mean and variance of x_{ij} given the current estimates and observed cells for observation i. The penalty weight q_j is chosen as $q_j = \chi^2_{1,0.99} + \ln(2\pi) + \ln(C_{ij})$ such that cells are flagged if the standardized residuals exceed a χ^2-quantile,

$$\frac{(x_{ij} - \hat{x}_{ij})^2}{C_{ij}} > \chi^2_{1,0.99},$$

the 99-th quantile of the chi-square distribution with one degree of freedom.

In the multi-group GMM, the original distributions of the observations are not clear, and we first need an initial estimate to which distribution each observation belongs to. Given initial estimates $\hat{\boldsymbol{\pi}}^0, \hat{\boldsymbol{\mu}}^0$ and $\hat{\boldsymbol{\Sigma}}^0$, we can calculate the probabilities $\hat{t}^0_{g,i,k}$ according to Equation (8) and use a weighted penalty parameter for each observation,

$$q_{g,ij} = \chi^2_{1,0.99} + \ln(2\pi) + \sum_{k=1}^{N} \hat{t}^0_{g,i,k} \ln(C^0_{k,j}),$$

where $C^0_{k,j} = \frac{1}{(\hat{\boldsymbol{\Sigma}}^0_{reg,k})^{-1}_{jj}}$.

4 Robustness properties

In this section, we introduce an extension of the additive breakdown point for cluster and finite mixture model settings to the cellwise paradigm. As common in these settings, the breakdown point is data dependent and in unfavorable constellations, a robust estimator can break down if even one point is added. Thus, often an idealized setting of well clustered data points is considered, introduced

Algorithm 1 Multi-group GMM

Require: $\boldsymbol{X}_1, \boldsymbol{X}_2, \ldots, \boldsymbol{X}_N$; initial estimates $\hat{\boldsymbol{\Sigma}}_{reg}^0$, $\hat{\boldsymbol{\mu}}^0$, $\hat{\boldsymbol{\pi}}^0$, $\hat{\boldsymbol{W}}^0$; hyperparameters $q_{g,ij}$, $\boldsymbol{T}_k$, ρ_k, ϵ_{conv}, h_g, α

$\boldsymbol{W} \leftarrow \hat{\boldsymbol{W}}^0$
$(\boldsymbol{\Sigma}_{reg}, \boldsymbol{\mu}, \boldsymbol{\pi}) \leftarrow (\hat{\boldsymbol{\Sigma}}_{reg}^0, \hat{\boldsymbol{\mu}}^0, \hat{\boldsymbol{\pi}}^0)$
$\texttt{crit} \leftarrow \infty$
while $\texttt{crit} > \epsilon_{conv}$ **do**
  $\boldsymbol{\Sigma}_{reg}^{prev} \leftarrow \boldsymbol{\Sigma}_{reg}$
  $\boldsymbol{W} \leftarrow \texttt{wstep}(\boldsymbol{X}, \boldsymbol{\Sigma}_{reg}, \boldsymbol{\mu}, \boldsymbol{\pi}, \boldsymbol{W}, q_{g,ij}, h_g)$
  $(\boldsymbol{\Sigma}_{reg}, \boldsymbol{\mu}, \boldsymbol{\pi}) \leftarrow \texttt{emstep}(\boldsymbol{X}, \boldsymbol{\Sigma}_{reg}, \boldsymbol{\mu}, \boldsymbol{\pi}, \boldsymbol{W}, \boldsymbol{T}, \rho, \alpha)$
  $\texttt{crit} \leftarrow \max_{k,j,j'} |\Sigma_{reg,k,jj'}^{prev} - \Sigma_{reg,k,jj'}|$
end while
return $\boldsymbol{\Sigma}_{reg}, \boldsymbol{\mu}, \boldsymbol{\pi}, \boldsymbol{W}$

by Hennig (2004) for univariate and extended by Cuesta-Albertos et al. (2008) to multivariate data in the rowwise paradigm (described in Appendix B.1). In this section we transfer the idealized setting from the rowwise outlier paradigm to the notion of cellwise outliers (see Section 4.1) as well as to the complex grouped structure of the targeted data sets (see Section 4.2) and prove the corresponding breakdown point of the proposed estimator.

4.1 Cellwise breakdown in an idealized scenario

Compared to the well-known rowwise outliers, where an outlier is considered to be a whole observation, in the cellwise outlier paradigm introduced by Alqallaf et al. (2009), outliers are considered to be only single cells of observations. For the corresponding cellwise replacement breakdown point, only single cells are replaced by arbitrary values. The maximal fraction of contaminated cells per variable without breakdown of the estimator is then its breakdown point (Raymaekers and Rousseeuw, 2023).

When considering cellwise outlyingness in a mixture model setting, the scenario of well-clustered data used for the assessment of the breakdown behavior in the rowwise paradigm is not sufficiently separating the clusters when it comes to cellwise outlyingness. In the cellwise contamination scheme, the removal of a subset of variables could still lead to cluster overlap (see Figure 1a) and thus, the ideal scenario should be adapted to cluster separation in all subsets (see Figure 1b). Note that a separation in all variable subsets is equivalent to a separation in each variable.

To formalize well-separated clusters in the cellwise paradigm, a sequence of clusters $(\mathcal{X}_m)_{m\in\mathbb{N}}$ is considered ideal when the distances of observations within clusters are bounded by a constant $b < \infty$ and observations from different clusters are increasingly far away. Formally, let $s \geq 2$ be the number of clusters, and $\tilde{n}_1 < \tilde{n}_2 < \ldots < \tilde{n}_s = \tilde{n} \in \mathbb{N}$. For each m-th part of the sequence, the

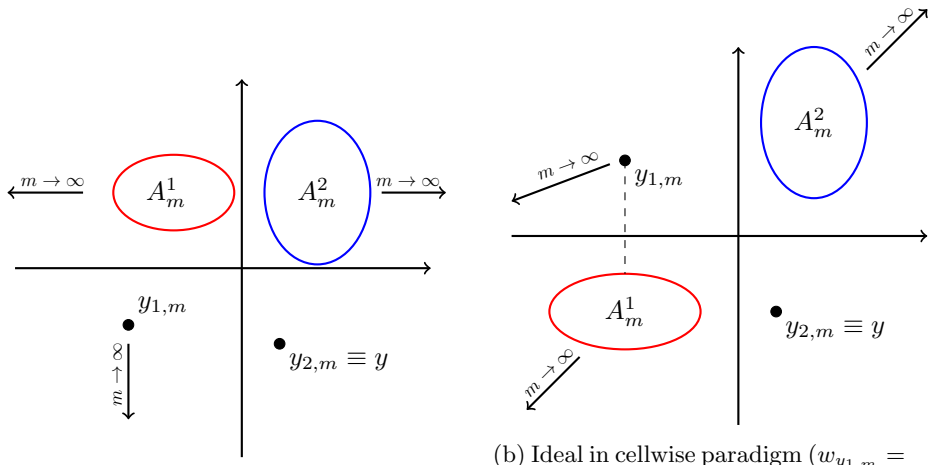

(a) Not ideal in cellwise paradigm. Clusters A_m^1, A_m^2 and $y_{2,m}$ not separated vertically, $y_{1,m}$ and $y_{2,m}$ not separated horizontally.

(b) Ideal in cellwise paradigm ($w_{y_{1,m}} = (1,0)$, $w_{y_{2,m}} = \mathbf{0}$, $y_{1,m} \in B_m^1$, $y_{2,m}$ in any B_m^l). The dashed line for $y_{2,m}$ indicates bounded horizontal but increasing vertical distance.

Figure 1: Horizontally overlapping clusters in Figure a) and ideally separated clusters in the cellwise outlier paradigm in Figure b).

data $\mathcal{X}_m$ are clustered into s clusters $A_m^1, \ldots, A_m^s$ such that

$$A_m^1 = \{\boldsymbol{x}_{1,m}, \ldots, \boldsymbol{x}_{\tilde{n}_1,m}\}, \ldots, A_m^s = \{\boldsymbol{x}_{\tilde{n}_{s-1}+1,m}, \ldots, \boldsymbol{x}_{\tilde{n}_s,m}\}$$

and $\mathcal{X}_m = \bigcup_{l=1}^s A_m^l$ and $\boldsymbol{x}_{i,m} = (x_{i1,m}, \ldots, x_{ip,m})$ for $i = 1, \ldots, \tilde{n}, m \in \mathbb{N}$.

Thus, to ensure that clusters are well separated in each variable, we enforce

$$\lim_{m\to\infty} \min\{|x_{i'j,m} - x_{ij,m}| : \boldsymbol{x}_{i',m} \in A_m^l, \boldsymbol{x}_{i,m} \in A_m^h, h \neq l, j = 1, \ldots, p\} = \infty. \tag{11}$$

Additionally, well-clustered also means that data points of each cluster are close to each other. Thus, a bounded distance within clusters in all variables separately is assumed,

$$\max_{1\leq l\leq s} \max\{|x_{i'j,m} - x_{ij,m}| : \boldsymbol{x}_{i',m}, \boldsymbol{x}_{i,m} \in A_m^l, j = 1, \ldots, p\} < b \quad \forall m \in \mathbb{N}. \tag{12}$$

Note, that Equation (12) is equivalent to the corresponding assumption in the rowwise setting stated in Equation (19).

We now consider added cellwise outliers, $\mathcal{Y}_m = \{\boldsymbol{y}_{1,m}, \ldots, \boldsymbol{y}_{\tilde{r},m}\}$, such that $0 \leq \tilde{r}_1 \leq \ldots \leq \tilde{r}_s = \tilde{r}$ and

$$B_m^1 = \{\boldsymbol{y}_{1,m}, \ldots, \boldsymbol{y}_{\tilde{r}_1,m}\}, \ldots, B_m^s = \{\boldsymbol{y}_{\tilde{r}_{s-1}+1,m}, \ldots, \boldsymbol{y}_{\tilde{r}_s,m}\}.$$

For each added observation $\boldsymbol{y}_{i,m}$, there exists a $\boldsymbol{w}(\boldsymbol{y}_{i,m}) \in \{0,1\}^p$ indicating the outlying cells by $w(\boldsymbol{y}_{i,m})_j = 0$ and non-outlying cells by $w(\boldsymbol{y}_{i,m})_j = 1$. The non-outlying part of cellwise outliers should originate from one of the constructed clusters,

$$\max_{1\leq l\leq s} \max\{|y_{i'j,m} - x_{ij,m}| : \boldsymbol{x}_{i,m} \in A_m^l, \boldsymbol{y}_{i',m} \in B_m^l, \\ j = 1,\ldots,p \text{ with } w(\boldsymbol{y}_{i',m})_j = 1\} < b \quad \forall m \in \mathbb{N},$$

and outlying cells should be infinitely far away from all other outlying cells and clusters,

$$\lim_{m\to\infty} \min\{|y_{i'j,m} - x_{ij,m}| : \boldsymbol{x}_{i,m} \in \mathcal{X}_m, \boldsymbol{y}_{i',m} \in \mathcal{Y}_m, w(\boldsymbol{y}_{i',m})_j = 0\} = \infty, \quad (13)$$

$$\lim_{m\to\infty} \min\{|y_{i'j,m} - y_{ij,m}| : \boldsymbol{y}_{i',m}, \boldsymbol{y}_{i,m} \in \mathcal{Y}_m, i \neq i', w(\boldsymbol{y}_{i',m})_j = 0\} = \infty. \quad (14)$$

The breakdown of an estimator $\hat{E}$ of location, covariance or cluster weight is defined equivalently to the rowwise setting. Thus, the breakdown of an estimator is relatively defined by estimates based on $\mathcal{X}_m$ and on $\mathcal{X}_m \cup \mathcal{Y}_m$ and the location breakdown for a cluster l occurs, if for all $h = 1,\ldots,N$

$$||\hat{\boldsymbol{\mu}}_l(\mathcal{X}_m) - \hat{\boldsymbol{\mu}}_h(\mathcal{X}_m \cup \mathcal{Y}_m)||_2 \to \infty, \quad (15)$$

where $||\cdot||_2$ denotes the Euclidean norm. Denoting the smallest and largest eigenvalue of a covariance matrix with λ_p and λ_1, respectively, a covariance estimator of a cluster l would implode (explode) if $\lambda_p(\hat{\boldsymbol{\Sigma}}_l(\mathcal{X}_m)) \to 0$ ($\lambda_1(\hat{\boldsymbol{\Sigma}}_l(\mathcal{X}_m)) \to \infty$) and $\lambda_p(\hat{\boldsymbol{\Sigma}}_l(\mathcal{X}_m \cup \mathcal{Y}_m)) \nrightarrow 0$ ($\lambda_1(\hat{\boldsymbol{\Sigma}}_l(\mathcal{X}_m \cup \mathcal{Y}_m)) \nrightarrow \infty$) or vice versa. The weight estimator $\hat{\pi}_l$ of a cluster l breaks down if $\hat{\pi}_l \in \{0,1\}$.

The cellwise additive breakdown point is then defined as

$$\epsilon^*(\hat{E}) = \min\left\{\frac{\max_{j=1,\ldots,p}\sum_{i=1}^{\tilde{r}}(1 - w(\boldsymbol{y}_{i,m})_j)}{\tilde{n} + \tilde{r}} : \hat{E} \text{ breaks down}\right\},$$

where $\sum_{i=1}^{\tilde{r}}(1 - w(\boldsymbol{y}_{i,m})_j)$ denotes the number of contaminated cells per column j.

4.2 Cellwise breakdown for multi-group data

For analyzing the breakdown point in an ideal setting for a multi-group mixture model as described in Section 2.1, we assume N many underlying clusters and outliers constructed to be cellwise, separated as described in Section 4.1. All observations $\mathcal{X}_m \cup \mathcal{Y}_m$, contaminated or not, are partitioned into groups $\boldsymbol{Z}_m^1,\ldots,\boldsymbol{Z}_m^N$ of size $n_1 + r_1,\ldots,n_N + r_N$ (where n_g is the number of clean and r_g is the number of added observations of group g) by a function $\tilde{g} : \mathcal{X}_m \bigcup \mathcal{Y}_m \to \{1,\ldots,N\}$, thus $\mathcal{Z}_m = \bigcup_{g=1}^N \boldsymbol{Z}_m^g = \mathcal{X}_m \bigcup \mathcal{Y}_m$. Moreover, we

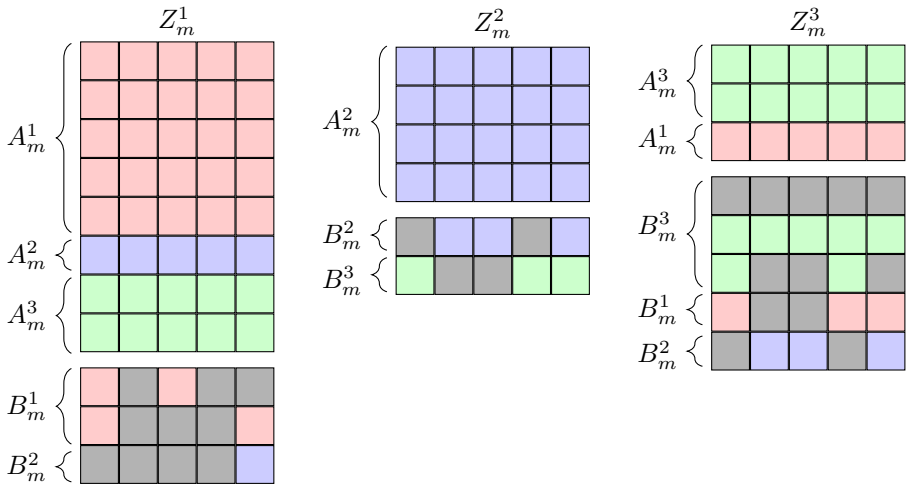

Figure 2: Possible group structure of groups for $N = 3$. Each column block corresponds to a group and each row within a column block to an observation. Red, violet and green rows are indicating from which cluster the observation originates from, gray indicates outlying cells. The gray line in the third block is assigned to B_m^3, but could stem from any other cluster too.

assume that for each group g a certain fraction $\tilde{\alpha}_g$ of its n_g observations and r_g added outliers are from cluster g,

$$\frac{|\{\boldsymbol{x} : \boldsymbol{x} \in A_m^g, \tilde{g}(\boldsymbol{x}) = g\}|}{n_g} \geq \tilde{\alpha}_g, \quad \frac{|\{\boldsymbol{y} : \boldsymbol{y} \in B_m^g, \tilde{g}(\boldsymbol{y}) = g\}|}{r_g} \geq \tilde{\alpha}_g, \tag{16}$$

thus, reflecting the major distribution per group. An illustration of the groups and the cluster origins per observation for a fictitious ideal data set is shown in Figure 2, where each row corresponds to an observation, each column block corresponds to a group and each column per group to a variable. The first (row) block per group includes the clean data, and the second block the added, possibly contaminated data. The color indicates the ideal cluster each observation is originating from (red, green, violet) for clean cells or whether a cell is outlying (grey). For each group the majority of observations comes from the main cluster for clean and for contaminated observations, respectively. Cellwise contamination can affect single cells (group 2), all cells of single variables (group 1, variable 2 and 4) and/or whole observations (group 3, first contaminated row).

For the ideal scenario we assume that at least $\left\lceil \frac{n_g+r_g+1}{2} \right\rceil$ observations from group g are from cluster g and thus, $\tilde{\alpha}_g$ is restricted to fulfill $(n_g + r_g)\tilde{\alpha}_g \geq \left\lceil \frac{n_g+r_g+1}{2} \right\rceil$ for all $g = 1, \ldots, N$. Note, for the proposed estimation this implies that for any variable j and group g there always exists at least one observation in $\boldsymbol{Z}_m^g$ originating from cluster g which is observed for variable j.

Cellwise breakdown is defined equivalently to the ungrouped setting and the breakdown point is defined as the minimal fraction of outlying cells for at least one variable in at least one group necessary to break down one estimator $\hat{E}$,

$$\epsilon^*_{group}(\hat{E}) = \min_{g=1,\dots,N} \min \left\{ \frac{\max_{j=1,\dots,p} \sum_{\boldsymbol{y} \in \boldsymbol{Z}^g_m \cap \mathcal{Y}_m} (1 - w(\boldsymbol{y})_j)}{n_g + r_g} : \hat{E} \text{ breaks down} \right\}.$$

Corollary 1. *Given the ideal setting and fixed $\rho_k > 0, \boldsymbol{T}_k > 0$ (positive definite), the following statements hold.*

a. *For all m and no contamination, $\mathcal{Z}_m = \mathcal{X}_m$, there exist feasible estimates $\hat{\boldsymbol{\pi}}$, $\hat{\boldsymbol{\mu}}$, $\hat{\boldsymbol{\Sigma}}$ such that the objective function is finite for any feasible set of $\boldsymbol{W}$ in Equation (5). Thus, the value of the objective function for a minimizer of Equation (3) under the constraints (4) to (7) is bounded.*

b. *Given the contaminated data $\mathcal{Z}_m$ and sets of estimates $\hat{\boldsymbol{\pi}}(\mathcal{Z}_m)$, $\hat{\boldsymbol{\mu}}(\mathcal{Z}_m)$, $\hat{\boldsymbol{\Sigma}}(\mathcal{Z}_m)$, $\hat{\boldsymbol{W}}(\mathcal{Z}_m)$ for $m \in \mathbb{N}$. If there exists an l such that $\lambda_1(\hat{\boldsymbol{\Sigma}}_{reg,l}(\mathcal{Z}_m)) \to \infty$ for $m \to \infty$, then the value of the objective function of the estimates goes to infinity.*

c. *Given the contaminated data $\mathcal{Z}_m$ and sets of estimates $\hat{\boldsymbol{\pi}}(\mathcal{Z}_m)$, $\hat{\boldsymbol{\mu}}(\mathcal{Z}_m)$, $\hat{\boldsymbol{\Sigma}}(\mathcal{Z}_m)$, $\hat{\boldsymbol{W}}(\mathcal{Z}_m)$ for $m \in \mathbb{N}$. If there exists a variable j^*, l, k and a constant $\tilde{b}$ such that $|\hat{\mu}_{k,j^*}(\mathcal{Z}_m) - \hat{\mu}_{l,j^*}(\mathcal{Z}_m)| < \tilde{b}$ for $l \neq k$, then the objective function of these estimates goes to infinity.*

The proof leverages the ideal scenario and subsequent intuition about reasonable estimates to bound the objective function in the uncontaminated case and to further show that an observation cannot "escape" from one cluster to another if it is originating from an exploding cluster since clusters move apart from each other. It is given in Appendix B.2.

Theorem 2 (Breakdown point)**.** *For the ideal scenario and fixed $\rho_k, \boldsymbol{T}_k > 0$ the following breakdown results in the cellwise paradigm hold.*

a. *The implosion breakdown point is* 1.

b. *The weight breakdown point is* 1.

c. *The explosion breakdown point is at least* $\min_g\{(n_g - h_g + 1)/n_g\}$.

d. *The location breakdown point is 0.*

e. *The explosion breakdown point is exactly* $\min_g\{(n_g - h_g + 1)/n_g\}$, *when assuming that the location estimator is not broken down.*

The proof leverages the strong cellwise separation between the clusters and the results of Corollary 1 and is given in Appendix B.3.

5 Simulations

In order to test the proposed method, we focus on five main scenarios: 1) a basic setting with $N = 2$ balanced groups, 2) a balanced setting with $N = 5$ groups, 3) an unbalanced two-group setting, 4) a balanced two-group setting with increasing singularity issues, and 5) a high-dimensional balanced two-group setting. Setting 1) and 2) are described in detail in the main text; for the remaining settings and further detailed evaluations we refer to Appendix D.

In Section 5.1 the generation of clean and contaminated data for two covariance structures is described in detail. Competing methods and evaluation criteria are summarized in Section 5.2 and 5.3, respectively, and corresponding results are shown in Section 5.4.

5.1 Data generation

Clean data are generated according to the underlying multi-group Gaussian mixture model, formulated in Equation (1), for given dimensions $p \in \{10, 20, 60\}$. For $N \in \{2, 5\}$ groups we vary the mixture between the groups indicated by the parameter $\pi_{diag} \in \{0.75, 0.9\}$. The mixture probabilities are then given by $\pi_{gg} = \pi_{diag}$ and $\pi_{g,k} = \frac{1-\pi_{diag}}{N-1}$ for $g, k = 1, \ldots, N, g \neq k$.

We differentiate between two different covariance structures applied to all covariances in the mixture distributions. The first type is of Toeplitz structure (similar to Raymaekers and Rousseeuw, 2023) and each covariance $\boldsymbol{\Sigma}_k \in \mathbb{R}^{p \times p}$ is constructed by $\boldsymbol{\Sigma}_{k,ij} = \zeta_k^{|i-j|}$ where ζ_k is randomly drawn from a uniform distribution in $[0.5, 1]$. Toeplitz covariances share the relationships between variables but to a different extent. The second type is based on the approach of Agostinelli et al. (2015) (ALYZ) to construct well-conditioned correlation matrices. We allow for more variation of the variances and stop the iterative procedure early, specifically when the trace of a covariance is bounded by $[p/2, 2p]$. Compared to the Toeplitz structure, here the correlation between the variables can vary more strongly between the groups, making it more difficult for local methods to account for outliers.

Two types of scenarios are discussed for the mean of the distributions. On the one hand, we consider a scenario where there are just differences in the covariance, thus setting all means to zero, $\boldsymbol{\mu}_k = \mathbf{0}$. On the other hand, the more realistic scenario with different means is considered, by applying the concept of c-separation (Dasgupta, 1999) that gives a notion of how strongly the distributions overlap. We assume significant overlap (0.5-separated clusters) due to an underlying smooth variable and construct the means inductively, starting with $\boldsymbol{\mu}_1 = \mathbf{0}_p$. Given $\boldsymbol{\mu}_1, \ldots, \boldsymbol{\mu}_{k-1}$ a new vector $\boldsymbol{\mu}_{tmp}$ is drawn from $\mathcal{N}(\mathbf{0}_p, \boldsymbol{I}_p)$. To ensure a certain level of separation and overlap we set the next distributional mean to $\boldsymbol{\mu}_k = t^*(\boldsymbol{\mu}_{tmp} - \frac{1}{k-1}\sum_{l=1}^{k-1} \boldsymbol{\mu}_l) + \frac{1}{k-1}\sum_{l=1}^{k-1} \boldsymbol{\mu}_l$, where t^* fulfills

$$||\boldsymbol{\mu}_l - \boldsymbol{\mu}_k||_2 \geq 0.5\sqrt{p \max(\lambda_1(\boldsymbol{\Sigma}_l), \lambda_1(\boldsymbol{\Sigma}_k))}$$

for all $l = 1, \ldots, k-1$, with equality for at least one l. Each group g consists

of $n_g \in \{30, 40, 50, 100\}$ many clean observations drawn with probability $\pi_{g,k}$ from $\mathcal{N}(\boldsymbol{\mu}_k, \boldsymbol{\Sigma}_k)$.

For each group a percentage $\epsilon_{cell} = 10\%$ of random cells per variable is contaminated as in Raymaekers and Rousseeuw (2023). Given an observation from group g which is drawn from distribution k and where a subset of variables indexed with $\mathcal{J}$ should be contaminated, cells indexed by $\mathcal{J}$ are replaced with

$$\boldsymbol{\mu}_{k,\mathcal{J}} + \boldsymbol{v}_{k,\mathcal{J}} \frac{\gamma_{cell}\sqrt{|\mathcal{J}|}}{\sqrt{\boldsymbol{v}'_{k,\mathcal{J}} \boldsymbol{\Sigma}^{-1}_{k,\mathcal{J}} \boldsymbol{v}_{k,\mathcal{J}}}}.$$

Here, $\mathcal{J}$ as subscript denotes the part of the vectors/matrices corresponding to the indexed variables, and $\boldsymbol{v}_{k,\mathcal{J}}$ denotes the eigenvector with the smallest eigenvalue of $\boldsymbol{\Sigma}_{k,\mathcal{J}}$. The parameter $\gamma_{cell} \in \{2, 6, 10\}$ controls the strength of the outlyingness of contaminated cells with respect to $\boldsymbol{\mu}_k$. For $\gamma_{cell} = 2$ the cellwise outliers are hard to distinguish from regular cells, while $\gamma_{cell} = 10$ produces clear outliers which are easier to detect for robust methods, and very influential to non-robust procedures.

5.2 Competing methods

Regarding the performance comparison of our proposed method, we include the following seven methods in our simulation study, starting with their acronyms.

cellgGMM: The proposed cellwise robust multi-group GMM.

sample: The sample covariance applied to each group separately as a non-robust alternative.

mclust: A non-robust basic finite GMM implemented via an EM-algorithm in the R-Package `mclust` (Fraley et al., 2024) applied globally, with the correct number of groups provided. Since there is no clear attribution of an estimated cluster to a group, mclust will only be calculated for two-group settings and clusters will be assigned to groups in the most favorable way[1].

MRCD (Boudt et al., 2020): Rowwise robust covariance estimator applicable to high dimensions and applied separately to each group. It is available in the R-package `rrcov` (Todorov, 2024).

ssMRCD (Puchhammer and Filzmoser, 2024): An estimator targeted towards a multi-group setting robust against rowwise contamination available in the R-package `ssMRCD` (Puchhammer, 2023). It is calculated with the default values for smoothing and equal weights for all groups, and the unsmoothed covariance estimates are assumed to correspond to the covariance matrices of the mixture distribution.

[1]The assignment of groups and clusters is such that it minimizes the evaluation measure of the KL-divergence. Thus, it is possible that the performance of estimating locations might suffer for the considered performance criteria.

cellMCD (Raymaekers and Rousseeuw, 2023): A cellwise robust method for covariance and location available in the R-package `cellWise`(Raymaekers et al., 2023).

OC (Öllerer and Croux, 2015): The cellwise robust covariance estimator is applied separately to each group. The OC-estimator does not provide a location estimate but it can calculate a covariance matrix in high-dimensional settings. A fast implementation is available in the R-package Filzmoser et al. (2009).

5.3 Evaluation criteria

The performance of covariance estimation is compared across all methods, where possible. Given an estimated covariance $\hat{\boldsymbol{\Sigma}}_k$, the Kullback-Leibler divergence to the real covariance $\boldsymbol{\Sigma}_k$ is used as evaluation criterion,

$$KL(\hat{\boldsymbol{\Sigma}}_k, \boldsymbol{\Sigma}_k) = \mathrm{tr}(\hat{\boldsymbol{\Sigma}}_k \boldsymbol{\Sigma}_k^{-1}) - p - \log\det(\hat{\boldsymbol{\Sigma}}_k \boldsymbol{\Sigma}_k^{-1}).$$

For $N \geq 2$, the final performance metric is the average over all distributions, $KL = \frac{1}{N}\sum_{k=1}^{N} KL(\hat{\boldsymbol{\Sigma}}_k, \boldsymbol{\Sigma}_k)$.

The mean estimates $\hat{\boldsymbol{\mu}}_k$ and the mixture probabilities $\hat{\boldsymbol{\pi}}$ are evaluated by the Mean Squared Error (MSE)

$$MSE(\hat{\boldsymbol{\mu}}_k, \boldsymbol{\mu}_k) = \frac{1}{p}\sum_{j=1}^{p}(\mu_{kj} - \hat{\mu}_{kj})^2,$$

$$MSE(\hat{\boldsymbol{\pi}}, \boldsymbol{\pi}) = \frac{1}{N^2}\sum_{g=1}^{N}\sum_{k=1}^{N}(\pi_{g,k} - \hat{\pi}_{g,k})^2$$

and averaged over the groups for the mean, $MSE(\mu) = \frac{1}{N}\sum_{k=1}^{N} MSE(\hat{\boldsymbol{\mu}}_k, \boldsymbol{\mu}_k)$.

Additionally, the correctness of flagged cellwise outliers is measured by the standard recall, precision and F1-score and compared only to the cellMCD, since this is the only other method providing flagged cells.

5.4 Results

As introduced at the beginning of Section 5, we focus on two out of the five different settings in the main text, and additional figures regarding the MSE for location and mixture probabilities as well as outlier detection performance are included in Appendix D. Each combination is repeated 100 times. Note that cellMCD cannot be calculated if too many marginal outliers are present, in which case the failed runs are removed for all methods reducing the number of repetitions shown in the plots (see Appendix D for corresponding tables stating the number of effective runs).

We start with the basic balanced setting where we consider $p = 10$ variables, $N = 2$ groups and $n_1 = n_2 = 100$ observations per group. Figure 3 and 4

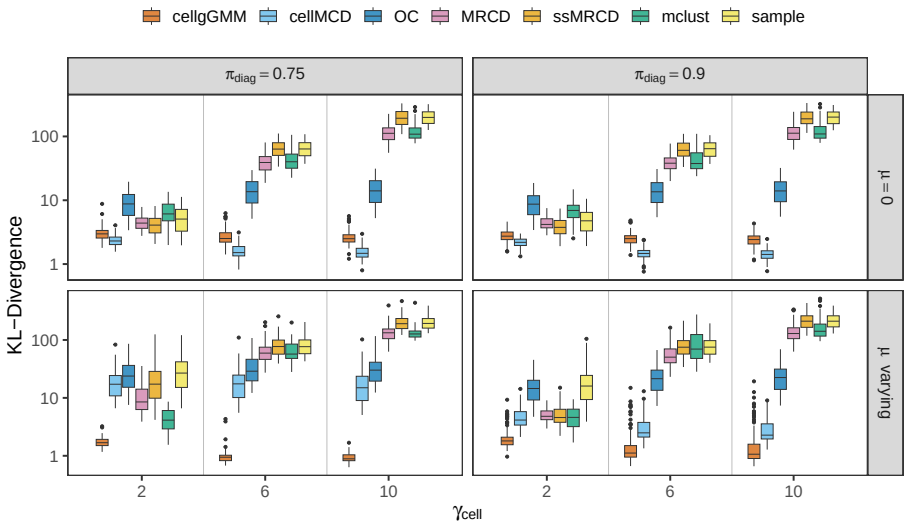

Figure 3: KL-divergence for the basic balanced setting and Toeplitz covariance structure for varying strength γ of outlyingness.

show the KL-divergence for covariance estimation across all seven competing methods and a varying strength of outlyingness γ_{cell} for the Toeplitz and ALYZ covariance structure, respectively. The four subpanels differ regarding the coherency in the predefined groups. For example, observations of one group are very coherent for $\pi_{diag} = 0.9$ and $\mu = 0$ (top right panel) or less coherent for $\pi_{diag} = 0.75$ and varying μ. For both covariance structures and among all four coherency types it is visible that only the cellwise robust methods can manage outlying cells as γ_{cell} increases. Our proposed method cellgGMM and cellMCD are the most reliable while OC local is somehow robust against an increase in the degree of outlyingness of cells. However, OC local starts already with suboptimal estimates for $\gamma_{cell} = 2$. At the bottom panels it is evident that differences in location, even for strong overlapping distributions like here, is sufficient to drastically decrease performance for all competitor methods regarding covariance estimation. Especially for the cellMCD, non-coherency in the mean and covariance structures (ALYZ structure) confuse the algorithm in detecting cells and precision deteriorates (see also Figure 13 and 15 in the appendix) while for the proposed cellgGMM it facilitates the correct clustering (see also Figure 12 and 14).

In the setting with an extended number of $N = 5$ groups, $p = 10$ variables and $n_1 = \ldots = n_5 = 100$ observations per group, we see similar and even more prominent patterns. In Figure 5, the KL-divergence for the ALYZ covariance structure[2] is shown. Again, methods that are not robust against cellwise outliers

[2]Due to the difficulties of the cellMCD based on the amount of marginal outliers, some

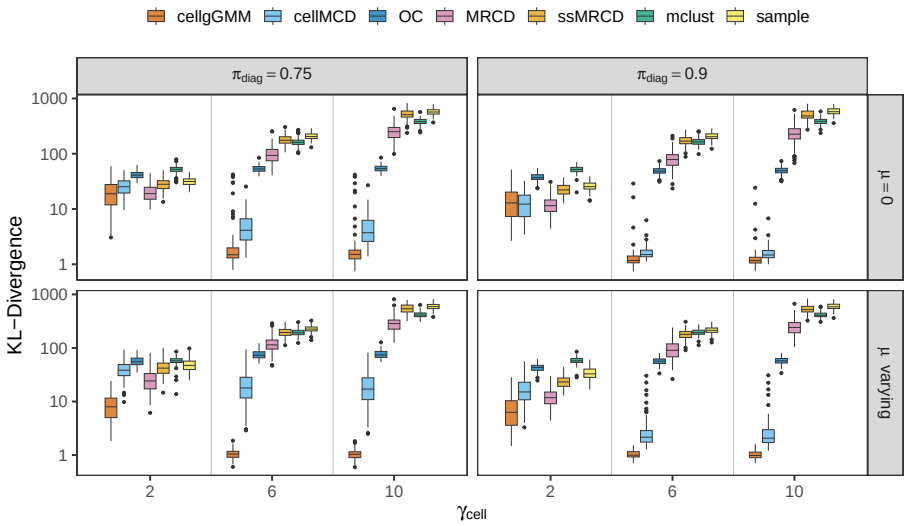

Figure 4: KL-divergence for the basic balanced setting and ALYZ covariance structure for varying strength γ of outlyingness.

suffer increasingly with the degree of outlyingness when it comes to covariance estimation. While for varying μ, the findings are the same as in the basic setting, we see that here cellgGMM performs better than cellMCD even in the most coherent setting (top right panel). Thus, the more groups are available to our proposed method, the better it can leverage the given context.

With respect to the other three settings, the findings are similarly good for the proposed cellgGMM. The results of the competing methods in the unbalanced setting with $N = 2, p = 10, n_1 = 100$ and $n_2 = 50$ are comparable to the balanced settings described above. When increasing the p-to-n-ratio ($N = 2$, $p = 20$, $n_1 = n_2 = 30$), we see that cellMCD struggles a lot with flagging cellwise outliers due to low precision and subsequently with covariance estimation, often delivering worse covariance estimates than the OC local method. In the high dimensional scenario ($N = 2$, $p = 60$, $n_1 = n_2 = 40$) the results depend on the covariance structure. For the Toeplitz structure, OC local performs comparably well, while for ALYZ-structured covariances, cellgGMM generally outperforms OC local more clearly.

In general, cellgGMM consistently performs well in all five settings considered and in multiple coherency constellations. While it is often comparable to cellMCD when $\mu = 0$, in real multi-group settings this is a rare exception and one has to consider real life data to be closer to settings where locations vary over groups. In these simulation scenarios, cellgGMM outperforms all other

parameter combinations for the Toeplitz-structured covariances lead to a very low number of repetitions (down to 16). Thus, corresponding results are stated in the appendix and should be treated with caution.

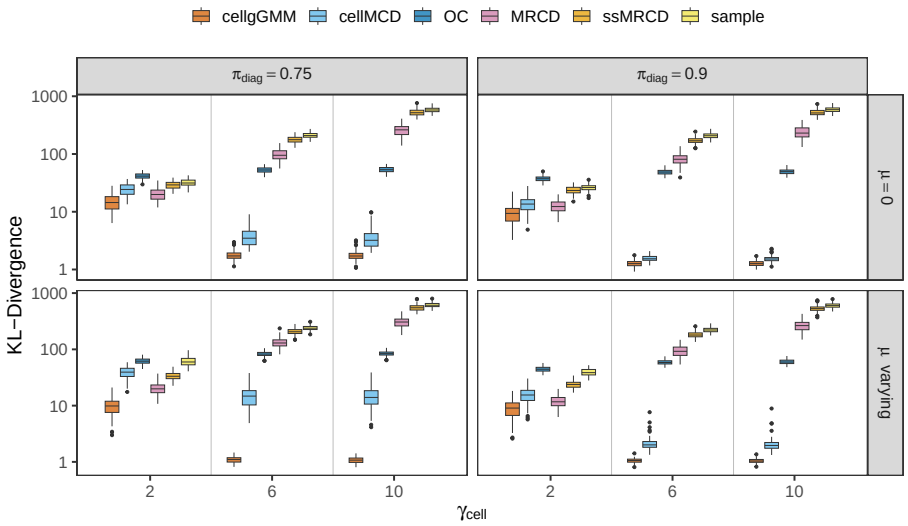

Figure 5: KL-divergence for the balanced setting with five groups and ALYZ covariance structure for varying strength γ of outlyingness.

considered methods.

6 Applications

We illustrate possible application scenarios of the proposed method by data from the fields meteorology, medicine and oenology. Weather measurements of Austrian weather stations are analyzed in Section 6.1, and in Section 6.2 we investigate handwriting data of healthy and Alzheimer patients. In the third application in Section 6.3 we analyze patterns of high to low rated wine samples.

6.1 Austrian weather data

We illustrate our method on data provided by GeoSphere Austria (2022), with $p = 6$ monthly measured weather variables at 183 Austrian weather stations, including air pressure (p) and temperature (t), amount of rain (rsum), relative humidity (rel), hours of sunshine (s) and wind velocity (vv), which are averaged over the year 2021. The data set is publicly available in the R-Package `ssMRCD` (Puchhammer, 2023) under the name `weatherAUT2021` on CRAN. Figure 6 shows the spatial locations and the underlying diverse geographical and thus also meteorological structure caused by the Alps. We proposed a separation of the stations into $N = 5$ more coherent groups, visible by the dashed lines in the figure. The most western area (group 1, $n_1 = 31$) is characterized by very mountainous terrain, which extends to the east into the next area (group 2,

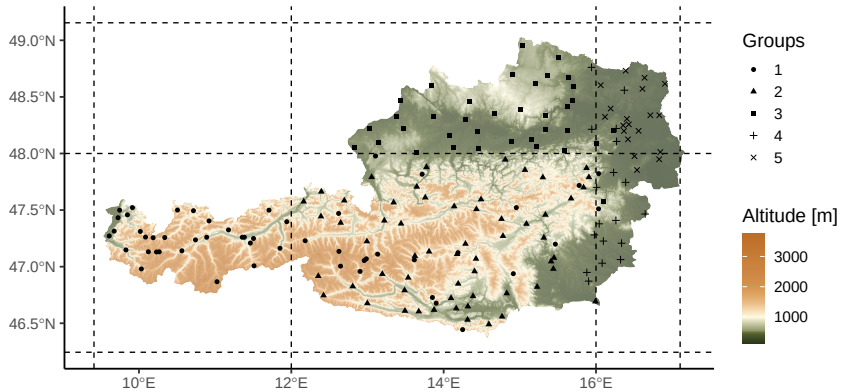

Figure 6: Altitude map of Austria with spatial locations of weather stations indicated by black symbols and separation into groups indicated by dashed grid lines. Shapes are based on the maximal class probability of the corresponding observation.

$n_2 = 80$), where high and low mountains are present. The most northern part (group 3, $n_3 = 35$) consists of low mountains and hills along the Danube river which flows through Vienna and the Vienna Basin (group 5, $n_5 = 21$). The last area to the East (group 4, $n_4 = 16$) hosts some hills but is mainly flat.

Our goal is to identify weather stations with cellwise outliers given the spatial context and to further analyze why these stations are atypical. Moreover, we are also interested in the coherency of the pre-defined groups. To this end, we apply our method with default values $h_g = 0.75n_g$, allowing for up to 25% of flagged cells per variable, and $\alpha = 0.5$, indicating a strong flexibility of observations to switch between the five groups. The highest class probabilities $\max_k \hat{t}_{g,i,k}$ per observations are shown in Figure 6 with different plot symbols.

Observations with at least one flagged cell are shown in Figure 7. The top panel shows the estimated class probabilities $\hat{t}_{g,i,k}$ by the color of the tiles, while the membership to one of the original groups is marked by a dot. In the bottom panel, outlying cells are colored according to their standardized residuals $r_{g,ij}$ (Raymaekers and Rousseeuw, 2023),

$$r_{g,ij} = \sum_{k=1}^{N} \hat{t}_{g,i,k} \frac{x_{g,ij} - \hat{x}^k_{g,ij}}{\sqrt{\hat{\boldsymbol{\Sigma}}^{(j|j)}_{reg,k} - \hat{\boldsymbol{\Sigma}}^{(j|\hat{\boldsymbol{w}}_{g,i})}_{reg,k} \left(\hat{\boldsymbol{\Sigma}}^{(\hat{\boldsymbol{w}}_{g,i}|\hat{\boldsymbol{w}}_{g,i})}_{reg,k}\right)^{-1} \hat{\boldsymbol{\Sigma}}^{(\hat{\boldsymbol{w}}_{g,i}|j)}_{reg,k}}},$$

where $\hat{x}^k_{g,ij}$ denotes the expected value of $x_{g,ij}$ given that it is from distribution k and using only unflagged cells $\hat{\boldsymbol{w}}_{g,i}$, see also Equation (9). The proposed method can identify if observations are outlying in all groups, indicated by a high number of cellwise outliers (e.g. half of the cells are outlying), or whether

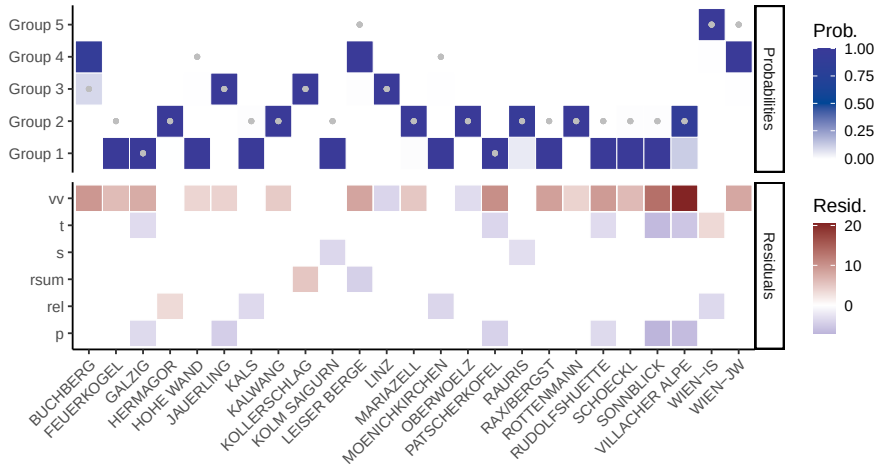

Figure 7: Outlying weather stations with group probabilities $\hat{t}_{g,i,k}$ on the top panel with dots at the original groups and the residuals of each cell on the bottom panel.

they are outlying specifically in their pre-defined group, indicated by a high probability for another group. In the upper panel of Figure 7 showing only observations with outlying cells, this is expressed by non-overlapping dots and dark blue tiles.

Positive values of the residual indicate that the observed value is higher than what would be expected, and negative values refer to observed values which are lower than expected, given the other non-flagged cells. Many outliers are connected to cell outliers in the variable wind velocity, likely due to the diverse exposure of weather stations even in the same area. Moreover, a pattern of unexpected high values in wind velocity and low values in air pressure and temperature is visible for the five weather stations with half of their cells outlying (Villacher Alpe, Sonnblick, Rudolfshütte, Patscherkofel, Galzig) - exactly the five highest weather stations with an altitude of more than 2000 meters.

Figure 8 presents a more detailed analysis of the variables wind velocity and air temperature. The tolerance ellipses, based on the estimated locations and covariance matrices per group, show a smooth transition from groups connected to mountainous landscapes (group 1 and 2) with higher variation in temperature to flatter landscapes (group 3 to 5) with increased variation in wind velocity and generally higher temperature. The only cellwise outlier with unexpectedly high temperature is the weather station Wien-IS, which is located in the city center of the capital Vienna.

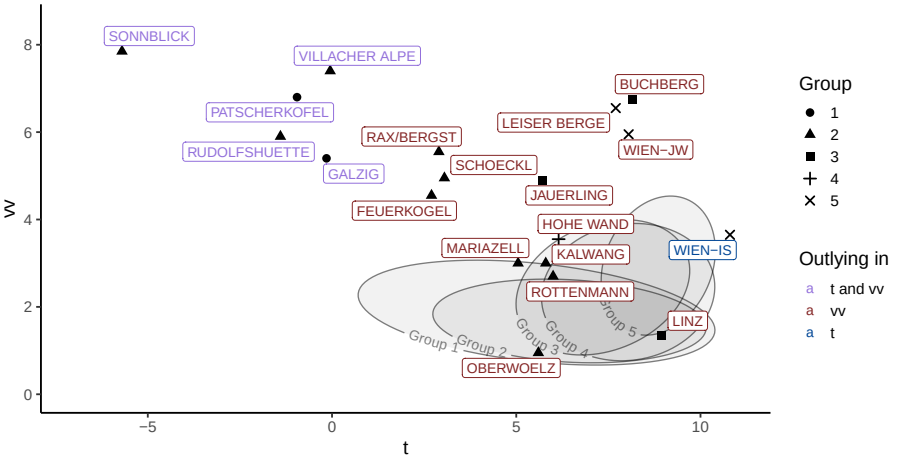

Figure 8: Bivariate feature space of wind velocity (vv) and air temperature (t). The 95% tolerance ellipses are based on the estimated smoothed covariance matrices and locations per group. Stations outlying in at least one of the two variables are shown. Shapes correspond to the original group of each observation, the color of the label indicates which cells are outlying.

6.2 Darwin - Alzheimer disease

Alzheimer disease is a non-curable neuro-degenerative disease which progresses over time, leading to cognitive impairment. To mitigate the negative effects of Alzheimer disease on affected patients and their loved ones, early diagnoses and treatment is essential. In contrast to Cilia et al. (2022) who train a classifier to discriminate between the two groups, we propose to use the developed multi-group GMM methodology as a tool to analyze the gray area between diagnosed Alzheimer patients and subjects considered healthy. While the groups are given by an official diagnosis, some persons can be on the verge to Alzheimer and not yet being diagnosed or at very early stages. Thus, the strict separation into groups might not be beneficial, and a more smoothed approach can help to better analyze the intertwinings between the two groups and identify corresponding influential variables.

The DARWIN (Diagnosis AlzheimeR WIth haNdwriting) data set (Cilia et al., 2022), available in the R-package `robustmatrix` (Mayrhofer et al., 2024), contains handwriting samples from $n_1 = 85$ healthy persons and $n_2 = 89$ patients with diagnosed Alzheimer disease (AD). Each subject was asked to execute 25 different handwriting tasks on a tablet from which 18 summary features where extracted: total time, air time, paper time, mean speed on paper, mean speed in air, mean acceleration on paper, mean acceleration on air, mean jerk on paper, mean jerk in air, mean of pressure, variance of pressure, generalization of the mean relative tremor (GMRT) on paper, GMRT in air, mean GMRT,

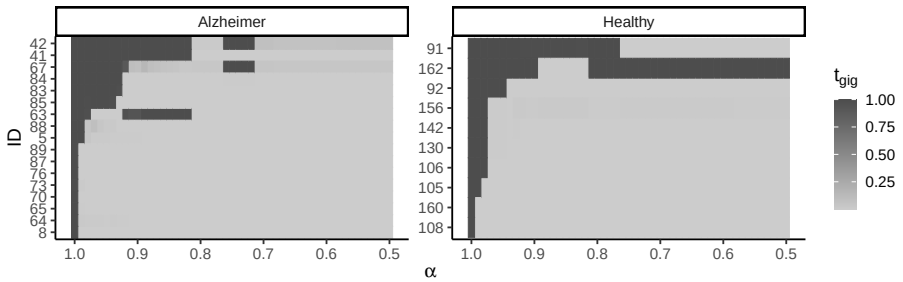

Figure 9: Class probabilities $t_{g,i,g}$ for subjects whose probabilities change based on α sorted by time of switching.

number of pendowns, maximal x-extension, maximal y-extension and dispersion index. For a detailed explanation of the tasks and measured variables we refer to Cilia et al. (2018). Similar to Mayrhofer et al. (2025) we also exclude the variables total time, mean GMRT and air time due to linear dependencies and unreliable measurements. The remaining variables are summarized over the 25 tasks by the median and the median absolute deviation (mad). Thus, we include $p = 30$ variables and the groups are given by the Alzheimer disease status ($N = 2$).

One way to focus on the overlap of the two groups is to vary the parameter $\alpha \in \{1, 0.99, \ldots, 0.51, 0.5\}$ in the calculations. While $\alpha = 1$ forces the observations to belong to the predefined group, decreasing values are less and less strict and enable switching to the other group if the multivariate distribution of that group is more appropriate. Figure 9 presents the class probabilities $\hat{t}_{g,i,g}$ for varying α for subjects whose probability of being in their predefined class $\hat{t}_{g,i,g}$ is lower than 50% for at least one value of α (*switchers*). We can see that a subset of 8 AD diagnosed patients and 2 healthy subjects move to the opposite group as soon as the procedure starts to allow for a switch, i.e. when $\alpha < 1$, indicating strong multivariate similarities to the opposite group.

Figure 10 shows all cells of the data matrix, with the observations split into Alzheimer patients and healthy people. Additionally, within these groups we show the switchers, which are sorted according to increasing values of α, thus in the same order as shown in Figure 9. The cells of the matrix present information about outlyingness of the cells when varying α (no symbol, crosses or dots), and color according to the standard deviation of the residuals over varying α. If a cell is white, it is not outlying for all α. Cells marked by dots are outlying for several or even all values of α. Higher variability of the residuals can occur for different reasons: (a) the person switches to the other group, (b) the cell is identified as an outlier for particular values of α, or both (a) and (b) occur. Case (a) mainly appears for the switching persons. For example, the variable `pressure_mean` (both median and mad) which shows many cells with increased residual variability. Several of those cells are outliers as soon as the given diagnosis is not enforced to the statistical model, revealing the

inhomogeneity of the subjects with respect to this variable. However, there is also a block of cells which are not outliers, and this block appears for persons switching from the healthy to the AD group, as this group provides a better model fit. It might be worth looking closer at the data collection of this variable, since either possible unfavorable measurement conditions or other undiagnosed or progressive diseases affecting the variable could cause the detected unusual behavior. The variable `pressure_mean` (as well as some other features) also leads to cellwise outliers for many observations, while other variables such as `mean_speed_in_air` are inconspicuous.

This plot also provides insights into multivariate cluster overlaps given by the distribution estimates for values of a specific subject. For example, Alzheimer patient 8 switches immediately to the healthy group without any change in residuals, indicating that patient 8 is at the overlap of the clusters in all variables but relatively closer to the center of the healthy cluster. It is likely that such persons have an early diagnosis of Alzheimer and low cognitive impairment.

6.3 Wine quality

Lastly, we leverage the model flexibility to investigate how qualitative expert evaluations of wine are consistent with their quantitative chemical features. To this end, we use a data set of Cortez et al. (2009b), available at the UCI Machine Learning Repository (Cortez et al., 2009a). The data were collected over the years 2004 to 2007 and consist of $p = 11$ physicochemical measurements, including fixed acidity, volatile acidity, citric acid, residual sugar, chlorides, free sulfur dioxide, total sulfur dioxide, density, pH-level, sulphates, and alcohol percentage, for $n = 4898$ samples of white *vinho verde*, a known Portuguese wine. Additionally, each wine was qualitatively graded from 0 (very bad) to 10 (excellent) by three different sensory assessors by blind tasting. The median of the three grades is reported as the variable quality.

Originally, Cortez et al. (2009b) trained a Support Vector Machine classifier given the quality variable. However, we are more interested in the coherency of each group and whether expert evaluations are consistent regarding the chemical features reported. We partition the data into three groups based on the quality assessment: the first group with low wine quality includes $n_1 = 1640$ wine samples with quality assessments 3 to 5 (20 wine samples with quality level 3, 163 with 4, and 1457 with 5), the second group with medium quality contains $n_2 = 2198$ samples with quality level 6, and the third group includes $n_3 = 1060$ good quality wine samples (880 samples with level 7, 175 with 8, and 5 samples with quality 9). Due to prominent skewness in multiple variables we apply a robust transformation to each variable to achieve central normality (see Raymaekers and Rousseeuw, 2024). We then apply the cellgGMM estimator with $\alpha = 0.75$. The increase in α compared to the minimal 0.5 should stabilize the estimation due to the low number of unbalanced groups as well as some incoherency within the groups.

The parallel coordinate plot in Figure 11 displays the resulting parameter estimates alongside the feature values of the wine samples. Each panel represents

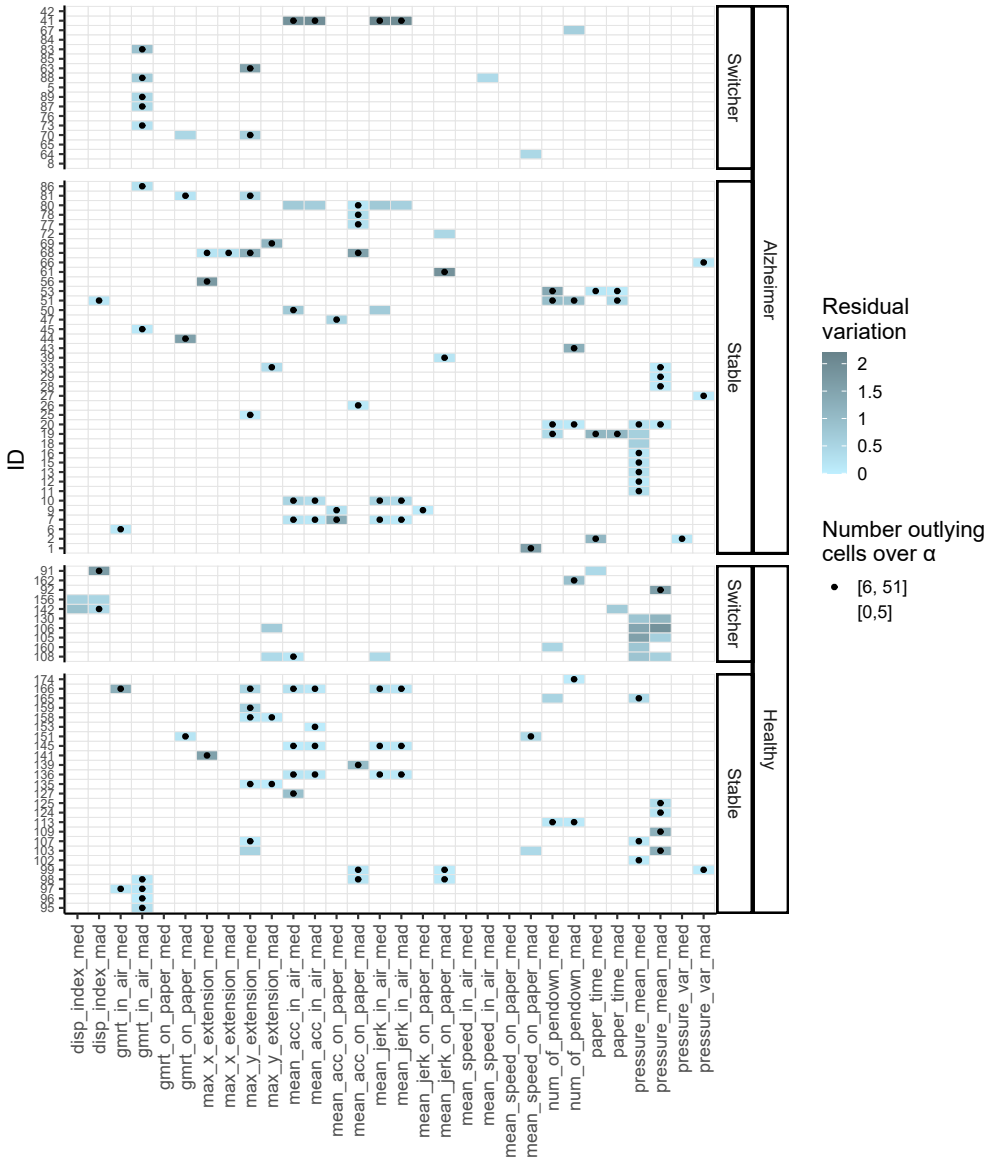

Figure 10: Standard deviation of residuals over α shown in color per individual and variable. Dots indicate that cells are outlying frequently for 51 different α values. White tiles represent non-outlying cells (no dot) and no calculable variation of residuals.

wine samples that are of low, medium or high quality according to the experts (column) and of low, medium or high quality according to the predicted group assignment of our model (rows). Consequently, the diagonal panels highlight wine samples where both expert evaluations and statistical methodology agree on their quality.

Panels below the main diagonal show wine samples that experts rate lower than their physicochemical measurements would suggest, while panels above the diagonal show samples rated higher than expected based on their quantitative features. Additionally, each panel includes the estimated location (solid black line) and standard deviation (black error bars) provided by the cellgGMM for the expert-proposed group (thus they are identical in each column). We see a strong heterogeneity within each expert group. While the wine samples where experts and cellgGMM agree are quite coherent, clear structural differences are visible in case of deviations. The two bottom left panels show quantitatively good wines that are rated low by experts. They differ clearly from less qualitative wines, most prominently by low density and residual sugar while containing a relatively high amount of alcohol. On the opposite, wines rated too high by experts (middle right panel) show adverse results for residual sugar, density and alcohol.

Moreover, there are many cellwise outliers detected by the algorithm that are also visible in the parallel coordinate plot. Especially the high amount of outlying chloride values is noticeable, as well as low citric acid values. Here, robustness against cellwise outliers is key to get reliable estimates and to avoid clusters basically modeling one variable with a high number of extreme values.

Overall, we get a good insight into the physicochemical features connected to the quality of wines as given by experts. While we achieve a nice pattern for high quality wines by our proposed multi-group GMM, the heterogeneity of the expert ratings is high. Possible factors might be chemical or physical properties that are not measured but are decisive for assessors when rating wine highly, a somewhat subjective notion of quality, or both. The strong heterogeneity together with multiple prominent cellwise outliers might also explain why previous classification attempts for this specific data set only achieve an accuracy of up to 64.6% in Cortez et al. (2009b).

7 Summary and conclusions

We establish a flexible GMM that accounts for external group information and can deliver moment estimates matched to given groups. Underlying progressive structures of the multi-group setting are present in many multi-group data sets and can be leveraged. To this end, we introduce a probabilistic multi-group GMM allowing observations to originate from other than their pre-defined group. An objective function is formulated based on its likelihood together with a penalty term.

A further contribution of this paper is the introduction of an appropriate notion of breakdown of the estimator in the cellwise multi-group setting. A

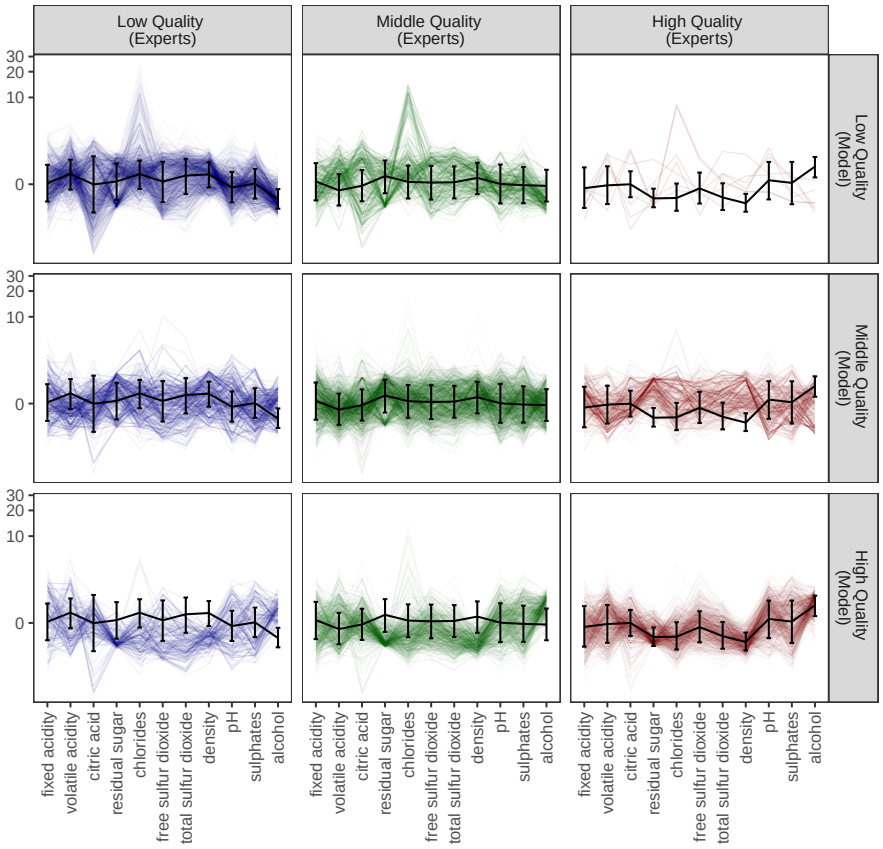

Figure 11: Differences in wine quality assessment of expert rating (columns) and physicochemical features. Black lines show estimated location and standard deviation for expert groups, colored lines show wine measurements, divided in expert group (column) and the statistically most likely group (rows).

novel setting of ideally cellwise well-clustered data is described for which the cellwise robustness properties can theoretically be evaluated and compared between different methods. This optimal setting is further extended to multi-group data for which we prove the breakdown point for the proposed cellwise robust multi-group GMM.

An iterative algorithm based on the EM algorithm guarantees convergence to a local optimum and due to the additional regularization the resulting estimator is applicable in high-dimensions. The robustness of the estimator is confirmed also in extensive simulation covering multiple relevant scenarios, and its usefulness is further demonstrated on three versatile real life examples where possible interpretation angles of the rich output of the method are illustrated in detail.

Compared to other methods, the cellgGMM provides a one-to-one match of estimated covariance and location parameters with pre-defined groups while allowing observations to be assigned flexibly to other groups if they are better fitting – a combination not offered by other methods. In contrast, classical GMMs deliver estimates that are not clearly matching known groups, and separate analysis forces observation to be always of the original group. The approach is in a way also more refined than robust discriminant analysis (for an overview see Hubert et al., 2024) which would discard observations in the covariance estimation that might not fit to the pre-defined groups due to misgrouping or being in the gray area between groups, e.g. when groups are related to progressive medical diseases or diagnoses. In applications, especially the parameter α that specifies the strictness of the membership to the given groups is a particularly well-suited tool to shed light on transition dynamics when varied. In a broader sense, the parameter α continuously bridges the gap between a separate parameter estimation via the cellMCD for each group when $\alpha = 1$ and a classical (cellwise robust) GMM with a given number of clusters in the extreme (and excluded) case of $\alpha = 0$.

The proposed method is applicable in many fields of research where assignments to pre-defined groups can be viewed more flexibly. Future research might leverage the resulting moment estimates for other prominent multivariate methods like principal component analysis, discriminant analysis or graphical modeling, and possibly further extend classical methods towards a joint approach for group dependent and group independent features.

Acknowledgements

Co-funded by the European Union (SEMACRET, Grant Agreement no. 101057741) and UKRI (UK Research and Innovation). Ines Wilms is supported by a grant from the Dutch Research Council (NWO), research program Vidi under the grant number VI.Vidi.211.032.

A Derivation of group moments

Given the multi-group Gaussian mixture model in Equation (1) we can derive the group moments.

Expected value: Due to the law of total expectation it follows that

$$\mathbb{E}[\boldsymbol{x}_g] = \sum_{k=1}^{N} \mathbb{P}[\boldsymbol{x}_g \in k]\mathbb{E}[\boldsymbol{x}_g | \boldsymbol{x}_g \in k] = \sum_{k=1}^{N} \pi_{g,k}\boldsymbol{\mu}_k.$$

Covariance: We want to show Equation (2),

$$\mathrm{Cov}[\boldsymbol{x}_g] = \sum_{k=1}^{N} \pi_{g,k}\boldsymbol{\Sigma}_k + \sum_{k=1}^{N} \pi_{g,k}(\boldsymbol{\mu}_k - \mathbb{E}[\boldsymbol{x}_g])(\boldsymbol{\mu}_k - \mathbb{E}[\boldsymbol{x}_g])'.$$

For fixed variables j, j' (that can also be equal), the corresponding covariance based on Equation (2) can be reformulated as

$$\begin{aligned}
\mathrm{Cov}[\boldsymbol{x}_g]_{j,j'} &= \sum_{k=1}^{N} \pi_{g,k}\Sigma_{k,j,j'} + \sum_{k=1}^{N} \pi_{g,k}((\boldsymbol{\mu}_k - \mathbb{E}[\boldsymbol{x}_g])(\boldsymbol{\mu}_k - \mathbb{E}[\boldsymbol{x}_g])')_{j,j'} \\
&= \sum_{k=1}^{N} \pi_{g,k}\Sigma_{k,j,j'} + \sum_{k=1}^{N} \pi_{g,k}(\boldsymbol{\mu}_k - \mathbb{E}[\boldsymbol{x}_g])_j(\boldsymbol{\mu}_k - \mathbb{E}[\boldsymbol{x}_g])_{j'} \\
&= \sum_{k=1}^{N} \pi_{g,k}\Sigma_{k,j,j'} \\
&\quad + \sum_{k=1}^{N} \pi_{g,k}(\mu_{k,j}\mu_{k,j'} - \mu_{k,j}\mathbb{E}[\boldsymbol{x}_g]_{j'} - \mu_{k,j'}\mathbb{E}[\boldsymbol{x}_g]_j + \mathbb{E}[\boldsymbol{x}_g]_{j'}\mathbb{E}[\boldsymbol{x}_g]_j) \\
&= \sum_{k=1}^{N} \pi_{g,k}\Sigma_{k,j,j'} + \sum_{k=1}^{N} \pi_{g,k}\mu_{k,j}\mu_{k,j'} - \sum_{k=1}^{N} \pi_{g,k}\mu_{k,j}\mathbb{E}[\boldsymbol{x}_g]_{j'} \\
&\quad - \sum_{k=1}^{N} \pi_{g,k}\mu_{k,j'}\mathbb{E}[\boldsymbol{x}_g]_j + \sum_{k=1}^{N} \pi_{g,k}\mathbb{E}[\boldsymbol{x}_g]_{j'}\mathbb{E}[\boldsymbol{x}_g]_j \\
&= \sum_{k=1}^{N} \pi_{g,k}\Sigma_{k,j,j'} + \sum_{k=1}^{N} \pi_{g,k}\mu_{k,j}\mu_{k,j'} - \mathbb{E}[\boldsymbol{x}_g]_{j'} \sum_{k=1}^{N} \pi_{g,k}\mu_{k,j} \\
&\quad - \mathbb{E}[\boldsymbol{x}_g]_j \sum_{k=1}^{N} \pi_{g,k}\mu_{k,j'} + \mathbb{E}[\boldsymbol{x}_g]_{j'}\mathbb{E}[\boldsymbol{x}_g]_j \\
&= \sum_{k=1}^{N} \pi_{g,k}\Sigma_{k,j,j'} + \sum_{k=1}^{N} \pi_{g,k}\mu_{k,j}\mu_{k,j'} - \mathbb{E}[\boldsymbol{x}_g]_{j'}\mathbb{E}[\boldsymbol{x}_g]_j. \qquad (17)
\end{aligned}$$

We can introduce the random variable $Z_{g,i}$ indicating from which distribution observation $\boldsymbol{x}_g$ comes. From the law of total covariance we get that

$$\begin{aligned}
\mathrm{Cov}(\boldsymbol{x}_{g,j}, \boldsymbol{x}_{g,j'}) &= \mathbb{E}[\mathrm{Cov}(\boldsymbol{x}_{g,j}, \boldsymbol{x}_{g,j'}|Z)] + \mathrm{Cov}(\mathbb{E}[\boldsymbol{x}_{g,j'}|Z], \mathbb{E}[\boldsymbol{x}_{g,j}|Z]) \\
&= \sum_{k=1}^{N} \pi_{g,k}\Sigma_{k,jj'} + \mathrm{Cov}(\mu_{Z,j'}, \mu_{Z,j}) \\
&= \sum_{k=1}^{N} \pi_{g,k}\Sigma_{k,jj'} + \mathbb{E}(\mu_{Z,j'}\mu_{Z,j}) - \mathbb{E}(\mu_{Z,j'})\mathbb{E}(\mu_{Z,j}) \\
&= \sum_{k=1}^{N} \pi_{g,k}\Sigma_{k,jj'} + \sum_{k=1}^{N} \pi_{g,k}\mu_{k,j'}\mu_{k,j} \\
&\quad - (\sum_{k=1}^{N} \pi_{g,k}\mu_{k,j'})(\sum_{k=1}^{N} \pi_{g,k}\mu_{k,j}) \\
&= \sum_{k=1}^{N} \pi_{g,k}\Sigma_{k,jj'} + \sum_{k=1}^{N} \pi_{g,k}\mu_{k,j'}\mu_{k,j} - \mathbb{E}[\boldsymbol{x}_g]_{j'}\mathbb{E}[\boldsymbol{x}_g]_j. \qquad (18)
\end{aligned}$$

We can see that the right hand sides of Equation (17) and (18) are the same.

B Derivation of the breakdown point

B.1 Idealized scenario in a rowwise outlier paradigm

The classical finite sample addition (replacement) breakdown point describes the maximal fraction of observations that need to be added to (replaced with arbitrary values in) a given sample to make the estimator useless. An estimator of location $\hat{\boldsymbol{\mu}}$ breaks down if it becomes unbounded, $||\hat{\boldsymbol{\mu}}||_2 \to \infty$. An estimated covariance matrix $\hat{\boldsymbol{\Sigma}}$ becomes either unbounded and explodes (*explosion breakdown point*), $\lambda_1(\hat{\boldsymbol{\Sigma}}) \to \infty$, or singular (*implosion breakdown point*), $\lambda_p(\hat{\boldsymbol{\Sigma}}) = 0$, where λ_1 and λ_p describe the largest and smallest eigenvalue, respectively.

However, in the setting of mixture models, pathological settings where (robust) estimators break down by just changing one observation can occur. Thus, we focus on the additive breakdown point for parameter estimation in ideal settings of well-clustered data points for mixture models, as described in Hennig (2004) for univariate and extended by Cuesta-Albertos et al. (2008) to multivariate data. A sequence of clusters $(\mathcal{X}_m)_{m\in\mathbb{N}}$ is considered to be ideal when the distances of observations within clusters are bounded by a constant $b < \infty$ and observations from different clusters are increasingly far away. Formally, let $s \geq 2$ be the number of clusters and $\tilde{n}_1 < \tilde{n}_2 < \ldots < \tilde{n}_s = \tilde{n} \in \mathbb{N}$. For each m-th part of the sequence, the data $\mathcal{X}_m$ is clustered into s clusters $A_m^1, \ldots, A_m^s$ such that

$$A_m^1 = \{\boldsymbol{x}_{1,m}, \ldots, \boldsymbol{x}_{\tilde{n}_1,m}\}, \ldots, A_m^s = \{\boldsymbol{x}_{\tilde{n}_{s-1}+1,m}, \ldots, \boldsymbol{x}_{\tilde{n}_s,m}\}$$

and $\mathcal{X}_m = \bigcup_{l=1}^{s} A_m^l$. The formal conditions for ideal clusters above are

$$\max_{1\leq l\leq s} \max\{||\boldsymbol{x}_{i',m} - \boldsymbol{x}_{i,m}||_2 : \boldsymbol{x}_{i',m}, \boldsymbol{x}_{i,m} \in A_m^l\} < b \quad \forall m \in \mathbb{N}, \tag{19}$$

$$\lim_{m\to\infty} \min\{||\boldsymbol{x}_{i',m} - \boldsymbol{x}_{i,m}||_2 : \boldsymbol{x}_{i',m} \in A_m^l, \boldsymbol{x}_{i,m} \in A_m^h, h \neq l\} = \infty, \tag{20}$$

where $||.||_2$ denotes the Euclidean norm. The added outliers denoted as $\mathcal{Y}_m = \{\boldsymbol{y}_{1,m}, \ldots, \boldsymbol{y}_{\tilde{r},m}\}$ should be clearly distinguished from all clusters and not build a cluster on their own,

$$\lim_{m\to\infty} \min\{||\boldsymbol{y}_{i',m} - \boldsymbol{x}_{i,m}||_2 : \boldsymbol{x}_{i,m} \in \mathcal{X}_m, \boldsymbol{y}_{i',m} \in \mathcal{Y}_m\} = \infty,$$
$$\lim_{m\to\infty} \min\{||\boldsymbol{y}_{i',m} - \boldsymbol{y}_{i,m}||_2 : \boldsymbol{y}_{i',m}, \boldsymbol{y}_{i,m} \in \mathcal{Y}_m, i \neq i'\} = \infty.$$

The breakdown of an estimator is then relatively defined by estimates based on $\mathcal{X}_m$ and on $\mathcal{X}_m \cup \mathcal{Y}_m$. Location breakdown for a cluster l occurs, if for all $h = 1, \ldots, N$

$$||\hat{\boldsymbol{\mu}}_l(\mathcal{X}_m) - \hat{\boldsymbol{\mu}}_h(\mathcal{X}_m \cup \mathcal{Y}_m)||_2 \to \infty. \tag{21}$$

A covariance estimator of a cluster l would implode if $\lambda_p(\hat{\boldsymbol{\Sigma}}_l(\mathcal{X}_m)) \to 0$ and $\lambda_p(\hat{\boldsymbol{\Sigma}}_l(\mathcal{X}_m \cup \mathcal{Y}_m)) \nrightarrow 0$ or if $\lambda_p(\hat{\boldsymbol{\Sigma}}_l(\mathcal{X}_m)) \nrightarrow 0$ and $\lambda_p(\hat{\boldsymbol{\Sigma}}_l(\mathcal{X}_m \cup \mathcal{Y}_m)) \to 0$. Analogously, the explosion breakdown occurs when $\lambda_1(\hat{\boldsymbol{\Sigma}}_l(\mathcal{X}_m)) \to \infty$ and $\lambda_1(\hat{\boldsymbol{\Sigma}}_l(\mathcal{X}_m \cup \mathcal{Y}_m)) \nrightarrow \infty$ or vice versa. The weight estimator $\hat{\pi}_l$ of a cluster l breaks down if $\hat{\pi}_l \in \{0, 1\}$. The addition breakdown point is then defined as $\frac{\tilde{r}}{\tilde{n}+\tilde{r}}$ where $\tilde{r}$ is the minimal number of added outliers necessary to break down the parameter estimate. Both illustrations in Figure 1 depict ideal settings in the rowwise outlier paradigm.

B.2 Proof of Corollary (1)

Corollary 1. *Given the ideal setting and fixed $\rho_k > 0, \boldsymbol{T}_k > 0$ (positive definite), the following statements hold.*

a. *For all m and no contamination, $\mathcal{Z}_m = \mathcal{X}_m$, there exist feasible estimates $\hat{\boldsymbol{\pi}}$, $\hat{\boldsymbol{\mu}}$, $\hat{\boldsymbol{\Sigma}}$ such that the objective function is finite for any feasible set of $\boldsymbol{W}$ in Equation (5). Thus, the value of the objective function for a minimizer of Equation (3) under the constraints (4) to (7) is bounded.*

b. *Given the contaminated data $\mathcal{Z}_m$ and sets of estimates $\hat{\boldsymbol{\pi}}(\mathcal{Z}_m)$, $\hat{\boldsymbol{\mu}}(\mathcal{Z}_m)$, $\hat{\boldsymbol{\Sigma}}(\mathcal{Z}_m)$, $\hat{\boldsymbol{W}}(\mathcal{Z}_m)$ for $m \in \mathbb{N}$. If there exists an l such that $\lambda_1(\hat{\boldsymbol{\Sigma}}_{reg,l}(\mathcal{Z}_m)) \to \infty$ for $m \to \infty$, then the value of the objective function of the estimates goes to infinity.*

c. *Given the contaminated data $\mathcal{Z}_m$ and sets of estimates $\hat{\boldsymbol{\pi}}(\mathcal{Z}_m)$, $\hat{\boldsymbol{\mu}}(\mathcal{Z}_m)$, $\hat{\boldsymbol{\Sigma}}(\mathcal{Z}_m)$, $\hat{\boldsymbol{W}}(\mathcal{Z}_m)$ for $m \in \mathbb{N}$. If there exists a variable j^*, l, k and a constant $\tilde{b}$ such that $|\hat{\mu}_{k,j^*}(\mathcal{Z}_m) - \hat{\mu}_{l,j^*}(\mathcal{Z}_m)| < \tilde{b}$ for $l \neq k$, then the objective function of these estimates goes to infinity.*

Proof. For ease of notation we drop the superscript m for observations and the explicit dependence of the estimators on $\mathcal{Z}_m$ or $\mathcal{X}_m$. All limits are corresponding to $m \to \infty$. The notation $\boldsymbol{w}(\boldsymbol{y})$ marks the real outlying cells of $\boldsymbol{y}$ while the notation $\boldsymbol{w}_{\boldsymbol{y}}$ indicates the missingness pattern of $\boldsymbol{y}$ for a given $\boldsymbol{W}$ from the objective function if the indexation of $\boldsymbol{y}$ is irrelevant. Then penalty term can generally be left out since it is always bounded,

$$|\sum_{g=1}^{N}\sum_{i=1}^{n_g}\sum_{j=1}^{p} q_{g,ij}(1-w_{g,ij})| \leq pN \max_g n_g \max_{g,i,j} q_{g,ij} < \infty.$$

a. Given a data matrix $\mathcal{X}$ we construct a set of estimators with finite value of the objective function. For all $k = 1, \ldots, N$ set $\hat{\Sigma}_{k,jj} = 1$ and zero otherwise and $\hat{\boldsymbol{\mu}}_k = \frac{1}{|A_m^k|}\sum_{\boldsymbol{x}\in A_m^k} \boldsymbol{x}$, where $|A_m^k|$ denotes the number of elements in A_m^k. Then, also regularized covariance matrices $\hat{\boldsymbol{\Sigma}}_{reg,k}$ have finite positive eigenvalues.

   1. Assume $\alpha \neq 1$. Set $\hat{\pi}_{k,k} = \alpha \geq 0.5$, $\hat{\pi}_{k,l} = \frac{1-\alpha}{N-1} > 0$ for $k \neq l$. For each observation $\boldsymbol{x}_{g,i}$ with $\boldsymbol{w}_{g,i}$ originating from any cluster l it holds that

$$\begin{aligned}
&\ln\left(\sum_{k=1}^{N}\hat{\pi}_{g,k}\varphi\left(\boldsymbol{x}_{g,i}^{(\boldsymbol{w}_{g,i})};\hat{\boldsymbol{\mu}}_k^{(\boldsymbol{w}_{g,i})},\hat{\boldsymbol{\Sigma}}_{reg,k}^{(\boldsymbol{w}_{g,i})}\right)\right)\\
&\quad\geq \ln\left(\frac{1-\alpha}{N-1}\varphi\left(\boldsymbol{x}_{g,i}^{(\boldsymbol{w}_{g,i})};\hat{\boldsymbol{\mu}}_l^{(\boldsymbol{w}_{g,i})},\hat{\boldsymbol{\Sigma}}_{reg,l}^{(\boldsymbol{w}_{g,i})}\right)\right)\\
&\quad= \ln\frac{1-\alpha}{N-1} + \ln\frac{e^{-\frac{1}{2}(\boldsymbol{x}_{g,i}^{(\boldsymbol{w}_{g,i})}-\hat{\boldsymbol{\mu}}_l^{(\boldsymbol{w}_{g,i})})'(\hat{\boldsymbol{\Sigma}}_{reg,l}^{(\boldsymbol{w}_{g,i})})^{-1}(\boldsymbol{x}_{g,i}^{(\boldsymbol{w}_{g,i})}-\hat{\boldsymbol{\mu}}_l^{(\boldsymbol{w}_{g,i})})}}{\sqrt{(2\pi)^{\sum_j w_{g,ij}}\det\hat{\boldsymbol{\Sigma}}_{reg,l}^{(\boldsymbol{w}_{g,i})}}}\\
&\quad= \ln\frac{1-\alpha}{N-1} - \frac{1}{2}\Bigg((\boldsymbol{x}_{g,i}^{(\boldsymbol{w}_{g,i})}-\hat{\boldsymbol{\mu}}_l^{(\boldsymbol{w}_{g,i})})'(\hat{\boldsymbol{\Sigma}}_{reg,l}^{(\boldsymbol{w}_{g,i})})^{-1}(\boldsymbol{x}_{g,i}^{(\boldsymbol{w}_{g,i})}-\hat{\boldsymbol{\mu}}_l^{(\boldsymbol{w}_{g,i})})\\
&\qquad+\sum_j w_{g,ij}\ln(2\pi) + \ln\det\hat{\boldsymbol{\Sigma}}_{reg,l}^{(\boldsymbol{w}_{g,i})}\Bigg)\\
&\quad\geq \ln\frac{1-\alpha}{N-1} - \frac{1}{2}(\boldsymbol{b}^{(\boldsymbol{w}_{g,i})})'(\hat{\boldsymbol{\Sigma}}_{reg,l}^{(\boldsymbol{w}_{g,i})})^{-1}(\boldsymbol{b}^{(\boldsymbol{w}_{g,i})})\\
&\qquad-\frac{1}{2}p\ln(2\pi) - \frac{1}{2}\ln\det\hat{\boldsymbol{\Sigma}}_{reg,l}^{(\boldsymbol{w}_{g,i})},
\end{aligned}$$

   where $\boldsymbol{b}$ denotes the vector $\boldsymbol{b} = (b, \ldots, b) \in \mathbb{R}^p$ with b corresponding to Equation (12) and the last inequality follows from Equation (19) with the Euclidean norm. Since all terms on the right hand side are bounded, the objective function is bounded from above. For the

lower bound, it follows that

$$
\begin{aligned}
&\ln\left(\sum_{k=1}^{N}\hat{\pi}_{g,k}\varphi\left(\boldsymbol{x}_{g,i}^{(\boldsymbol{w}_{g,i})};\hat{\boldsymbol{\mu}}_k^{(\boldsymbol{w}_{g,i})},\hat{\boldsymbol{\Sigma}}_{reg,k}^{(\boldsymbol{w}_{g,i})}\right)\right)\\
&\quad\leq \ln N+\max_k \ln\left(\varphi\left(\boldsymbol{x}_{g,i}^{(\boldsymbol{w}_{g,i})};\hat{\boldsymbol{\mu}}_k^{(\boldsymbol{w}_{g,i})},\hat{\boldsymbol{\Sigma}}_{reg,k}^{(\boldsymbol{w}_{g,i})}\right)\right)\\
&\quad\leq \ln N+\max_k(\underbrace{-\frac{1}{2}(\boldsymbol{x}_{g,i}^{(\boldsymbol{w}_{g,i})}-\hat{\boldsymbol{\mu}}_k^{(\boldsymbol{w}_{g,i})})'(\hat{\boldsymbol{\Sigma}}_{reg,k}^{(\boldsymbol{w}_{g,i})})^{-1}(\boldsymbol{x}_{g,i}^{(\boldsymbol{w}_{g,i})}-\hat{\boldsymbol{\mu}}_k^{(\boldsymbol{w}_{g,i})})}_{\leq 0})\\
&\qquad\underbrace{-\frac{1}{2}\sum_j w_{g,ij}\ln(2\pi)}_{\leq 0}+\max_k(-\frac{1}{2}\ln\det\hat{\boldsymbol{\Sigma}}_{reg,k}^{(\boldsymbol{w}_{g,i})})\\
&\quad\leq \ln N-\frac{1}{2}\ln\min_k\det\hat{\boldsymbol{\Sigma}}_{reg,k}^{(\boldsymbol{w}_{g,i})}.
\end{aligned}
$$

Since the covariance estimates are finite, the objective function is bounded for any feasible $\boldsymbol{W}$.

2. Assume $\alpha=1$. Set $\hat{\pi}_{k,k}=1$, $\hat{\pi}_{k,l}=0$ for all $k\neq l$. All observations from a group g originate from cluster g, $\boldsymbol{Z}^g=A^g$, see Equation (16). Thus, for any $\boldsymbol{x}_{g,i}$ it holds that

$$
\begin{aligned}
&\ln\left(\sum_{k=1}^{N}\hat{\pi}_{g,k}\varphi\left(\boldsymbol{x}_{g,i}^{(\boldsymbol{w}_{g,i})};\hat{\boldsymbol{\mu}}_k^{(\boldsymbol{w}_{g,i})},\hat{\boldsymbol{\Sigma}}_{reg,k}^{(\boldsymbol{w}_{g,i})}\right)\right)\\
&\qquad=-\frac{1}{2}(\boldsymbol{x}_{g,i}^{(\boldsymbol{w}_{g,i})}-\hat{\boldsymbol{\mu}}_g^{(\boldsymbol{w}_{g,i})})'(\hat{\boldsymbol{\Sigma}}_{reg,g}^{(\boldsymbol{w}_{g,i})})^{-1}(\boldsymbol{x}_{g,i}^{(\boldsymbol{w}_{g,i})}-\hat{\boldsymbol{\mu}}_g^{(\boldsymbol{w}_{g,i})})\\
&\qquad\quad-\frac{1}{2}\sum_j w_{g,ij}\ln(2\pi)-\frac{1}{2}\ln\det\hat{\boldsymbol{\Sigma}}_{reg,g}^{(\boldsymbol{w}_{g,i})}\\
&\qquad\geq-\frac{1}{2}\left((\boldsymbol{b}^{(\boldsymbol{w}_{g,i})})'(\hat{\boldsymbol{\Sigma}}_{reg,g}^{(\boldsymbol{w}_{g,i})})^{-1}(\boldsymbol{b}^{(\boldsymbol{w}_{g,i})})+p\ln(2\pi)+\ln\det\hat{\boldsymbol{\Sigma}}_{reg,g}^{(\boldsymbol{w}_{g,i})}\right)
\end{aligned}
$$

and the objective function is bounded from above. For the lower

bound, it follows

$$
\begin{aligned}
&\ln\left(\sum_{k=1}^{N}\hat{\pi}_{g,k}\varphi\left(\boldsymbol{x}_{g,i}^{(\boldsymbol{w}_{g,i})};\hat{\boldsymbol{\mu}}_k^{(\boldsymbol{w}_{g,i})},\hat{\boldsymbol{\Sigma}}_{reg,k}^{(\boldsymbol{w}_{g,i})}\right)\right)\\
&\qquad=\underbrace{-\frac{1}{2}(\boldsymbol{x}_{g,i}^{(\boldsymbol{w}_{g,i})}-\hat{\boldsymbol{\mu}}_g^{(\boldsymbol{w}_{g,i})})'(\hat{\boldsymbol{\Sigma}}_{reg,g}^{(\boldsymbol{w}_{g,i})})^{-1}(\boldsymbol{x}_{g,i}^{(\boldsymbol{w}_{g,i})}-\hat{\boldsymbol{\mu}}_g^{(\boldsymbol{w}_{g,i})})}_{\leq 0}\\
&\qquad\quad\underbrace{-\frac{1}{2}\sum_j w_{g,ij}\ln(2\pi)}_{\leq 0}-\frac{1}{2}\ln\det\hat{\boldsymbol{\Sigma}}_{reg,g}^{(\boldsymbol{w}_{g,i})}\\
&\qquad\leq -\frac{1}{2}\ln\det\hat{\boldsymbol{\Sigma}}_{reg,g}^{(\boldsymbol{w}_{g,i})}.
\end{aligned}
$$

Thus, the objective function is bounded for any feasible $\boldsymbol{W}$.

b. Assume that under the given estimates the objective function is bounded. By construction, the estimated covariances $\hat{\boldsymbol{\Sigma}}_{reg,k}$ are regular and thus, the lowest eigenvalues $\lambda_p(\hat{\boldsymbol{\Sigma}}_{reg,k}) \geq \tilde{b}_k(\rho_k, \boldsymbol{T}_k) > 0$ are bounded away from zero. According to the proof of Proposition 2b) from Raymaekers and Rousseeuw (2023) it holds for all k and any feasible $\hat{\boldsymbol{w}}$ that

$$\ln\det\hat{\boldsymbol{\Sigma}}_{reg,k}^{(\hat{\boldsymbol{w}})} \geq \ln\max_{j=1,\ldots,p}\hat{\Sigma}_{reg,k,jj}^{(\hat{\boldsymbol{w}})} + (p-1)\ln\tilde{b}_k(\rho_k, \boldsymbol{T}_k).$$

where $\tilde{b}_k(\rho_k, \boldsymbol{T}_k)$ is a constant depending only on ρ_k and $\boldsymbol{T}_k$.

From part a. we know that for all $\boldsymbol{x}_{g,i}$ from group g it holds that

$$\begin{aligned}
&\ln\left(\sum_{k=1}^{N}\hat{\pi}_{g,k}\varphi\left(\boldsymbol{x}_{g,i}^{(\hat{\boldsymbol{w}}_{g,i})};\hat{\boldsymbol{\mu}}_k^{(\hat{\boldsymbol{w}}_{g,i})},\hat{\boldsymbol{\Sigma}}_{reg,k}^{(\hat{\boldsymbol{w}}_{g,i})}\right)\right)\\
&\quad\leq \ln N-\frac{1}{2}\min_k\Bigg((\boldsymbol{x}_{g,i}^{(\hat{\boldsymbol{w}}_{g,i})}-\hat{\boldsymbol{\mu}}_k^{(\hat{\boldsymbol{w}}_{g,i})})'(\hat{\boldsymbol{\Sigma}}_{reg,k}^{(\hat{\boldsymbol{w}}_{g,i})})^{-1}(\boldsymbol{x}_{g,i}^{(\hat{\boldsymbol{w}}_{g,i})}-\hat{\boldsymbol{\mu}}_k^{(\hat{\boldsymbol{w}}_{g,i})})\\
&\qquad+\ln\det\hat{\boldsymbol{\Sigma}}_{reg,k}^{(\hat{\boldsymbol{w}}_{g,i})}\Bigg)\\
&\quad\leq \ln N-\frac{1}{2}\min_k\Bigg((\boldsymbol{x}_{g,i}^{(\hat{\boldsymbol{w}}_{g,i})}-\hat{\boldsymbol{\mu}}_k^{(\hat{\boldsymbol{w}}_{g,i})})'(\hat{\boldsymbol{\Sigma}}_{reg,k}^{(\hat{\boldsymbol{w}}_{g,i})})^{-1}(\boldsymbol{x}_{g,i}^{(\hat{\boldsymbol{w}}_{g,i})}-\hat{\boldsymbol{\mu}}_k^{(\hat{\boldsymbol{w}}_{g,i})})\\
&\qquad+\ln\max_{j=1,\ldots,p}\hat{\Sigma}_{reg,k,jj}^{(\hat{\boldsymbol{w}}_{g,i})}+(p-1)\ln\tilde{b}_k(\rho_k,\boldsymbol{T}_k)\Bigg)\\
&\quad\leq \ln N-\frac{1}{2}\min_k(p-1)\ln\tilde{b}_k(\rho_k,\boldsymbol{T}_k)-\frac{1}{2}\min_k\Bigg((\boldsymbol{x}_{g,i}^{(\hat{\boldsymbol{w}}_{g,i})}-\hat{\boldsymbol{\mu}}_k^{(\hat{\boldsymbol{w}}_{g,i})})'\\
&\qquad\times(\hat{\boldsymbol{\Sigma}}_{reg,k}^{(\hat{\boldsymbol{w}}_{g,i})})^{-1}(\boldsymbol{x}_{g,i}^{(\hat{\boldsymbol{w}}_{g,i})}-\hat{\boldsymbol{\mu}}_k^{(\hat{\boldsymbol{w}}_{g,i})})+\ln\max_{j=1,\ldots,p}\hat{\Sigma}_{reg,k,jj}^{(\hat{\boldsymbol{w}}_{g,i})}\Bigg).
\end{aligned}\tag{22}$$

Let $j^*(l)=\max_{j=1,\ldots,p}\hat{\Sigma}_{reg,l,jj}$ for the distribution where $\lambda_1(\hat{\boldsymbol{\Sigma}}_{reg,l})\to\infty$. For each group g there exists at least one observation $\boldsymbol{x}_{g,i^*(g)}$ from cluster g for which variable $j^*(l)$ is observed, $w_{g,i^*(g)j^*(l)}=1$. For these observations, we have

$$\begin{aligned}
&(\boldsymbol{x}_{g,i^*(g)}^{(\hat{\boldsymbol{w}}_{g,i^*(g)})}-\hat{\boldsymbol{\mu}}_l^{(\hat{\boldsymbol{w}}_{g,i^*(g)})})'(\hat{\boldsymbol{\Sigma}}_{reg,l}^{(\hat{\boldsymbol{w}}_{g,i^*(g)})})^{-1}\\
&\quad\times(\boldsymbol{x}_{g,i^*(g)}^{(\hat{\boldsymbol{w}}_{g,i^*(g)})}-\hat{\boldsymbol{\mu}}_l^{(\hat{\boldsymbol{w}}_{g,i^*(g)})})+\ln\max_{j=1,\ldots,p}\hat{\Sigma}_{reg,l,jj}^{(\hat{\boldsymbol{w}}_{g,i^*(g)})}\geq\ln\max_{j=1,\ldots,p}\hat{\Sigma}_{reg,l,jj}\\
&\qquad=\ln\max_{j,j'=1,\ldots,p}|\hat{\Sigma}_{reg,l,jj'}|\\
&\qquad\geq\ln\frac{\lambda_1(\hat{\boldsymbol{\Sigma}}_{reg,l})}{p}\to\infty.
\end{aligned}$$

Thus, for all $\boldsymbol{x}_{g,i^*(g)}, g=1,\ldots,N$ the argument l cannot be the minimizer. Without loss of generality, assume that all other covariance matrices are bounded, $\lambda_1(\hat{\boldsymbol{\Sigma}}_{reg,k})<\infty$ if $k\neq l$. Due to Equation (11), (13) and (14) it holds that $|x_{g,i^*(g)j^*(l)}-x_{h,i^*(h)j^*(l)}|\to\infty$ if $g\neq h$. Also,

$$\begin{aligned}
&(\boldsymbol{x}_{g,i^*(g)}^{(\hat{\boldsymbol{w}}_{g,i^*(g)})}-\hat{\boldsymbol{\mu}}_k^{(\hat{\boldsymbol{w}}_{g,i^*(g)})})'(\hat{\boldsymbol{\Sigma}}_{reg,k}^{(\hat{\boldsymbol{w}}_{g,i^*(g)})})^{-1}(\boldsymbol{x}_{g,i^*(g)}^{(\hat{\boldsymbol{w}}_{g,i^*(g)})}-\hat{\boldsymbol{\mu}}_k^{(\hat{\boldsymbol{w}}_{g,i^*(g)})})\\
&\qquad\geq(x_{g,i^*(g)j^*(l)}-\hat{\mu}_{k,j^*(l)})^2(\hat{\boldsymbol{\Sigma}}_{reg,k}^{(\hat{\boldsymbol{w}}_{g,i^*(g)})})^{-1}_{j^*(l)j^*(l)}.
\end{aligned}$$

If $(\hat{\boldsymbol{\Sigma}}_{reg,k}^{(\hat{\boldsymbol{w}}_{g,i^*(g)})})^{-1}_{j^*(l)j^*(l)}\to 0$, then the smallest eigenvalue goes to zero, $\lambda_p((\hat{\boldsymbol{\Sigma}}_{reg,k}^{(\hat{\boldsymbol{w}}_{g,i^*(g)})})^{-1})\to 0$ implying $\lambda_1(\hat{\boldsymbol{\Sigma}}_{reg,k}^{(\hat{\boldsymbol{w}}_{g,i^*(g)})})\to\infty$ as well as $\lambda_1(\hat{\boldsymbol{\Sigma}}_{reg,k})\to$

∞, which contradicts that the other covariances are bounded in the first eigenvalue. Thus, $(\hat{\boldsymbol{\Sigma}}_{reg,k}^{(\hat{\boldsymbol{w}}_{g,i^*(g)})})^{-1}_{j^*(l)j^*(l)}$ is bounded away from zero.

Since all observations are increasingly far away, there exists at least one $\boldsymbol{x}_{g',i^*(g')}$ such that $(x_{g',i^*(g')j^*(l)} - \hat{\mu}_{k,j^*(l)})^2 \to \infty$ for all $k = 1, \ldots, N, k \neq l$ and for which the minimum from Equation (22) goes to infinity. Moreover, all parts are bounded from above,

$$\ln\left(\sum_{k=1}^{N} \hat{\pi}_{g,k}\varphi\left(\boldsymbol{x}_{g,i}^{(\hat{\boldsymbol{w}}_{g,i})}; \hat{\boldsymbol{\mu}}_k^{(\hat{\boldsymbol{w}}_{g,i})}, \hat{\boldsymbol{\Sigma}}_{reg,k}^{(\hat{\boldsymbol{w}}_{g,i})}\right)\right) \leq \ln N - \frac{p}{2}\min_k \ln \tilde{b}_k(\rho_k, \boldsymbol{T}_k).$$

Thus, the objective function has to explode.

c. Assume that the objective function of the estimators $\hat{\boldsymbol{\pi}}$, $\hat{\boldsymbol{\mu}}$, $\hat{\boldsymbol{\Sigma}}$, $\hat{\boldsymbol{W}}$ is finite. Then $\hat{\boldsymbol{\Sigma}}_{reg,k}$ are regular and not exploding due to part b. For all groups g there exists at least one observation $\boldsymbol{x}_{g,i*(g)} \in (A^g \cup B^g) \cap \boldsymbol{Z}^g$ such that $\hat{w}_{g,i*(g)j^*} = 1$. Let $C_1 = \min_{k,\hat{\boldsymbol{w}},j} \hat{\boldsymbol{\Sigma}}_{reg,k,jj}^{(\hat{\boldsymbol{w}})} > 0$ and $C_2 = \min_{k,\hat{\boldsymbol{w}},j} (\hat{\boldsymbol{\Sigma}}_{reg,k}^{(\hat{\boldsymbol{w}})})^{-1}_{jj} > 0$ (see part b.), then it holds

$$\begin{aligned}
&\ln\left(\sum_{k=1}^{N}\hat{\pi}_{g,k}\varphi\left(\boldsymbol{x}_{g,i*(g)}^{(\hat{\boldsymbol{w}}_{g,i*(g)})}; \hat{\boldsymbol{\mu}}_k^{(\hat{\boldsymbol{w}}_{g,i*(g)})}, \hat{\boldsymbol{\Sigma}}_{reg,k}^{(\hat{\boldsymbol{w}}_{g,i*(g)})}\right)\right) \\
&\quad \leq \ln N - \frac{1}{2}\min_k (p-1)\ln \tilde{b}_k(\rho_k, \boldsymbol{T}_k) - \frac{1}{2}\min_k \ln \max_{j=1,\ldots,p} \hat{\boldsymbol{\Sigma}}_{reg,k,jj}^{(\hat{\boldsymbol{w}}_{g,i*(g)})} \\
&\qquad - \frac{1}{2}\min_k \Bigg((\boldsymbol{x}_{g,i*(g)}^{(\hat{\boldsymbol{w}}_{g,i*(g)})} - \hat{\boldsymbol{\mu}}_k^{(\hat{\boldsymbol{w}}_{g,i*(g)})})' (\hat{\boldsymbol{\Sigma}}_{reg,k}^{(\hat{\boldsymbol{w}}_{g,i*(g)})})^{-1} \\
&\qquad \times (\boldsymbol{x}_{g,i*(g)}^{(\hat{\boldsymbol{w}}_{g,i*(g)})} - \hat{\boldsymbol{\mu}}_k^{(\hat{\boldsymbol{w}}_{g,i*(g)})}) \Bigg) \\
&\quad \leq \ln N - \frac{1}{2}\min_k (p-1)\ln \tilde{b}_k(\rho_k, \boldsymbol{T}_k) - \frac{1}{2}\ln C_1 \\
&\qquad - \frac{1}{2}C_2 \min_k \left((x_{g,i^*(g)j^*} - \hat{\mu}_{k,j^*})^2 \right).
\end{aligned}$$

There are N many observations observed in j^* that move increasingly far away from each other in variable j^*. Since there exists l', l such that to $|\hat{\mu}_{l',j^*} - \hat{\mu}_{l,j^*}| < \tilde{b}$ there are only $N-1$ location estimates that move infinitely far away from each other. It follows that $\max_g \min_k (x_{g,i^*(g)j^*} - \hat{\mu}_{k,j^*})^2 \to \infty$ and thus, there is one term in the objective function that explodes, while the others are bounded (see part b.).

□

B.3 Proof of breakdown points in Theorem 2

Theorem 2 (Breakdown point)**.** *For the ideal scenario and fixed $\rho_k, T_k > 0$ the following breakdown results in the cellwise paradigm hold.*

a. The implosion breakdown point is 1.

b. The weight breakdown point is 1.

c. The explosion breakdown point is at least $\min_g\{(n_g - h_g + 1)/n_g\}$.

d. The location breakdown point is 0.

e. The explosion breakdown point is exactly $\min_g\{(n_g - h_g + 1)/n_g\}$*, when assuming that the location estimator is not broken down.*

Proof.

a. Clear, since the lowest eigenvalues are always bound away from zero (see also proof of Theorem 2c in Puchhammer and Filzmoser, 2024).

b. Since constraint (7) restricts the estimates $\hat{\boldsymbol{\pi}}(\mathcal{Z}_m)$ such that $\hat{\pi}(\mathcal{Z}_m)_{g,g} \geq \alpha > 0$ for all g, the weight of each cluster k is $\frac{1}{N}\sum_{g=1}^{N} \hat{\pi}(\mathcal{Z}_m)_{g,k} \geq \frac{\alpha}{N} > 0$. Thus, all clusters have non-zero weight.

c. From Corollary 1a., we know for uncontaminated data $\mathcal{X}_m$ that the objective function is finite for the minimizers, and from Corollary 1b. we know that the covariance matrix estimates are not exploding. Thus, a breakdown occurs only when there exists an l such that $\lambda_1(\hat{\boldsymbol{\Sigma}}_{reg,l}(\mathcal{Z}_m)) \to \infty$.

Assume that for each group g only up to $n_g - h_g$ cells per column are contaminated and outlying in the idealized scenario. It is possible to set $\hat{\boldsymbol{W}}$ such that $w_{\boldsymbol{y},j} = 0$ for all cells of added outliers $\boldsymbol{y}$ exactly when $w(\boldsymbol{y})_j = 0$. Thus, there exists a copy of an uncontaminated ideal scenario $\tilde{\mathcal{X}}_m$, that has the same values if cells are observed as indicated by $\hat{\boldsymbol{W}}$ and non-outlying values if $w_{\boldsymbol{y},j} = 0$. From Corollary 1a. for the given $\hat{\boldsymbol{W}}$ it follows that there exist candidate estimates with finite objective function for $\tilde{\mathcal{X}}_m$ and the value of the objective function on $\mathcal{X}_m \cup \mathcal{Y}_m$ is the same (and finite). From Corollary 1b. it follows that if a covariance matrix explodes, the objective function explodes as well and the estimates cannot be minimizers of the objective function because there exist candidate estimates with a lower objective function. Thus, the breakdown point is at least $\min_g\{(n_g - h_g + 1)/n_g\}$.

d. We produce a special setting that is ideal and uncontaminated and in which there are two possible estimates for location that have increasing distance from each other for $m \to \infty$.

Assume $N = 2$ many groups[3], $\alpha = 0.5$, n_g is even for all $g = 1, \ldots, N$, and that there are no added outliers, $\mathcal{Y}_m = \emptyset$. Further assume that we have minimizing estimates of the objective function, $\hat{\boldsymbol{\pi}}$, $\hat{\boldsymbol{\mu}}$, $\hat{\boldsymbol{\Sigma}}$ and $\hat{\boldsymbol{W}}$. Assume $\mathcal{X}_m$ such that the minimizing $\hat{\boldsymbol{W}}$ has zeros in the first column and in the first $n_g/2$ cells and for all other columns there are zeros in the last half of the cells, for both groups. Assume $\mathcal{X}_m$ such that $\hat{\boldsymbol{\Sigma}}_{reg,1} = \hat{\boldsymbol{\Sigma}}_{reg,2}$ as well as $\hat{\pi}_{1,1} = \hat{\pi}_{2,2} = 0.5$. Construct $\tilde{\boldsymbol{\mu}}_1 = (\hat{\mu}_{2,1}, \hat{\mu}_{1,2}, \ldots, \hat{\mu}_{1,p})$ and $\tilde{\boldsymbol{\mu}}_2 = (\hat{\mu}_{1,1}, \hat{\mu}_{2,2}, \ldots, \hat{\mu}_{2,p})$ by exchanging the first coordinate of $\hat{\boldsymbol{\mu}}_1$ and $\hat{\boldsymbol{\mu}}_2$.

[3]This setting can be generalized to $N > 2$, e.g. by adding groups which consist entirely of one cluster each.

Then it holds for the constructed $\tilde{\boldsymbol{\mu}}_1, \tilde{\boldsymbol{\mu}}_2$ that

$$\begin{aligned}
\varphi\left(\boldsymbol{x}_{1,i}^{(\hat{\boldsymbol{w}}_{1,i})}; \hat{\boldsymbol{\mu}}_1^{(\hat{\boldsymbol{w}}_{1,i})}, \hat{\boldsymbol{\Sigma}}_{reg,1}^{(\hat{\boldsymbol{w}}_{1,i})}\right) &= \varphi\left(\boldsymbol{x}_{1,i}^{(\hat{\boldsymbol{w}}_{1,i})}; \tilde{\boldsymbol{\mu}}_1^{(\hat{\boldsymbol{w}}_{1,i})}, \hat{\boldsymbol{\Sigma}}_{reg,1}^{(\hat{\boldsymbol{w}}_{1,i})}\right) \quad \forall i \leq n_1/2 \\
\varphi\left(\boldsymbol{x}_{1,i}^{(\hat{\boldsymbol{w}}_{1,i})}; \hat{\boldsymbol{\mu}}_1^{(\hat{\boldsymbol{w}}_{1,i})}, \hat{\boldsymbol{\Sigma}}_{reg,1}^{(\hat{\boldsymbol{w}}_{1,i})}\right) &= \varphi\left(\boldsymbol{x}_{1,i}^{(\hat{\boldsymbol{w}}_{1,i})}; \tilde{\boldsymbol{\mu}}_2^{(\hat{\boldsymbol{w}}_{1,i})}, \hat{\boldsymbol{\Sigma}}_{reg,2}^{(\hat{\boldsymbol{w}}_{1,i})}\right) \quad \forall i \geq 1 + n_2/2 \\
\varphi\left(\boldsymbol{x}_{2,i}^{(\hat{\boldsymbol{w}}_{2,i})}; \hat{\boldsymbol{\mu}}_2^{(\hat{\boldsymbol{w}}_{2,i})}, \hat{\boldsymbol{\Sigma}}_{reg,2}^{(\hat{\boldsymbol{w}}_{2,i})}\right) &= \varphi\left(\boldsymbol{x}_{2,i}^{(\hat{\boldsymbol{w}}_{2,i})}; \tilde{\boldsymbol{\mu}}_2^{(\hat{\boldsymbol{w}}_{2,i})}, \hat{\boldsymbol{\Sigma}}_{reg,2}^{(\hat{\boldsymbol{w}}_{2,i})}\right) \quad \forall i \leq n_1/2 \\
\varphi\left(\boldsymbol{x}_{2,i}^{(\hat{\boldsymbol{w}}_{2,i})}; \hat{\boldsymbol{\mu}}_2^{(\hat{\boldsymbol{w}}_{2,i})}, \hat{\boldsymbol{\Sigma}}_{reg,2}^{(\hat{\boldsymbol{w}}_{2,i})}\right) &= \varphi\left(\boldsymbol{x}_{2,i}^{(\hat{\boldsymbol{w}}_{2,i})}; \tilde{\boldsymbol{\mu}}_1^{(\hat{\boldsymbol{w}}_{2,i})}, \hat{\boldsymbol{\Sigma}}_{reg,1}^{(\hat{\boldsymbol{w}}_{2,i})}\right) \quad \forall i \geq 1 + n_2/2.
\end{aligned}$$

Thus, the value of the objective function is the same and finite and the constructed estimates $\hat{\boldsymbol{\pi}}$, $\tilde{\boldsymbol{\mu}}$, $\hat{\boldsymbol{\Sigma}}$ and $\hat{\boldsymbol{W}}$ are also optimizers. However, $||\hat{\boldsymbol{\mu}}_l(\mathcal{X}_m) - \tilde{\boldsymbol{\mu}}_h(\mathcal{X}_m \cup \mathcal{Y}_m)||_2 \to \infty$ for all $l, h \in \{1, 2\}$ due to Corollary 1c.

e. For ease of notation we drop the superscript m for observations and the explicit dependence of the estimators of $\mathcal{Z}_m$ or $\mathcal{X}_m$. All limits are corresponding to $m \to \infty$. We construct a counter example that shows that the covariance needs to explode if the location estimator is not breaking down within the idealized scenario.

Given an uncontaminated sample $\mathcal{X}$ and one variable j^*, we assume that all cells from variable j^* of the uncontaminated data are positive. The uncontaminated data $\mathcal{X}$ is partitioned into groups $\boldsymbol{Z}^1, \ldots, \boldsymbol{Z}^N$ and only one group g' is contaminated with $n_{g'} - h_{g'} + 1$ many cellwise outliers $\mathcal{Y}$, outlying only in variable j^* with negative values. Thus, for any $\boldsymbol{W}_{g'}$ there is always at least one outlying cell in variable j^*, that is observed. The data used in the contaminated case is then $\mathcal{Z} = \bigcup_{g=1}^N \boldsymbol{Z}^g$. For an estimator $\hat{\boldsymbol{W}}(\mathcal{Z})$ let $\tilde{\boldsymbol{y}}$ be an outlier for which variable j^* is observed, $w(\tilde{\boldsymbol{y}})_{j^*} = 0$ and $\hat{w}_{\tilde{\boldsymbol{y}},j^*} = 1$.

Let $\hat{t}_k(\boldsymbol{z})$ denote the probability of an observation $\boldsymbol{z} \in \boldsymbol{Z}_g$ that it belongs to distribution k given the estimates $\hat{\boldsymbol{\pi}}(\mathcal{Z})$, $\hat{\boldsymbol{\mu}}(\mathcal{Z})$, $\hat{\boldsymbol{\Sigma}}(\mathcal{Z})$ and $\hat{\boldsymbol{W}}(\mathcal{Z})$,

$$\hat{t}_k(\boldsymbol{z}) = \frac{\hat{\pi}_{g,k}\varphi\left(\boldsymbol{z}^{(\hat{\boldsymbol{w}}_{\boldsymbol{z}})}; \hat{\boldsymbol{\mu}}_k^{(\hat{\boldsymbol{w}}_{\boldsymbol{z}})}, \hat{\boldsymbol{\Sigma}}_{reg,k}^{(\hat{\boldsymbol{w}}_{\boldsymbol{z}})}\right)}{\sum_{l=1}^N \hat{\pi}_{g,l}\varphi\left(\boldsymbol{z}^{(\hat{\boldsymbol{w}}_{\boldsymbol{z}})}; \hat{\boldsymbol{\mu}}_l^{(\hat{\boldsymbol{w}}_{\boldsymbol{z}})}, \hat{\boldsymbol{\Sigma}}_{reg,l}^{(\hat{\boldsymbol{w}}_{\boldsymbol{z}})}\right)}.$$

Note that due to the regularity of the covariance estimates the density goes to zero, $\varphi\left(\boldsymbol{z}^{(\hat{\boldsymbol{w}}_{\boldsymbol{z}})}; \hat{\boldsymbol{\mu}}_k^{(\hat{\boldsymbol{w}}_{\boldsymbol{z}})}, \hat{\boldsymbol{\Sigma}}_{reg,k}^{(\hat{\boldsymbol{w}}_{\boldsymbol{z}})}\right) \to 0$, if $||\boldsymbol{z}^{(\hat{\boldsymbol{w}}_{\boldsymbol{z}})} - \hat{\boldsymbol{\mu}}_k^{(\hat{\boldsymbol{w}}_{\boldsymbol{z}})}||_2 \to \infty$ and thus $\hat{t}_k(\boldsymbol{z}) \to 0$. Since there are N many possible distributions, for $\tilde{\boldsymbol{y}}$ there exists a distribution k^* with $\hat{t}_{k^*}(\tilde{\boldsymbol{y}}) \geq \frac{1}{N} > 0$.

Upon convergence of the EM-algorithm the location estimate of the j^*-th variable of distribution k^* is

$$\hat{\mu}_{k^*j^*}(\mathcal{Z}) = \frac{1}{\bar{t}_{k^*}} \sum_{g=1}^N \sum_{\boldsymbol{z} \in \boldsymbol{Z}_g} \hat{t}_{k^*}(\boldsymbol{z})\hat{z}_{j^*},$$

with $\bar{t}_{k^*} = \sum_{g=1}^N \sum_{\boldsymbol{z} \in \boldsymbol{Z}_g} \hat{t}_{k^*}(\boldsymbol{z})$ and $\hat{z}_{j^*}$ being the imputed value of $\boldsymbol{z}$ for variable

j^*. For $\hat{w}_{\boldsymbol{z},j^*} = 1$ it is equal to z_{j^*} and for $\hat{w}_{\boldsymbol{z},j^*} = 0$ it is equal to

$$\hat{\mu}_{k^*j^*} + \hat{\boldsymbol{\Sigma}}_{reg,k^*}^{(j^*|\hat{\boldsymbol{w}}_{\boldsymbol{z}})} \left(\hat{\boldsymbol{\Sigma}}_{reg,k^*}^{(\hat{\boldsymbol{w}}_{\boldsymbol{z}}|\hat{\boldsymbol{w}}_{\boldsymbol{z}})}\right)^{-1} \left(\boldsymbol{z}^{(\hat{\boldsymbol{w}}_{\boldsymbol{z}})} - \hat{\boldsymbol{\mu}}_{k^*}^{(\hat{\boldsymbol{w}}_{\boldsymbol{z}})}\right),$$

where $\hat{\boldsymbol{\Sigma}}_{reg,k^*}^{(j^*|\hat{\boldsymbol{w}}_{\boldsymbol{z}})}$ indicates the submatrix $\hat{\boldsymbol{\Sigma}}_{reg,k^*}$ consisting of the j^*-th row and the observed variables of $\boldsymbol{z}$ as columns, see also Equations (9) and (10).

Denoting the set of observations of $\mathcal{Z}$ where variable j^* is observed as $\mathcal{O}_{j^*} = \{\boldsymbol{z} \in \mathcal{Z} : \hat{w}_{\boldsymbol{z},j^*} = 1\}$, we can separate the sum term into

$$\begin{aligned}
\hat{\mu}_{k^*j^*}(\mathcal{Z}) &= \frac{1}{\bar{t}_{k^*}} \sum_{g=1}^{N} \sum_{\boldsymbol{z} \in \boldsymbol{Z}_g} \hat{t}_{k^*}(\boldsymbol{z}) \hat{z}_{j^*} \\
&= \frac{1}{\bar{t}_{k^*}} \sum_{g \neq g'} \sum_{\boldsymbol{x} \in \boldsymbol{Z}_g} \hat{t}_{k^*}(\boldsymbol{x}) \hat{x}_{j^*} + \frac{1}{\bar{t}_{k^*}} \sum_{\boldsymbol{z} \in \boldsymbol{Z}_{g'}} \hat{t}_{k^*}(\boldsymbol{z}) \hat{z}_{j^*} \\
&= \frac{1}{\bar{t}_{k^*}} \sum_{g=1}^{N} \sum_{\boldsymbol{x} \in \boldsymbol{Z}_g \cap \mathcal{X}} \hat{t}_{k^*}(\boldsymbol{x}) \hat{x}_{j^*} + \frac{1}{\bar{t}_{k^*}} \sum_{\boldsymbol{y} \in \boldsymbol{Z}_{g'} \cap \mathcal{Y}} \hat{t}_{k^*}(\boldsymbol{y}) \hat{y}_{j^*} \\
&= \frac{1}{\bar{t}_{k^*}} \sum_{g=1}^{N} \sum_{\boldsymbol{x} \in \boldsymbol{Z}_g \cap \mathcal{X} \cap \mathcal{O}_{j^*}} \hat{t}_{k^*}(\boldsymbol{x}) \hat{x}_{j^*} + \frac{1}{\bar{t}_{k^*}} \sum_{g=1}^{N} \sum_{\boldsymbol{x} \in \boldsymbol{Z}_g \cap \mathcal{X} \cap \mathcal{O}_{j^*}^c} \hat{t}_{k^*}(\boldsymbol{x}) \hat{x}_{j^*} \\
&\quad + \frac{1}{\bar{t}_{k^*}} \sum_{\boldsymbol{y} \in \boldsymbol{Z}_{g'} \cap \mathcal{Y} \cap \mathcal{O}_{j^*}} \hat{t}_{k^*}(\boldsymbol{y}) \hat{y}_{j^*} + \frac{1}{\bar{t}_{k^*}} \sum_{\boldsymbol{y} \in \boldsymbol{Z}_{g'} \cap \mathcal{Y} \cap \mathcal{O}_{j^*}^c} \hat{t}_{k^*}(\boldsymbol{y}) \hat{y}_{j^*} \\
&= \frac{1}{\bar{t}_{k^*}} \sum_{g=1}^{N} \sum_{\boldsymbol{x} \in \boldsymbol{Z}_g \cap \mathcal{X} \cap \mathcal{O}_{j^*}} \hat{t}_{k^*}(\boldsymbol{x}) x_{j^*} + \frac{1}{\bar{t}_{k^*}} \sum_{\boldsymbol{y} \in \boldsymbol{Z}_{g'} \cap \mathcal{Y} \cap \mathcal{O}_{j^*}} \hat{t}_{k^*}(\boldsymbol{y}) y_{j^*} \\
&\quad + \frac{1}{\bar{t}_{k^*}} \sum_{g=1}^{N} \sum_{\boldsymbol{x} \in \boldsymbol{Z}_g \cap \mathcal{X} \cap \mathcal{O}_{j^*}^c} \hat{t}_{k^*}(\boldsymbol{x}) \Big[\hat{\mu}_{k^*j^*}(\mathcal{Z}) + \hat{\boldsymbol{\Sigma}}_{reg,k^*}^{(j^*|\hat{\boldsymbol{w}}_{\boldsymbol{x}})} \left(\hat{\boldsymbol{\Sigma}}_{reg,k^*}^{(\hat{\boldsymbol{w}}_{\boldsymbol{x}}|\hat{\boldsymbol{w}}_{\boldsymbol{x}})}\right)^{-1} \\
&\quad \times \left(\boldsymbol{x}^{(\hat{\boldsymbol{w}}_{\boldsymbol{x}})} - \hat{\boldsymbol{\mu}}_{k^*}(\mathcal{Z})^{(\hat{\boldsymbol{w}}_{\boldsymbol{x}})}\right) \Big] + \frac{1}{\bar{t}_{k^*}} \sum_{\boldsymbol{y} \in \boldsymbol{Z}_{g'} \cap \mathcal{Y} \cap \mathcal{O}_{j^*}^c} \hat{t}_{k^*}(\boldsymbol{y}) \Big[\hat{\mu}_{k^*j^*}(\mathcal{Z}) \\
&\quad + \hat{\boldsymbol{\Sigma}}_{reg,k^*}^{(j^*|\hat{\boldsymbol{w}}_{\boldsymbol{y}})} \left(\hat{\boldsymbol{\Sigma}}_{reg,k^*}^{(\hat{\boldsymbol{w}}_{\boldsymbol{y}}|\hat{\boldsymbol{w}}_{\boldsymbol{y}})}\right)^{-1} \left(\boldsymbol{y}^{(\hat{\boldsymbol{w}}_{\boldsymbol{y}})} - \hat{\boldsymbol{\mu}}_{k^*}(\mathcal{Z})^{(\hat{\boldsymbol{w}}_{\boldsymbol{y}})}\right) \Big].
\end{aligned}$$

Subtracting the estimated location on the uncontaminated sample $\hat{\mu}_{k^*j^*}(\mathcal{X})$

and using that the location estimator is not breaking down, we further get

$$
\begin{aligned}
&\underbrace{\hat{\mu}_{k^*j^*}(\mathcal{Z}) - \hat{\mu}_{k^*j^*}(\mathcal{X})}_{\text{bounded}} = \\
&= \frac{1}{\bar{t}_{k^*}} \sum_{g=1}^{N} \sum_{\boldsymbol{x} \in \boldsymbol{Z}_g \cap \mathcal{X} \cap \mathcal{O}_{j^*}} \hat{t}_{k^*}(\boldsymbol{x}) \underbrace{(x_{j^*} - \hat{\mu}_{k^*j^*}(\mathcal{X}))}_{*} \\
&+ \frac{1}{\bar{t}_{k^*}} \sum_{\boldsymbol{y} \in \boldsymbol{Z}_{g'} \cap \mathcal{Y} \cap \mathcal{O}_{j^*}} \hat{t}_{k^*}(\boldsymbol{y}) \underbrace{(y_{j^*} - \hat{\mu}_{k^*j^*}(\mathcal{X}))}_{\to -\infty} \\
&+ \frac{1}{\bar{t}_{k^*}} \sum_{g=1}^{N} \sum_{\boldsymbol{x} \in \boldsymbol{Z}_g \cap \mathcal{X} \cap \mathcal{O}^c_{j^*}} \hat{t}_{k^*}(\boldsymbol{x}) \\
&\qquad \left[\underbrace{\hat{\mu}_{k^*j^*}(\mathcal{Z}) - \hat{\mu}_{k^*j^*}(\mathcal{X})}_{\text{bounded}} + \hat{\boldsymbol{\Sigma}}^{(j^*|\hat{\boldsymbol{w}}_{\boldsymbol{x}})}_{reg,k^*} \left(\hat{\boldsymbol{\Sigma}}^{(\hat{\boldsymbol{w}}_{\boldsymbol{x}}|\hat{\boldsymbol{w}}_{\boldsymbol{x}})}_{reg,k^*} \right)^{-1} \underbrace{\left(\boldsymbol{x}^{(\hat{\boldsymbol{w}}_{\boldsymbol{x}})} - \hat{\boldsymbol{\mu}}_{k^*}(\mathcal{Z})^{(\hat{\boldsymbol{w}}_{\boldsymbol{x}})} \right)}_{*} \right] \\
&+ \frac{1}{\bar{t}_{k^*}} \sum_{\boldsymbol{y} \in \boldsymbol{Z}_{g'} \cap \mathcal{Y} \cap \mathcal{O}^c_{j^*}} \hat{t}_{k^*}(\boldsymbol{y}) \\
&\qquad \left[\underbrace{\hat{\mu}_{k^*j^*}(\mathcal{Z}) - \hat{\mu}_{k^*j^*}(\mathcal{X})}_{\text{bounded}} + \hat{\boldsymbol{\Sigma}}^{(j^*|\hat{\boldsymbol{w}}_{\boldsymbol{y}})}_{reg,k^*} \left(\hat{\boldsymbol{\Sigma}}^{(\hat{\boldsymbol{w}}_{\boldsymbol{y}}|\hat{\boldsymbol{w}}_{\boldsymbol{y}})}_{reg,k^*} \right)^{-1} \left(\boldsymbol{y}^{(\hat{\boldsymbol{w}}_{\boldsymbol{y}})} - \hat{\boldsymbol{\mu}}_{k^*}(\mathcal{Z})^{(\hat{\boldsymbol{w}}_{\boldsymbol{y}})} \right) \right].
\end{aligned}
$$

Due to Corollary 1a. the objective function of the uncontaminated sample is finite and due to Theorem 2, part a. and c., the estimated covariances on the uncontaminated sample are bounded and regular. Since we assume that the location estimator is not breaking down, variables cannot be separated (otherwise a similar counter example to part d. can be constructed). Thus, for all $\boldsymbol{x} \in \mathcal{X}$ there exists k such that $|\boldsymbol{x}^{(\boldsymbol{w})} - \hat{\boldsymbol{\mu}}_k^{(\boldsymbol{w})}(\mathcal{X})|$ bounded for all feasible $\boldsymbol{w}$ – otherwise the objective function would explode – and thus, if $|\boldsymbol{x}^{(\boldsymbol{w})} - \hat{\boldsymbol{\mu}}_l^{(\boldsymbol{w})}(\mathcal{X})| \to \infty$ for $l \neq k$ it follows that $\hat{t}_l(\boldsymbol{x}) \to 0$ and $t_l(\boldsymbol{x})(\boldsymbol{x}^{(\boldsymbol{w})} - \hat{\boldsymbol{\mu}}_l^{(\boldsymbol{w})}(\mathcal{X})) \to 0$. Thus, all subtraction parts marked with $*$ are bounded. The last term $\hat{t}_{k^*}(\boldsymbol{y}) \left(\boldsymbol{y}^{(\hat{\boldsymbol{w}}_{\boldsymbol{y}})} - \hat{\boldsymbol{\mu}}_{k^*}(\mathcal{Z})^{(\hat{\boldsymbol{w}}_{\boldsymbol{y}})} \right)$ is also bounded, since outliers are only outlying in variable j^* and otherwise they are part of one cluster. Thus, with the same argument as for uncontaminated data, the term is bounded.

Since $\hat{t}_{k^*}(\tilde{\boldsymbol{y}}) \geq 1/N$ and $\tilde{\boldsymbol{y}} \in \boldsymbol{Z}_{g'} \cap \mathcal{Y} \cap \mathcal{O}_{j^*}$ the whole sum of $\in \boldsymbol{Z}_{g'} \cap \mathcal{Y} \cap \mathcal{O}_{j^*}$ goes to minus infinity. To enable the equality of both sides, at least one of the covariances needs to explode (in variable j^*) to counteract the exploding sum.

□

C Algorithm

In this section details on initialization and additional derivations for the EM-step are provided.

C.1 Initialization

First, all data sets are standardized robustly on a global scale (meaning as if the group structure is not known) using the wrapped location (see also default options in function `estLocScale` from the R-package `cellWise` Raymaekers et al., 2023). This leads to global scale and shift invariance and is helpful to stabilize the regularization approach based on the condition number of the estimated covariance matrices. For a given α the initial estimate for $\hat{\boldsymbol{\pi}}^0$ is

$$\hat{\boldsymbol{\pi}}^0 = \begin{bmatrix} \alpha & \frac{1-\alpha}{N-1} & \cdots & \frac{1-\alpha}{N-1} \\ \frac{1-\alpha}{N-1} & \alpha & \cdots & \frac{1-\alpha}{N-1} \\ \vdots & \vdots & \ddots & \vdots \\ \frac{1-\alpha}{N-1} & \frac{1-\alpha}{N-1} & \cdots & \alpha \end{bmatrix}.$$

Then the other initial values are estimated for each group separately according to the following steps:

1. Based on the scaled and centered data sets, local robust scales $\hat{\sigma}_{k,j}$ for group k and variable j are calculated using the univariate MCD. The regularization matrices are then defined as $\boldsymbol{T}_k = \text{diag}(\hat{\sigma}_{k,1}, \ldots, \hat{\sigma}_{k,p})$.

2. Define the condition number to achieve for distribution k as

$$\kappa_k = \max\left\{100, 1.1\frac{\lambda_1(\boldsymbol{T}_k)}{\lambda_p(\boldsymbol{T}_k)}\right\}.$$

3. We use the DDCW as in Raymaekers and Rousseeuw (2023), applied separately for each group, to get initial estimates $\hat{\boldsymbol{\Sigma}}^0_{reg,k}$ and $\hat{\boldsymbol{\mu}}^0_k$. While this approach is not feasible in normal clustering, here we assume that each group has a main distribution enforced by Equation (7). Thus, taking a robust estimate of the covariance and mean of the main bulk of the observations for each group separately is reasonable and a good initial estimate of the corresponding main distribution. To ensure regularity also in cases with low number of observation in a group k, each time a covariance is calculated during the DDCW-algorithm, it is regularized with regularization matrix $\boldsymbol{T}_k$ and an adaptive regularization factor ρ_k ensuring a maximal condition number of κ_k.

4. Similar to the initialization in Raymaekers and Rousseeuw (2023) the entries of the matrices $\boldsymbol{W}^0$ are all set to one.

After the convergence of the algorithm all data are rescaled to the original scale.

C.2 EM-Step

The Expectation-Maximization Algorithm (Dempster et al., 1977; McLachlan and Krishnan, 2008) is often used to find maximum likelihood estimates in setting where data is incomplete - meaning that some random variables are not observed. Here, this includes the values of missing cells indicated by the given $\boldsymbol{W}$ and the class of an observation which is an often used approach in the context of mixture models.

For each observation $\boldsymbol{x}_{g,i}$ a binary random variable $z_{g,i,k}$ indicates whether it was drawn from distribution k. The likelihood resulting from including the additional random variables $z_{g,i,k}$ is called the *complete log-likelihood* and the resulting objective function the *complete objective function* $\mathrm{CObj}(\boldsymbol{\pi}, \boldsymbol{\mu}, \boldsymbol{\Sigma}, \boldsymbol{W}, \boldsymbol{Z})$ is -2 times

$$\sum_{g=1}^{N}\sum_{i=1}^{n_g}\left[\sum_{\substack{k=1\\ \pi_{g,k}\neq 0}}^{N} z_{g,i,k}\ln\left(\pi_{g,k}\varphi\left(\boldsymbol{x}_{g,i}^{(\boldsymbol{w}_{g,i})};\boldsymbol{\mu}_k^{(\boldsymbol{w}_{g,i})},\boldsymbol{\Sigma}_{reg,k}^{(\boldsymbol{w}_{g,i})}\right)\right)+\sum_{j=1}^{p} q_{g,i,j}(1-w_{g,ij})\right],$$

where $\boldsymbol{Z}$ includes all random variables $z_{g,i,k}$. When taking the conditional expectation of $z_{g,i,k}$,

$$t_{g,i,k}=\mathbb{E}[z_{g,i,k}|\boldsymbol{x}_{g,i}^{(\boldsymbol{w}_{g,i})},\boldsymbol{\pi},\boldsymbol{\mu},\boldsymbol{\Sigma},\boldsymbol{W}]=\frac{\pi_{g,k}\varphi\left(\boldsymbol{x}_{g,i}^{(\boldsymbol{w}_{g,i})};\boldsymbol{\mu}_k^{(\boldsymbol{w}_{g,i})},\boldsymbol{\Sigma}_{reg,k}^{(\boldsymbol{w}_{g,i})}\right)}{\sum_{l=1}^{N}\pi_{g,l}\varphi\left(\boldsymbol{x}_{g,i}^{(\boldsymbol{w}_{g,i})};\boldsymbol{\mu}_l^{(\boldsymbol{w}_{g,i})},\boldsymbol{\Sigma}_{reg,l}^{(\boldsymbol{w}_{g,i})}\right)},$$

we can formulate the *expected objective function* $\mathrm{EObj}(\boldsymbol{\pi}, \boldsymbol{\mu}, \boldsymbol{\Sigma}, \boldsymbol{W})$, which is -2 times

$$\sum_{g=1}^{N}\sum_{i=1}^{n_g}\left[\sum_{\substack{k=1\\ \pi_{g,k}\neq 0}}^{N} t_{g,i,k}\ln\left(\pi_{g,k}\varphi\left(\boldsymbol{x}_{g,i}^{(\boldsymbol{w}_{g,i})};\boldsymbol{\mu}_k^{(\boldsymbol{w}_{g,i})},\boldsymbol{\Sigma}_{reg,k}^{(\boldsymbol{w}_{g,i})}\right)\right)+\sum_{j=1}^{p} q_{g,i,j}(1-w_{g,ij})\right]. \tag{23}$$

The Expectation-Maximization algorithm then leverages that we can iteratively take the expectation and then maximize the expected objective function in Equation (23). Overall this approach gives us at least the same or more optimal next estimates after each iteration.

The extension of the maximization step regarding the parameters $\boldsymbol{\mu}$ and $\boldsymbol{\Sigma}$ for the Gaussian Mixture Model with missing values (Eirola et al., 2014) to the multi-group GMM with missing values is straight forward since the group structure can be ignored once the conditional expectation of $z_{g,i,k}$ is calculated.

The only difference is the estimation of the mixture probabilities $\boldsymbol{\pi}$ due to the constraint $\pi_{g,g} \geq \alpha$ and $\sum_{k=1}^{N}\pi_{g,k} = 1$ for all $g = 1, \ldots, N$. To find the optimal mixture probability the Karush-Kuhn-Tucker theorem can be applied. We set the derivative of the expected objective function in Equation (23)with

respect to $\pi_{g,l}$ to zero, then the following conditions have to hold

$$\begin{aligned}\frac{\partial[EObj + \lambda(1 - \sum_{k=1}^{N} \pi_{g,k}) + \mu(\alpha - \pi_{g,g})]}{\partial \pi_{g,l}} &= 0\\ \mu(\alpha - \pi_{g,g}) &= 0\\ \mu &\geq 0\\ 1 - \sum_{k=1}^{N} \pi_{g,k} &= 0.\end{aligned}$$

Plugging in the concrete formula from Equation (23) leads to ($\mathbb{I}$ denoting the indicator function)

$$\begin{aligned}0 =& \frac{-2\sum_{i=1}^{n_g} t_{g,i,l}}{\pi_{g,l}} - \lambda - \mu \mathbb{I}_{l=g}\\ -2\sum_{i=1}^{n_g} t_{g,i,l} =& \lambda \pi_{g,l} + \mu \mathbb{I}_{l=g} \pi_{g,l}\\ -2\sum_{i=1}^{n_g}\sum_{l=1,l\neq g}^{N} t_{g,i,l} =& \lambda \sum_{l=1,l\neq g}^{N} \pi_{g,l} + \mu \sum_{l=1,l\neq g}^{N} \mathbb{I}_{l=g}\pi_{g,l}\\ \lambda =& \frac{-2\sum_{i=1}^{n_g}\sum_{l=1,l\neq g}^{N} t_{g,i,l}}{(1-\pi_{g,g})} = \frac{-2\sum_{i=1}^{n_g}(1-t_{g,i,g})}{(1-\pi_{g,g})},\end{aligned}$$

where we sum over all $l \neq g$ from the third row on. Plugging λ in leads to

$$\pi_{g,l} = \frac{(1-\pi_{g,g})\sum_{i=1}^{n_g} t_{g,i,l}}{\sum_{i=1}^{n_g}(1-t_{g,i,g})} = (1-\pi_{g,g})\frac{\frac{1}{n_g}\sum_{i=1}^{n_g} t_{g,i,l}}{1-\frac{1}{n_g}\sum_{i=1}^{n_g} t_{g,i,g}}.$$

For the Lagrange parameter μ we finally have

$$\begin{aligned}\frac{-\frac{1}{n_g}\sum_{i=1}^{n_g} t_{g,i,g}}{\pi_{g,g}} + \frac{(1-\frac{1}{n_g}\sum_{i=1}^{n_g} t_{g,i,g})}{(1-\pi_{g,g})} =& \frac{\mu}{2n_g} \geq 0\\ \frac{\pi_{g,g}}{(1-\pi_{g,g})} \geq& \frac{\frac{1}{n_g}\sum_{i=1}^{n_g} t_{g,i,g}}{(1-\frac{1}{n_g}\sum_{i=1}^{n_g} t_{g,i,g})}\end{aligned}$$

Since $f(x) = x/(1-x)$ is monotonously increasing, this is fulfilled if $\pi_{g,g} \geq \frac{1}{n_g}\sum_{i=1}^{n_g} t_{g,i,g}$. Thus, if the inequality is strict, $\mu > 0$ and $\pi_{g,g} = \alpha$. Otherwise, $\pi_{g,g} = \frac{1}{n_g}\sum_{i=1}^{n_g} t_{g,i,g}$ is a feasible solution which is equal to the unconstrained minimization problem. Overall, we have

$$\pi_{g,g} = \max\left\{\alpha, \frac{1}{n_g}\sum_{i=1}^{n_g} t_{g,i,g}\right\}, \quad \pi_{g,l} = (1-\pi_{g,g})\frac{\frac{1}{n_g}\sum_{i=1}^{n_g} t_{g,i,l}}{1-\frac{1}{n_g}\sum_{i=1}^{n_g} t_{g,i,g}}.$$

Also the regularity condition *linear independence constraint qualification* (LICQ) is fulfilled for all feasible $\boldsymbol{\pi}$.

D Additional simulation results

In the following subsections additional results for the five settings from Section 5 are presented. The settings analyzed are the balanced basic setting ($N = 2, p = 10, n_1 = n_2 = 100$), an unbalanced setting ($N = 2, p = 10, n_1 = 100, n_2 = 50$) as well as a balanced setting with nearly as many variables as observations per group ($N = 2, p = 20, n_1 = 30, n_2 = 30$), a setting with more groups ($N = 5, p = 10, n_1 = \ldots = n_5 = 100$) and a high-dimensional setting ($N = 2, p = 60, n_1 = n_2 = 40$).

For each setting, the performance of parameter estimation compared to competing methods is visualized as well as the correctness of flagging outlying cells. Moreover, for each setting a table with the number of repetitions considered in the figures is given. They can deviate from the default number of 100 due to the restriction of the cellMCD regarding the number of marginal outliers.

D.1 Basic balanced setting

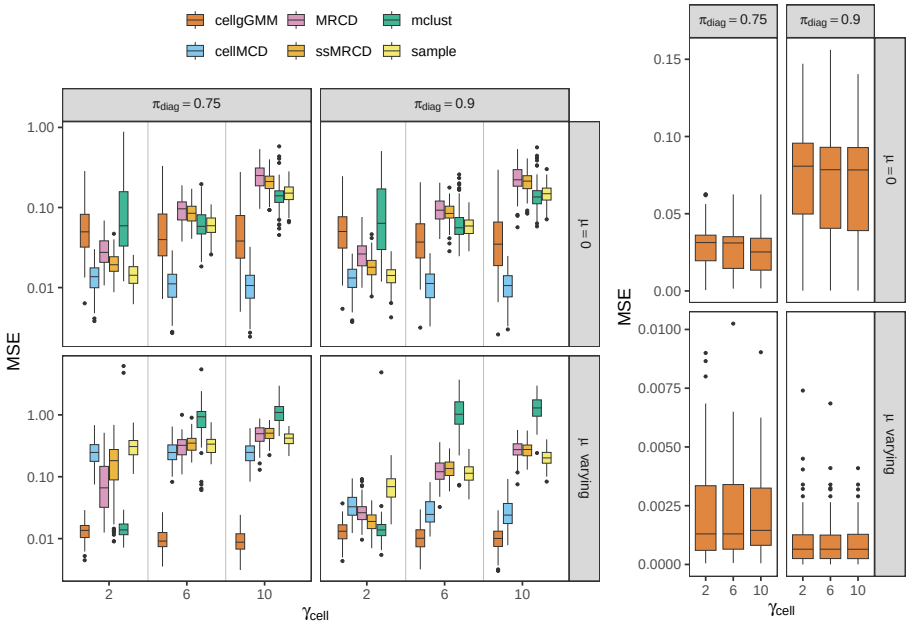

Figure 12: Parameter estimates for the basic balanced setting ($N = 2, p = 10, n_1 = n_2 = 100$) with Toeplitz structured covariances. In the left panel MSE of the mean estimation and in the right the MSE of the mixture probabilities $\boldsymbol{\pi}$.

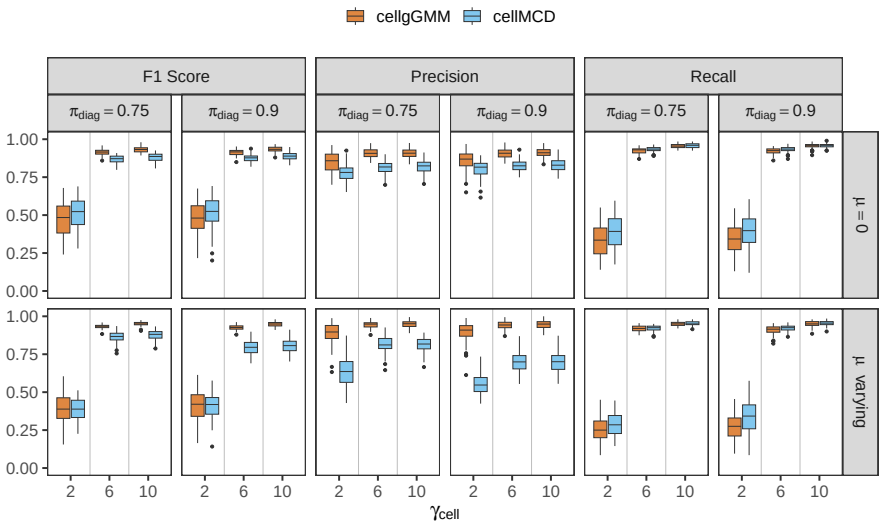

Figure 13: Performance of cellwise outlier detection in the basic balanced setting ($N = 2, p = 10, n_1 = n_2 = 100$) with Toeplitz structured covariances evaluated by precision, recall and F1-score.

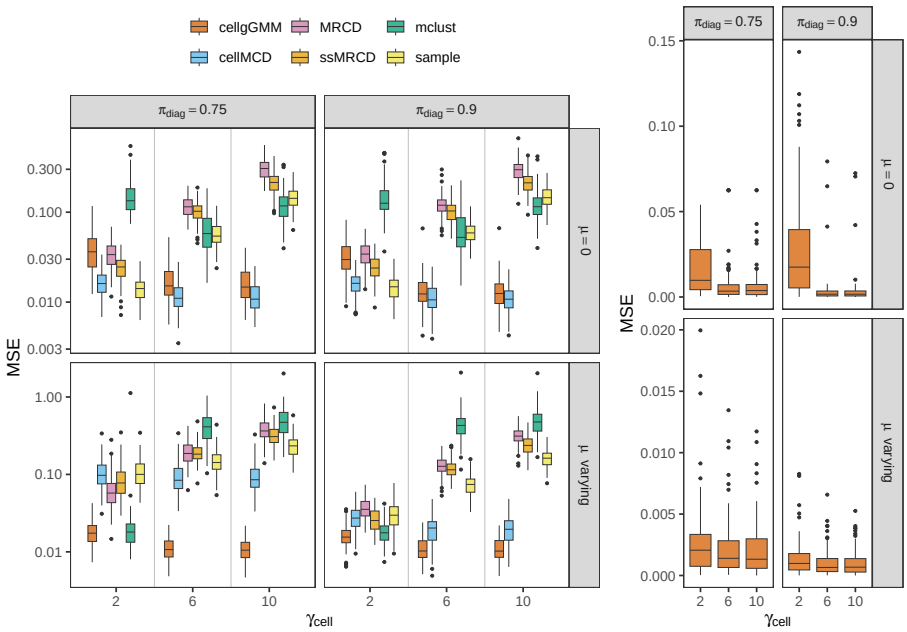

Figure 14: Parameter estimates for the basic balanced setting ($N = 2, p = 10, n_1 = n_2 = 100$) with covariances according to Agostinelli et al. (2015). In the left panel MSE of the mean estimation and in the right the MSE of the mixture probabilities $\boldsymbol{\pi}$.

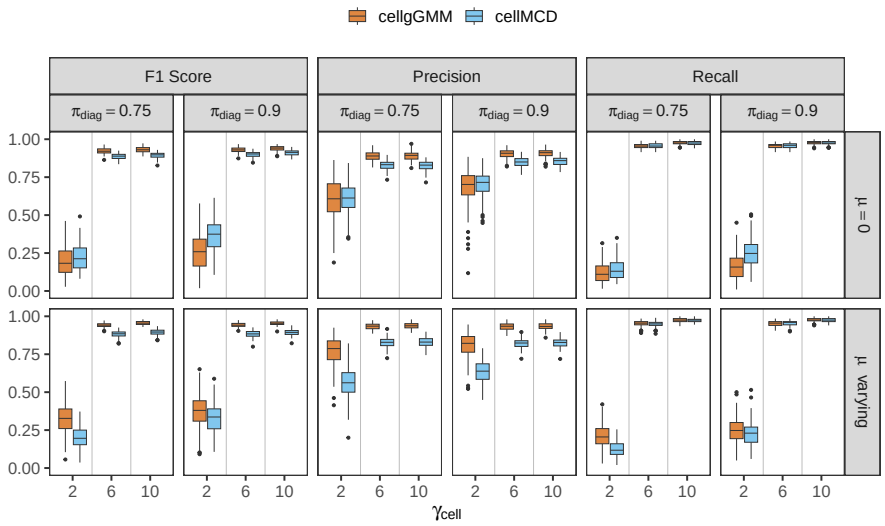

Figure 15: Performance of cellwise outlier detection in the basic balanced setting ($N = 2, p = 10, n_1 = n_2 = 100$) with covariances according to Agostinelli et al. (2015) evaluated by on precision, recall and F1-score.

γ_{cell}	π_{diag}	μ	#
10	0.75	0	100
10	0.75	varying	58
10	0.90	0	100
10	0.90	varying	98
6	0.75	0	100
6	0.75	varying	61
6	0.90	0	100
6	0.90	varying	99
2	0.75	0	100
2	0.75	varying	84
2	0.90	0	100
2	0.90	varying	100

(a) Toeplitz structure.

γ_{cell}	π_{diag}	μ	#
10	0.75	0	100
10	0.75	varying	100
10	0.90	0	100
10	0.90	varying	100
6	0.75	0	100
6	0.75	varying	100
6	0.90	0	100
6	0.90	varying	100
2	0.75	0	100
2	0.75	varying	100
2	0.90	0	100
2	0.90	varying	100

(b) Agostinelli et al. (2015) structure.

Table 1: Number of successful replications for the two covariance structures in the basic balanced setting ($N = 2, p = 10, n_1 = n_2 = 100$), depending on simulation parameters.

D.2 Balanced setting with increased group number

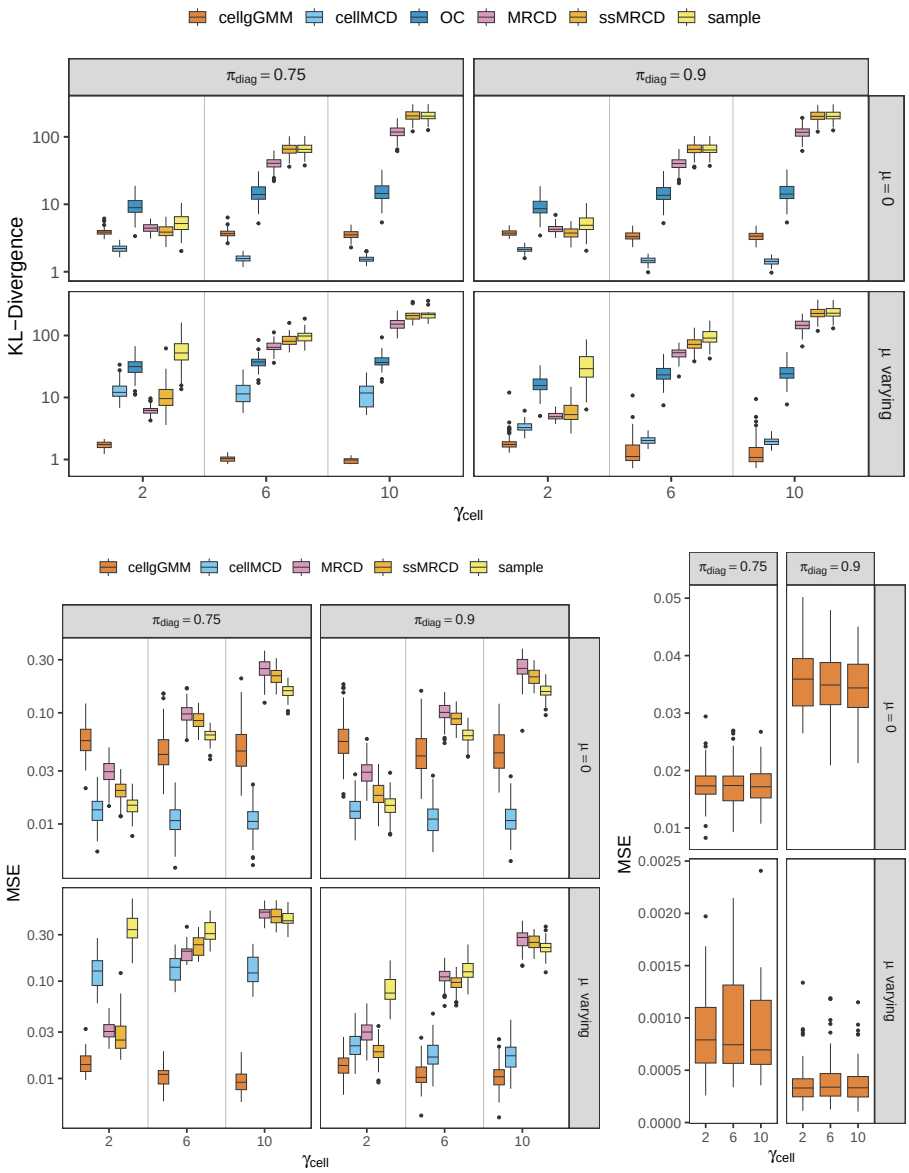

Figure 16: Parameter estimates for the balanced setting with increased number of groups ($N = 5, p = 10, n_1 = \ldots = n_5 = 100$) and Toeplitz structured covariances. On top the KL-divergence of the covariance estimates. On the bottom left panel MSE of the mean estimation and on the bottom right the MSE of the mixture probabilities $\boldsymbol{\pi}$.

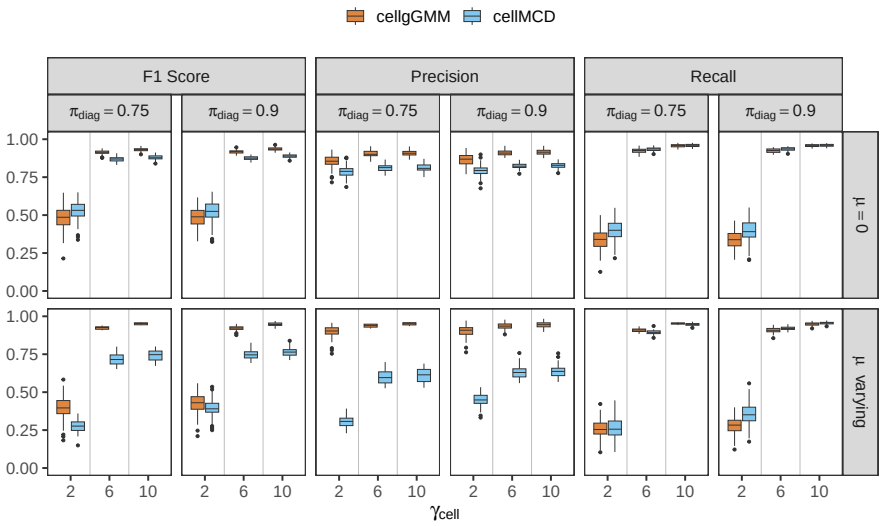

Figure 17: Performance of cellwise outlier detection in the balanced setting with increased number of groups ($N = 5, p = 10, n_1 = \ldots = n_5 = 100$) and Toeplitz structured covariances evaluated by precision, recall and F1-score.

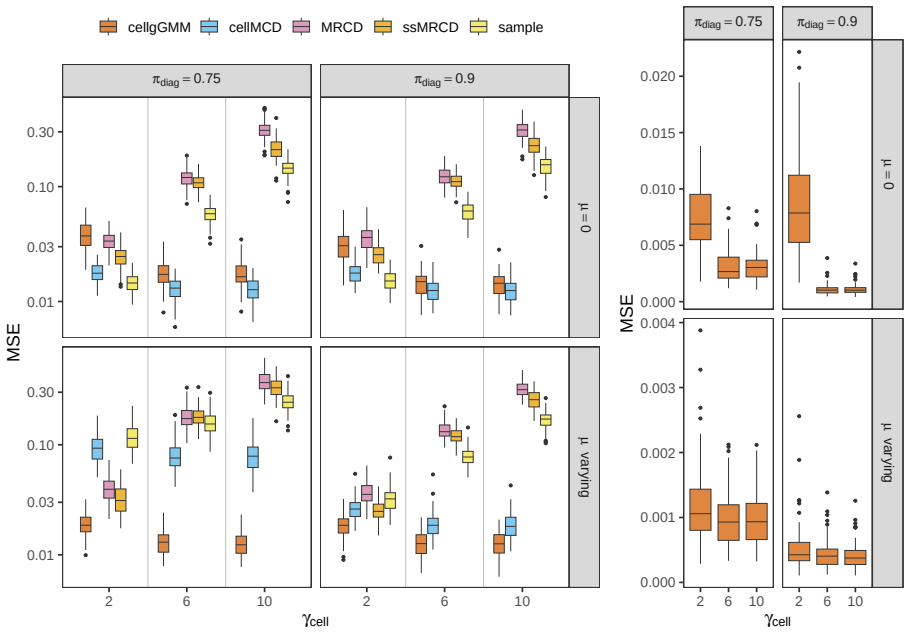

Figure 18: Parameter estimates for the balanced setting with increased number of groups ($N = 5, p = 10, n_1 = \ldots = n_5 = 100$) and covariances according to Agostinelli et al. (2015). in the left panel MSE of the mean estimation and in the right the MSE of the mixture probabilities $\boldsymbol{\pi}$.

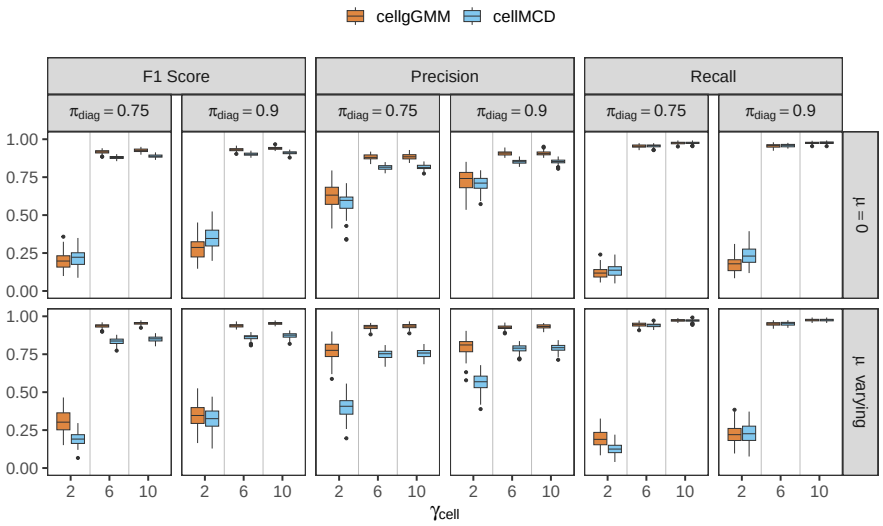

Figure 19: Performance of cellwise outlier detection in the balanced setting with increased number of groups ($N = 5, p = 10, n_1 = \ldots = n_5 = 100$) and covariances according to Agostinelli et al. (2015) evaluated by on precision, recall and F1-score.

γ_{cell}	π_{diag}	μ	#
10	0.75	0	100
10	0.75	varying	16
10	0.90	0	100
10	0.90	varying	99
6	0.75	0	100
6	0.75	varying	21
6	0.90	0	100
6	0.90	varying	100
2	0.75	0	100
2	0.75	varying	61
2	0.90	0	100
2	0.90	varying	100

(a) Toeplitz structure.

γ_{cell}	π_{diag}	μ	#
10	0.75	0	100
10	0.75	varying	96
10	0.90	0	100
10	0.90	varying	100
6	0.75	0	100
6	0.75	varying	96
6	0.90	0	100
6	0.90	varying	100
2	0.75	0	100
2	0.75	varying	100
2	0.90	0	100
2	0.90	varying	100

(b) Agostinelli et al. (2015) structure.

Table 2: Number of successful replications for the two covariance structures in the balanced setting with increased number of groups ($N = 5, p = 10, n_1 = \ldots = n_5 = 100$), depending on simulation parameters.

D.3 Unbalanced groups

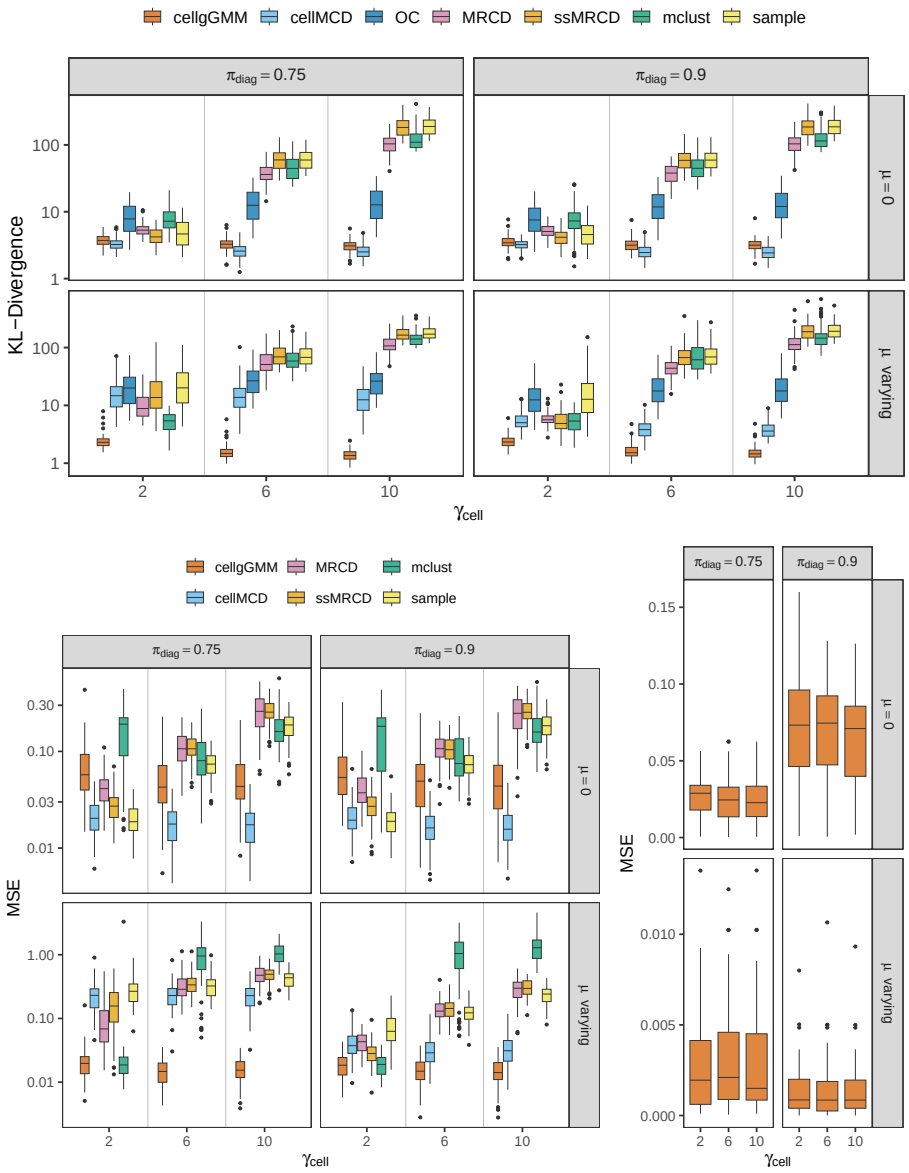

Figure 20: Parameter estimates for the unbalanced setting ($N = 2, p = 10, n_1 = 100, n_2 = 50$) with Toeplitz structured covariances. On top the KL-divergence of the covariance estimates. On the bottom left panel MSE of the mean estimation and on the bottom right the MSE of the mixture probabilities $\boldsymbol{\pi}$.

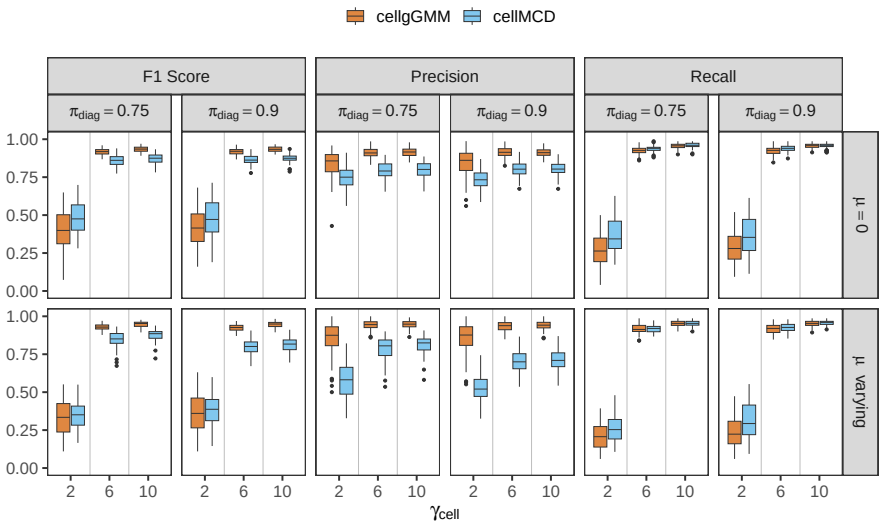

Figure 21: Performance of cellwise outlier detection in the unbalanced setting ($N = 2, p = 10, n_1 = 100, n_2 = 50$) with Toeplitz structured covariances evaluated by precision, recall and F1-score.

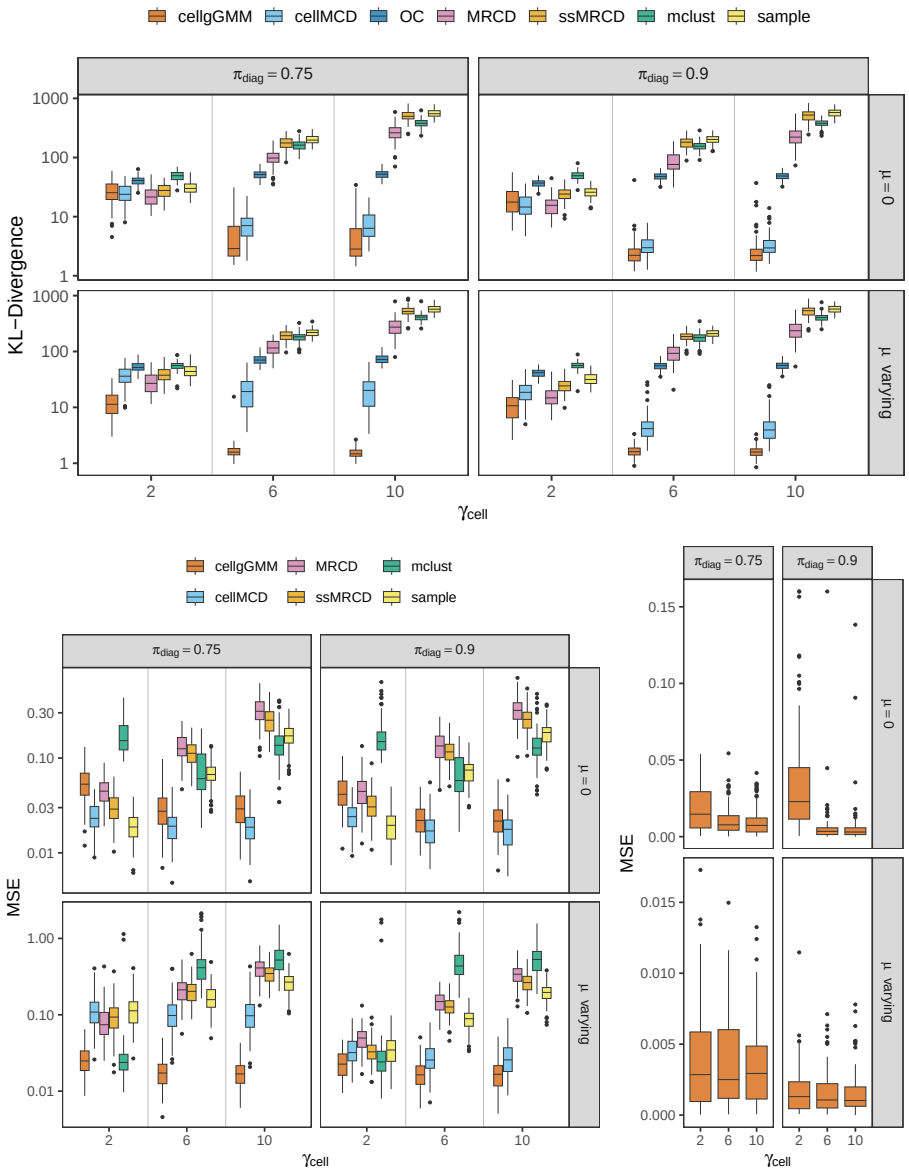

Figure 22: Parameter estimates for the unbalanced setting ($N = 2, p = 10, n_1 = 100, n_2 = 50$) with covariances according to Agostinelli et al. (2015) On top the KL-divergence of the covariance estimates. On the bottom left panel MSE of the mean estimation and on the bottom right the MSE of the mixture probabilities $\boldsymbol{\pi}$.

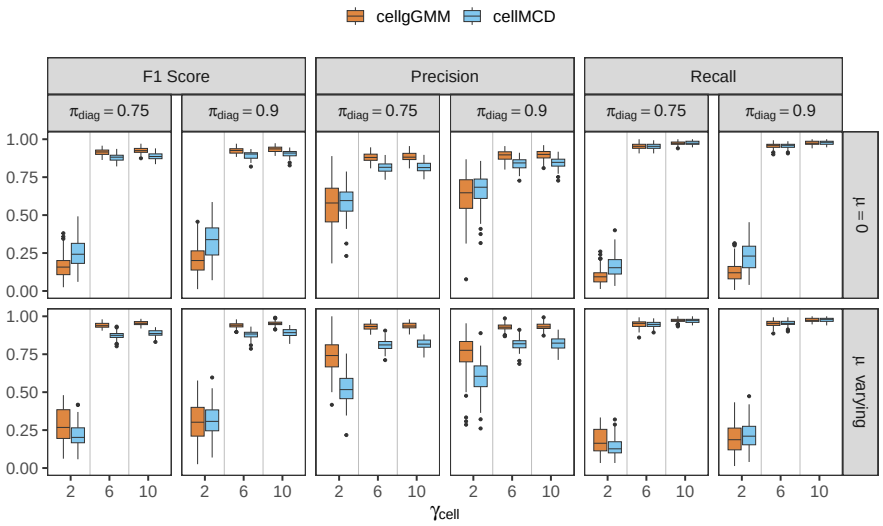

Figure 23: Performance of cellwise outlier detection in the unbalanced setting ($N = 2, p = 10, n_1 = 100, n_2 = 50$) with covariances according to Agostinelli et al. (2015) evaluated by on precision, recall and F1-score.

γ_{cell}	π_{diag}	μ	#
10	0.75	0	100
10	0.75	varying	58
10	0.90	0	100
10	0.90	varying	93
6	0.75	0	100
6	0.75	varying	68
6	0.90	0	100
6	0.90	varying	96
2	0.75	0	100
2	0.75	varying	84
2	0.90	0	100
2	0.90	varying	100

(a) Toeplitz structure.

γ_{cell}	π_{diag}	μ	#
10	0.75	0	100
10	0.75	varying	99
10	0.90	0	100
10	0.90	varying	100
6	0.75	0	100
6	0.75	varying	99
6	0.90	0	100
6	0.90	varying	100
2	0.75	0	100
2	0.75	varying	100
2	0.90	0	100
2	0.90	varying	100

(b) Agostinelli et al. (2015) structure.

Table 3: Number of successful replications for the two covariance structures in the unbalanced setting ($N = 2, p = 10, n_1 = 100, n_2 = 50$), depending on simulation parameters.

D.4 Balanced setting with similar n and p

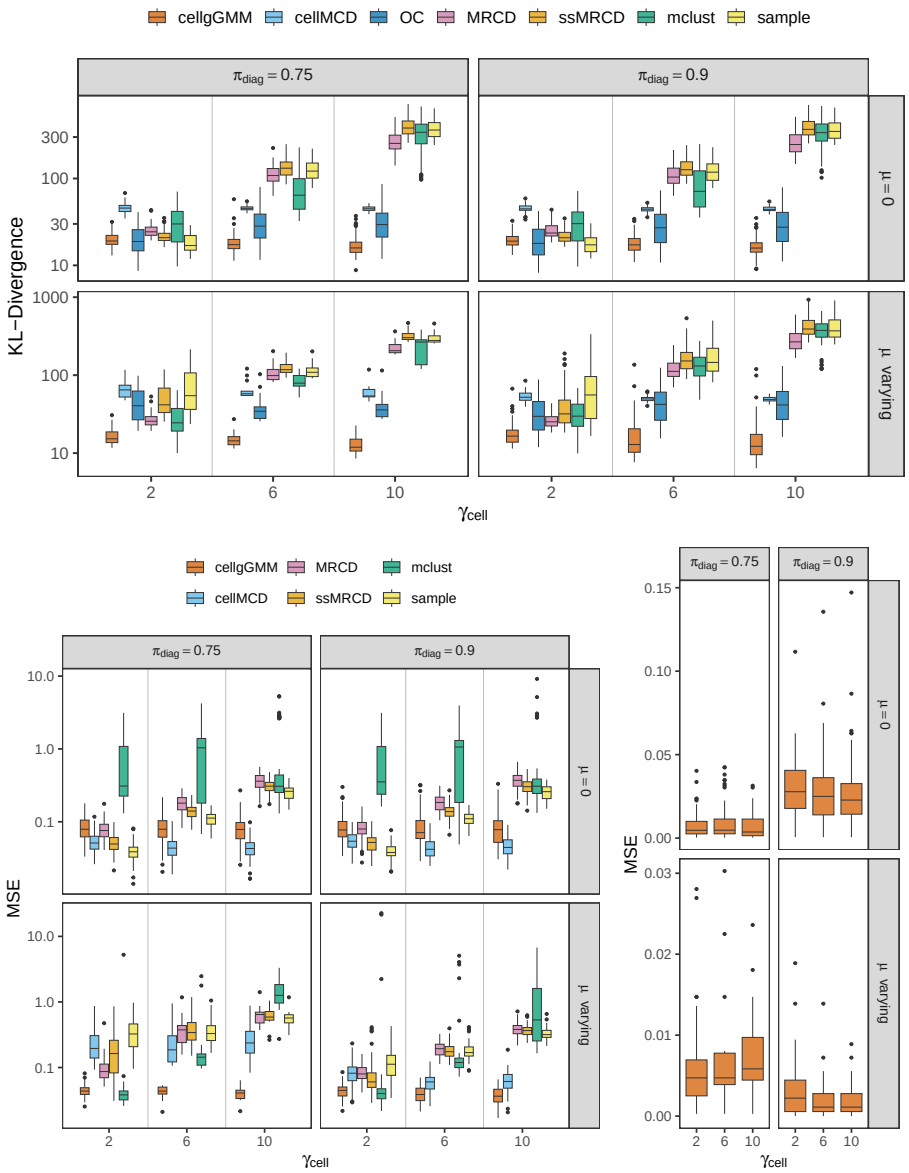

Figure 24: Parameter estimates for the balanced setting with n close to p ($N = 2, p = 20, n_1 = 30, n_2 = 30$) and Toeplitz structured covariances. On top the KL-divergence of the covariance estimates. On the bottom left panel MSE of the mean estimation and on the bottom right the MSE of the mixture probabilities $\boldsymbol{\pi}$.

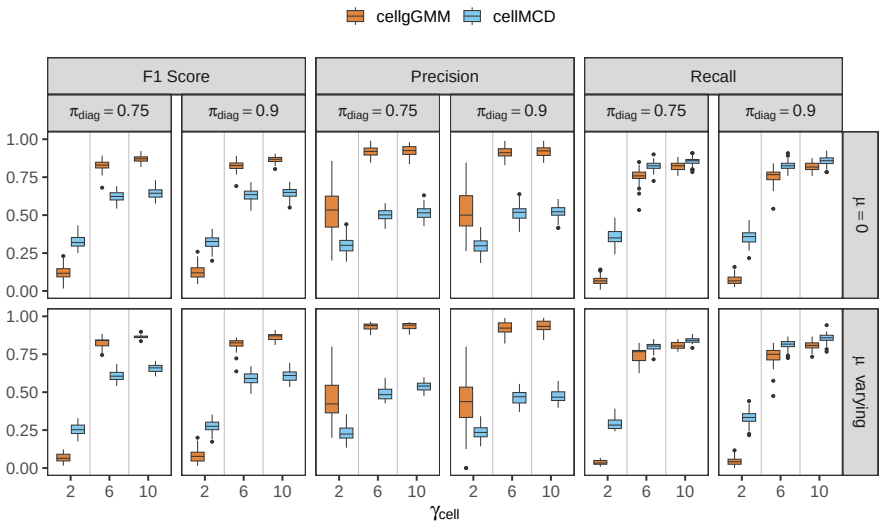

Figure 25: Performance of cellwise outlier detection in the balanced setting with n close to p ($N = 2, p = 20, n_1 = 30, n_2 = 30$) and Toeplitz structured covariances evaluated by precision, recall and F1-score.

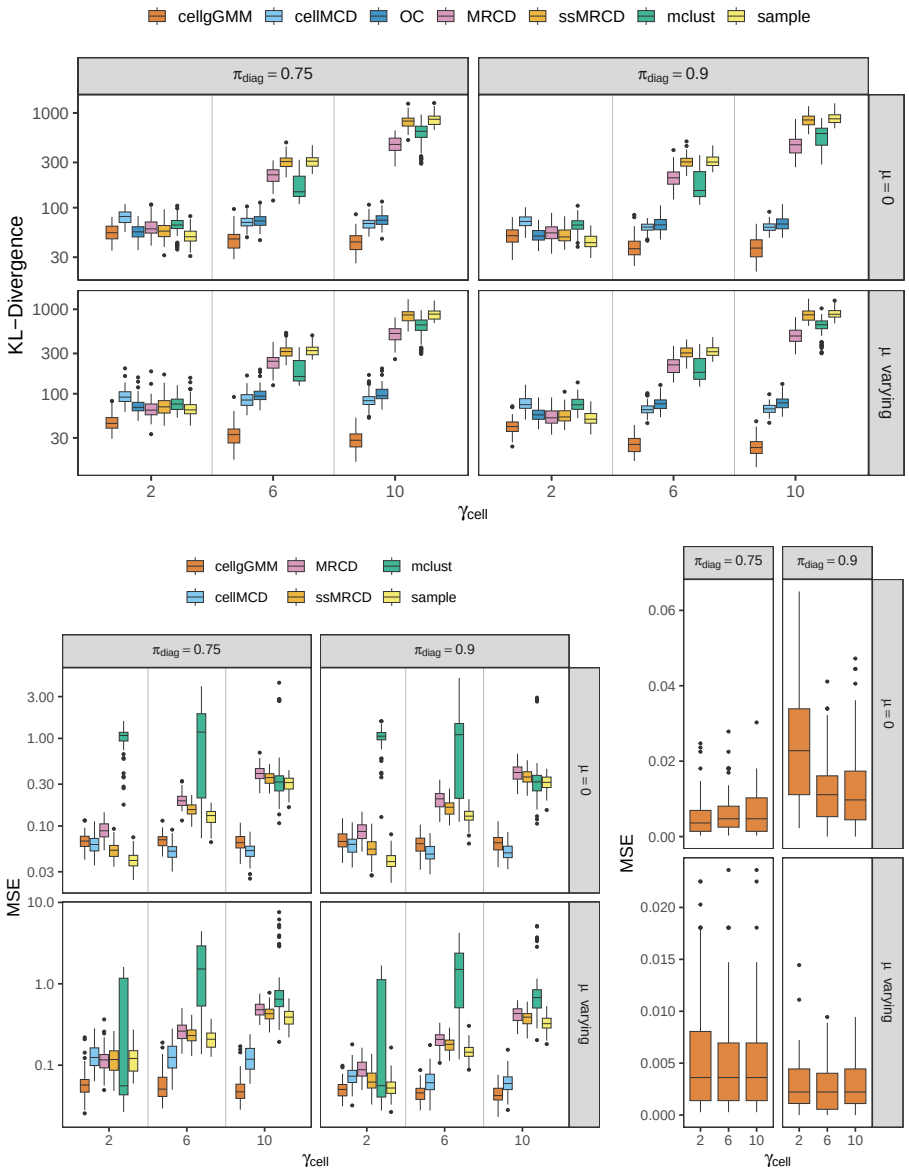

Figure 26: Parameter estimates for the balanced setting with n close to p ($N = 2, p = 20, n_1 = 30, n_2 = 30$) with covariances according to Agostinelli et al. (2015). On top the KL-divergence of the covariance estimates. On the bottom left panel MSE of the mean estimation and on the bottom right the MSE of the mixture probabilities $\boldsymbol{\pi}$.

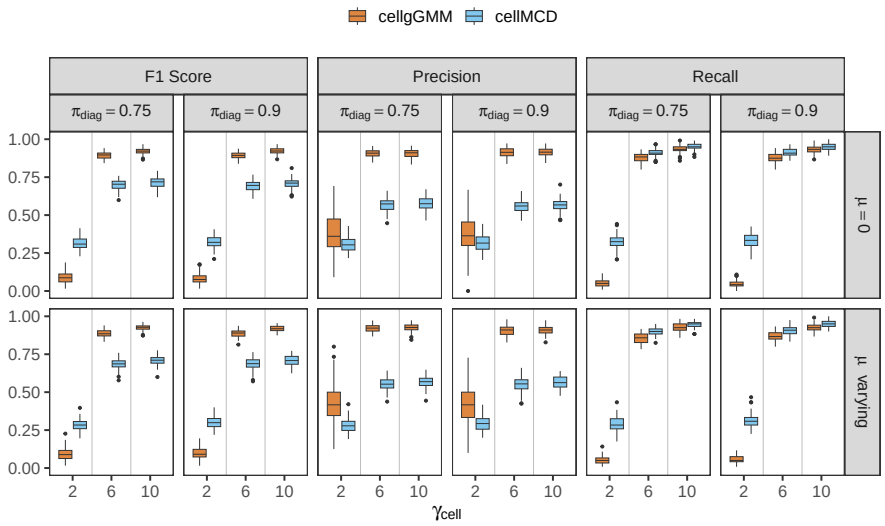

Figure 27: Performance of cellwise outlier detection in the balanced setting with n close to p ($N = 2, p = 20, n_1 = 30, n_2 = 30$) and covariances according to Agostinelli et al. (2015) evaluated by on precision, recall and F1-score.

γ_{cell}	π_{diag}	μ	#
10	0.75	0	84
10	0.75	varying	12
10	0.90	0	84
10	0.90	varying	53
6	0.75	0	84
6	0.75	varying	14
6	0.90	0	85
6	0.90	varying	55
2	0.75	0	89
2	0.75	varying	38
2	0.90	0	88
2	0.90	varying	85

(a) Toeplitz structure.

γ_{cell}	π_{diag}	μ	#
10	0.75	0	79
10	0.75	varying	81
10	0.90	0	82
10	0.90	varying	82
6	0.75	0	81
6	0.75	varying	82
6	0.90	0	83
6	0.90	varying	82
2	0.75	0	92
2	0.75	varying	92
2	0.90	0	88
2	0.90	varying	85

(b) Agostinelli et al. (2015) structure.

Table 4: Number of successful replications for the two covariance structures in the balanced setting with similar sized p and n ($N = 2, p = 20, n_1 = 30, n_2 = 30$), depending on simulation parameters.

D.5 High-dimensional setting

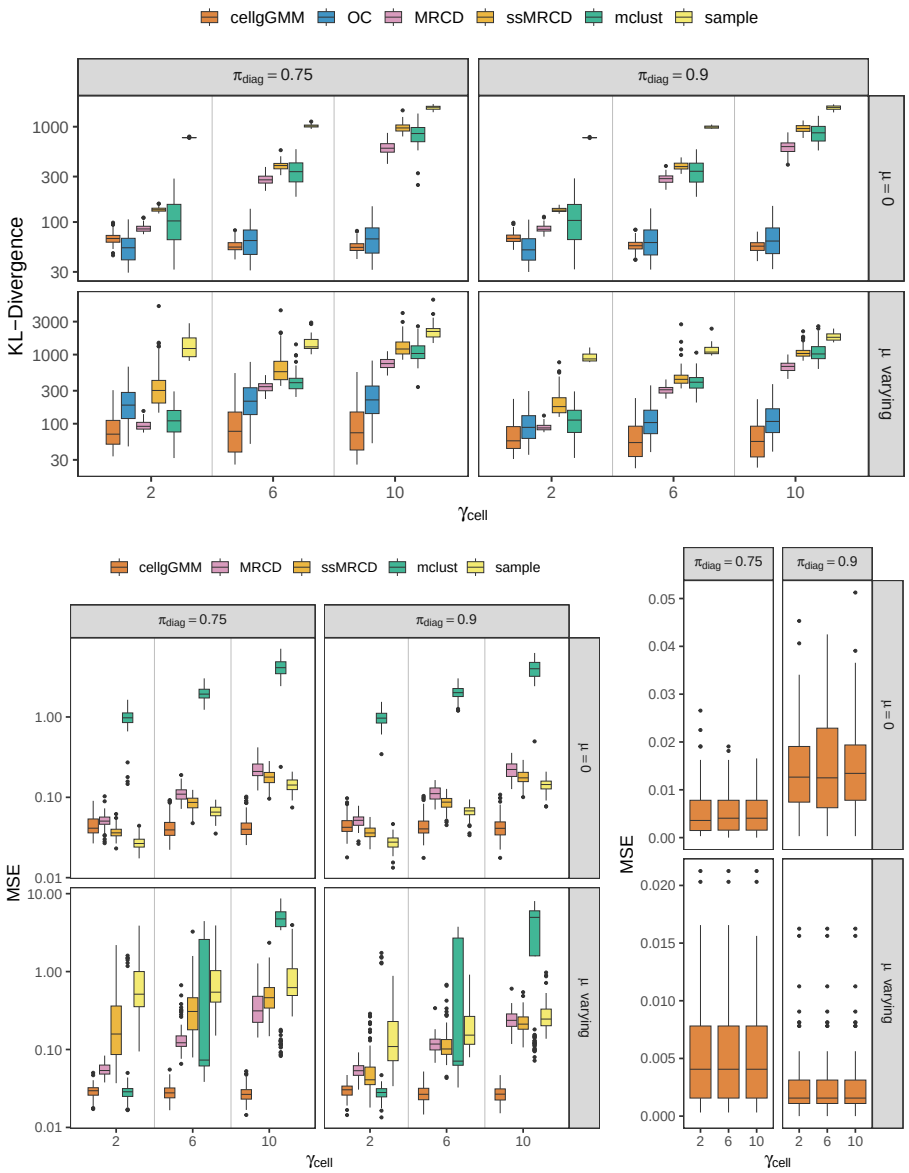

Figure 28: Parameter estimates for the balanced high-dimensional setting ($N = 2, p = 60, n_1 = n_2 = 40$) with Toeplitz structured covariances. On top the KL-divergence of the covariance estimates. On the bottom left panel MSE of the mean estimation and on the bottom right the MSE of the mixture probabilities $\boldsymbol{\pi}$.

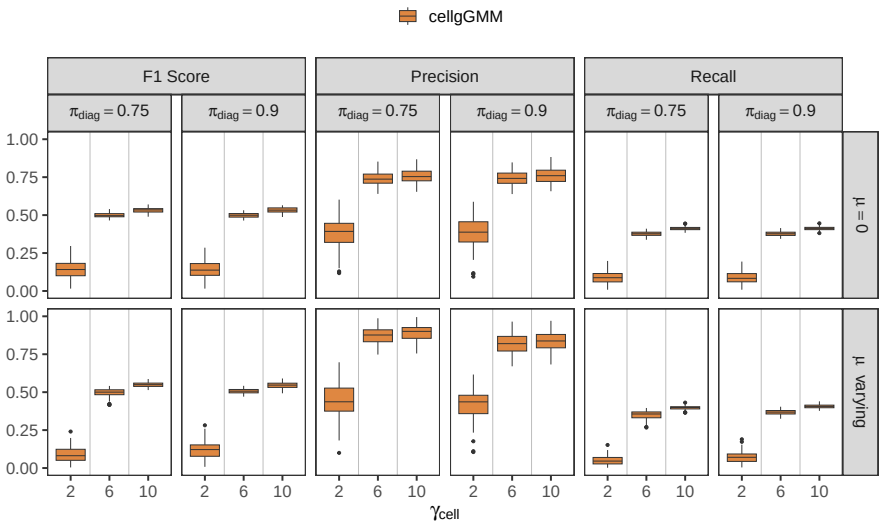

Figure 29: Performance of cellwise outlier detection in the balanced high-dimensional setting ($N = 2, p = 60, n_1 = n_2 = 40$) with Toeplitz structured covariances evaluated by precision, recall and F1-score.

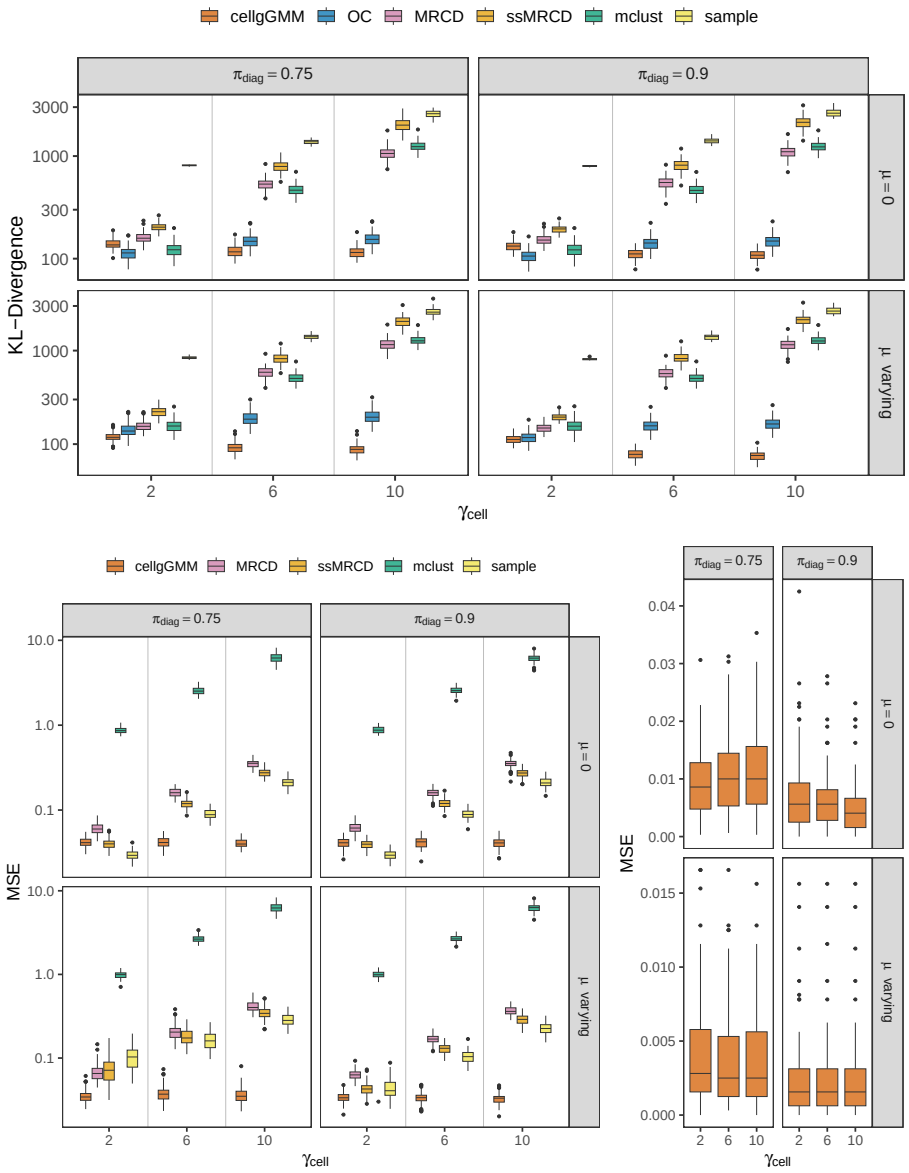

Figure 30: Parameter estimates for the balanced high-dimensional setting ($N = 2, p = 60, n_1 = n_2 = 40$) with covariances according to Agostinelli et al. (2015). On top the KL-divergence of the covariance estimates. On the bottom left panel MSE of the mean estimation and on the bottom right the MSE of the mixture probabilities $\boldsymbol{\pi}$.

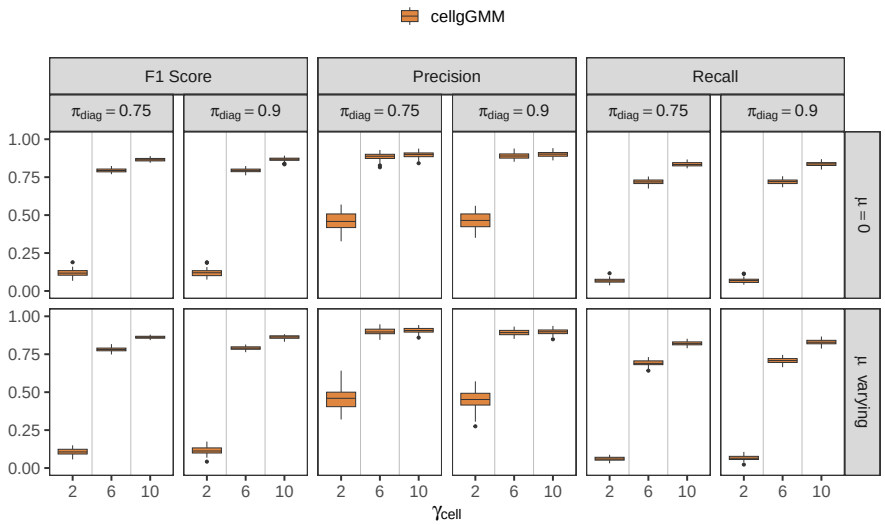

Figure 31: Performance of cellwise outlier detection in the balanced high-dimensional setting ($N = 2, p = 60, n_1 = n_2 = 40$) with covariances according to Agostinelli et al. (2015) evaluated by on precision, recall and F1-score.

γ_{cell}	π_{diag}	μ	#
10	0.75	0	100
10	0.75	varying	100
10	0.90	0	100
10	0.90	varying	100
6	0.75	0	100
6	0.75	varying	100
6	0.90	0	100
6	0.90	varying	100
2	0.75	0	100
2	0.75	varying	100
2	0.90	0	100
2	0.90	varying	100

(a) Toeplitz structure.

γ_{cell}	π_{diag}	μ	#
10	0.75	0	100
10	0.75	varying	100
10	0.90	0	100
10	0.90	varying	100
6	0.75	0	100
6	0.75	varying	100
6	0.90	0	100
6	0.90	varying	100
2	0.75	0	100
2	0.75	varying	100
2	0.90	0	100
2	0.90	varying	100

(b) Agostinelli et al. (2015) structure.

Table 5: Number of successful replications for the two covariance structures in the balanced high-dimensional setting ($N = 2, p = 60, n_1 = n_2 = 40$), depending on simulation parameters.

References

Agostinelli, C., Leung, A., Yohai, V. J., and Zamar, R. H. (2015). Robust estimation of multivariate location and scatter in the presence of cellwise and casewise contamination. *Test*, 24:441–461.

Alqallaf, F., Van Aelst, S., Yohai, V. J., and Zamar, R. H. (2009). Propagation of outliers in multivariate data. *The Annals of Statistics*, pages 311–331.

Boudt, K., Rousseeuw, P. J., Vanduffel, S., and Verdonck, T. (2020). The minimum regularized covariance determinant estimator. *Statistics and Computing*, 30(1):113–128.

Cilia, N. D., De Gregorio, G., De Stefano, C., Fontanella, F., Marcelli, A., and Parziale, A. (2022). Diagnosing alzheimer's disease from on-line handwriting: A novel dataset and performance benchmarking. *Engineering Applications of Artificial Intelligence*, 111:104822.

Cilia, N. D., De Stefano, C., Fontanella, F., and Di Freca, A. S. (2018). An experimental protocol to support cognitive impairment diagnosis by using handwriting analysis. *Procedia Computer Science*, 141:466–471.

Cortez, P., Cerdeira, A., Almeida, F., Matos, T., and Reis, J. (2009a). Wine Quality. UCI Machine Learning Repository. DOI: https://doi.org/10.24432/C56S3T.

Cortez, P., Cerdeira, A. L., Almeida, F., Matos, T., and Reis, J. (2009b). Modeling wine preferences by data mining from physicochemical properties. *Decis. Support Syst.*, 47:547–553.

Cuesta-Albertos, J., Matrán, C., and Mayo-Iscar, A. (2008). Robust estimation in the normal mixture model based on robust clustering. *Journal of the Royal Statistical Society Series B: Statistical Methodology*, 70(4):779–802.

Dasgupta, S. (1999). Learning mixtures of gaussians. In *40th Annual Symposium on Foundations of Computer Science (Cat. No. 99CB37039)*, pages 634–644. IEEE.

Dempster, A. P., Laird, N. M., and Rubin, D. B. (1977). Maximum likelihood from incomplete data via the em algorithm. *Journal of the royal statistical society: series B (methodological)*, 39(1):1–22.

Eirola, E., Lendasse, A., Vandewalle, V., and Biernacki, C. (2014). Mixture of gaussians for distance estimation with missing data. *Neurocomputing*, 131:32–42.

Filzmoser, P., Fritz, H., and Kalcher, K. (2009). *`pcaPP`: Robust PCA by projection pursuit.*

Fraley, C., Raftery, A. E., Scrucca, L., Murphy, T. B., and Fop, M. (2024). *`mclust`: Gaussian Mixture Modelling for Model-Based Clustering, Classification, and Density Estimation*. R package version 6.6.1.

GeoSphere Austria (2022). *https://data.hub.zamg.ac.at*.

Hennig, C. (2004). Breakdown points for maximum likelihood estimators of location–scale mixtures. *Ann. Statist.*, 32(1):1313–1340.

Hubert, M., Raymaekers, J., and Rousseeuw, P. J. (2024). Robust discriminant analysis. *Wiley Interdisciplinary Reviews: Computational Statistics*, 16(5):e70003.

Little, R. J. and Rubin, D. B. (2019). *Statistical analysis with missing data*. John Wiley & Sons.

Maronna, R. A., Martin, R. D., Yohai, V. J., and Salibián-Barrera, M. (2019). *Robust statistics: theory and methods (with R)*. John Wiley & Sons.

Mayrhofer, M., Radojičić, U., and Filzmoser, P. (2025). Robust covariance estimation and explainable outlier detection for matrix-valued data. *Technometrics*, (just-accepted):1–23.

Mayrhofer, M., Radojičić, U., and Filzmoser, P. (2024). *robustmatrix: Robust Matrix-Variate Parameter Estimation*. R package version 0.1.3.

McLachlan, G. J. and Krishnan, T. (2008). *The EM algorithm and extensions*. John Wiley & Sons.

Neykov, N., Filzmoser, P., Dimova, R., and Neytchev, P. (2007). Robust fitting of mixtures using the trimmed likelihood estimator. *Computational Statistics & Data Analysis*, 52(1):299–308.

Öllerer, V. and Croux, C. (2015). Robust high-dimensional precision matrix estimation. *Modern nonparametric, robust and multivariate methods*, pages 325–350.

Puchhammer, P. (2023). *`ssMRCD`: Spatially Smoothed MRCD Estimator*. R package version 1.1.0.

Puchhammer, P. and Filzmoser, P. (2024). Spatially smoothed robust covariance estimation for local outlier detection. *Journal of Computational and Graphical Statistics*, 33(3):928–940.

Raymaekers, J., Rousseeuw, P., den Bossche, W. V., and Hubert, M. (2023). *`cellWise`: Analyzing Data with Cellwise Outliers*. R package version 2.5.3.

Raymaekers, J. and Rousseeuw, P. J. (2023). The cellwise minimum covariance determinant estimator. *Journal of the American Statistical Association*, pages 1–12.

Raymaekers, J. and Rousseeuw, P. J. (2024). Transforming variables to central normality. *Machine Learning*, 113(8):4953–4975.

Rousseeuw, P. (1985). Multivariate estimation with high breakdown point. *Mathematical Statistics and Applications B*.

Rousseeuw, P. J. (1984). Least median of squares regression. *Journal of the American statistical association*, 79(388):871–880.

Rousseeuw, P. J. and Bossche, W. V. D. (2018). Detecting deviating data cells. *Technometrics*, 60(2):135–145.

Todorov, V. (2024). *`rrcov`: Scalable Robust Estimators with High Breakdown Point*. R package version 1.7-6.

Zaccaria, G., García-Escudero, L. A., Greselin, F., and Mayo-Íscar, A. (2024). Cellwise outlier detection in heterogeneous populations. *arXiv preprint arXiv:2409.07881*.